Dynamic Analysis for fatigue performances assessment in Floating Offshore Wind Turbines electrical cables

Supervisors

Prof, Ing Francesco Petrini

Prof, Ing Franco Bontempi

Ph.D. Candidate

Mohsen Sobhaniasl

February 2021

Table of Content

List of Figures

List of Tables

Abbreviate

WT	Wind Turbine
OWT	Offshore wind turbine
FOWT	Floating Offshore Wind Turbine
OWF	Offshore Wind Farms
O&G	Oil and Gas industry
SBFOWT	Spar-buoy FOWT
FEM	Finite element method
BEM	Blade element momentum
SS	Sea state
ULS	Ultimate load state
FLS	Fatigue load state
DLC	Design load case
CAPEX	Capital Costs
OPEX	operating expenditure
AEP	annual energy production
FE	Finite element
CS	Coordinate system
CL	Center Line
DOF	Degrees of freedom
COG	Center of gravity
SWL	Sea water level
BC	Boundary condition
PI	proportional integral
HVDC	High Voltage Direct Current
MI	mass impregnated
VSC	Voltage Source Converters
XLPE	cross-linked polyethylene
EPR	ethylene propylene rubber
TD	Time domain
FD	frequency domain
FFT	Fast Fourier Transform
PDF	probability density function
CM	Center of mass
MSL	Mean sea level
TLP	tension leg platform
FSI	fluid-structure interaction
$\boldsymbol{Dm}$	fatigue damage
$\boldsymbol{Dm_{year}}$	total annual fatigue damage
$\boldsymbol{Lf}$	fatigue life of the cable
$\boldsymbol{Lf_d}$	Design fatigue life
$\boldsymbol{SF\_DNV}$	DNV safety factor
WTG	wind turbine generators

Chapter 1: Introduction

The current chapter gives an overview of motivation, goals of the research, novelty of the thesis with a vision to the advantages and disadvantages of offshore wind turbines (OWT). Furthermore, current chapter discuss design and analysis challenges of floating offshore wind turbines (FOWT) and provides information of operational condition of floating offshore wind turbines.

In recent years, wind energy has become one of the most important and promising sources of renewable energy, which rapid expansion during last years leads to continuous demands for additional transmission capacity and better means of maintaining system reliability. As wind power continues its rapid growth worldwide, offshore wind farms (OWFs) are likely to comprise a significant portion of the total production of wind energy and may even become a sizable contributor to the total electricity production in some countries. Over recent years, the demand for renewable energy has increased significantly, the percentage of electricity produced by renewable energy sources increased 2% between 2007 and 2009 in the United Kingdom. According to the US Energy Information Administration, the total net primary energy production (renewable and not renewable), averaged over the period 1980-2006, increased 1.92% worldwide and 0.68% in Europe [1]. FOWTs offer a means to vastly expand the number of possible sites for offshore wind energy plants. Driven by the limitations of onshore wind power, the continuously growing demand and the availability of subsidies, wind farms have been installed offshore Europe since 1991. In first developments of the OWFs, monopiles (large single piles) were used as the support structure, providing a simple and cost-efficient structure. However, although relatively cheap, the applicability of a monopile support structure is limited to water depths of roughly 20m. To gain access to areas with larger water depths, alternative bottom-founded structures have been developed. With this innovation, the commercial applicability has been widened to water depths of 40 to 50m. In water deeper than 50 meters, they offer access to large areas with a strong wind resource and less proximity to population centers. For some countries, such as those with a narrow continental shelf, floating foundations offer the only opportunity for large-scale offshore wind deployment. FOWTs are generally considered for operation in deep water [1]. They will likely be the only economical solution for wind energy development at most deep-water sites.

1.1 Motivation

The high-quality offshore wind resource (e.g., lower turbulence and higher wind speed magnitude at a fixed height) with respect to onshore sites, make offshore wind energy a compelling proposition, and OWTs will be a significant contributor to global

energy production in the future. However, due to the addition of wave and current loads, offshore structures must be made stronger, and thus more expensive than their land-based counterparts. The reliability of OWTs suffers from the higher loading, and the difficult accessibility of the turbines for maintenance compounds. Besides, standard rotor diameters of commercial wind turbines (WT) are rapidly increasing in size for satisfying increasing requests of energy from the market thanks to the advancement in material technology. To sustain the expansion of the wind energy in the demanding offshore environment, a lot of the technologies have been adapted from the offshore oil and gas industry (O&G), but still, the system design differs drastically. Though lower targeted reliability levels hint at relatively cheaper structures, the coupled system dynamics of turbine/platform and lower profit margins in renewable energy necessitate a highly stabled design. What is abundantly clear is that the goal of an offshore wind farm is to produce electricity and send it to shore, and the way to do so is only by using a grid system that involves hundreds of meters of electrical cable in an offshore farm, some of which are seabed laying, and some of which are dynamic cables that connect to the floating structures and transfer the produced electricity. A crucial design issue for FOWTs regards the fatigue performances of structural and non-structural components, which are subjected to high number of loading cycles during their service in an aggressive environment.

One of the main failures causes of FOWT farms is the fatigue in marine power cables connecting the single turbines each other and with the shore, where the electrical transformation station is usually located. In fact, one of the important issues in dynamic cables is fatigue damage, which reduces cable life by less than the life of the wind farm. In addition, it is very costly and difficult to maintain, repair or adjust these cables when the wind farm is in service.

In this scenario, studying numerical aspects of FOWTs can be very helpful in understanding the behavior of the multi-physic model of supporting platform and floating wind turbine including additional components like power cables. The challenge is to develop reliable numerical models of the buoyancy of supporting platform and connected power cable.

1.2 Present study

This thesis will model a spar-buoy FOWT (SBFOWT) considering aerodynamic and hydrodynamic behavior of the floating structure stabilized by mooring line in deep water containing connected dynamic power cable. More specifically, the thesis studies the multi-physic numerical modeling SBFOWTs using the finite element method

(FEM), blade element momentum (BEM), the joint probabilistic distribution of wind and sea state, wave theory and floating dynamics to analyze the multi-physic model of a single and a group of FOWTs including the electrical marine cables connecting the single turbines, focusing on the fatigue calculation of such a elements as main purpose. During the study, efforts will be made to better understanding the system properties of FOWTs and to model a single floating offshore wind turbine consisting mooring lines and connected power cable in different sea states (SS) (environmental condition). The goal of the numerical analysis is first to estimate the fatigue life of an electrical cable connected to a single 5MW SBFOWT and later in a larger scale, to estimate the fatigue life of three different electrical cables connected to three FOWT with a simple connection layout modeled, which inspired by an optimum wind farm layout. The NREL 5 MW baseline wind turbine model, developed to represent a typical multi-megawatt wind turbine for offshore applications, is considered as SBFOWT prototype in the present study. ANSYS AQWA [2] commercial code will be used for modeling multi-physic behavior of OWT. On the other hand, hydrodynamic and aerodynamic responses of 5 MW NREL wind turbine will be calculated using the open-source code, FAST (Fatigue, Aerodynamics, Structures, and Turbulence), developed at the National Renewable Energy Laboratory (NREL) [3] to validate the model of the FOWT in ANSYS AQWA, furthermore, extracted rotor aerodynamic loads from FAST will apply as an input in ANSYS AQWA. Responses of a SBFOWT under current, wave and aerodynamic loads will be investigated.

The innovation of this study is to propose a procedure for full (turbine + floating platform+ mooring lines + cables) non-linear dynamic modelling of marine electrical cables connected to the floating platform in a variety of configurations for the accurate fatigue analysis of the of electrical cables. Analyses and models of the stand-alone floating electrical cables are provided in literature for offshore platforms (mainly for oil and gas industry studies, but such a cable is usually not modeled in the whole context of FOWT farms by considering the dynamics of the system. In order to determine the fatigue damage in the electrical cable, it is important to model the whole system, applying operating loads (wave, wind, current) and after validating the model. To incorporate all these aspects in a non-linear numerical mode is a big challenge, and it requires massive computational effort.

1.3 Design Challenges for FOWT

The main aim in designing a SBFOWT is to create a platform that can generate electricity safely at the lowest possible cost and the most stable configuration. Given the single platform's payload–estimated to be a single 5 MW wind turbine, weighing

approximately 700 tons, and generating a maximum steady-state thrust of approximately 800 kN at 90 m above sea level, an affordable configuration should be produced that can safely generate electricity as part of a larger wind farm. Construction costs, which constitute a large part of the total initial investment is very depend on the structural design. The structural design, in turn, depends on the ultimate (ULS) and fatigue (FLS) loads encountered over the lifetime of the structure. SBFOWTs are subjected to a wide range of load conditions dictated by the environment (wind, waves, current, ice), by their operation (tow-out and installation, start-up, shut-down, normal operation, idling, parked and possibly defective) and possibility of the accident (ship collision, ballast system failure, mooring line loss, fire). The design standards for wind turbines require the consideration of extensive design loading cases (DLCs) [4-7]. New design standards for FOWTs introduce additional criteria related to the mooring system and the interaction between the operating platform and the wind turbine [8,9]. Nonetheless, the issue of which DLCs are design-driving in terms of both fatigue and overall strength for the existing types of FOWTs remains open. While various researchers have suggested possible designs, there is very little consensus, with 5 MW designs reported ranging from 846 tons [8] to 12,187 tons [9]. Even the concept of self-stable construction is open to discussion, as it can be claimed that the cost savings of installing a whole farm of operating wind turbines will cover the costs of constructing a specialized installation tool to provide stability during marine operations [10].

1.4 Analysis Challenges for FOWT

Besides the inherent research difficulties of a novel multidisciplinary architecture topic, SBFOWTs pose specific challenges regarding the variety of time scales involved in the problem, coupled structural modes, aerodynamics, and complex hydrodynamic loads. Considerable time scales for global SBFOWT analysis vary from approximately 0.2 s (for platform pitch and tower bending mode) to approximately 4000 s (for platform motions), with much longer times present in wind and difference-frequency wave forcing. Under these thresholds, there are contributions from rotor frequencies, controller frequencies, high-and low-frequency system resonances, and wave excitation. An analysis method must be capable of capturing critical high-frequency events while being accurately calculated to allow the simulation of several cycles of slower events. Hydrodynamic loads on SBFOWTs are an especially important challenge: such structures that lie at the boundary between slender and large-structures, so that the use of Morison's equation could be well fitted option. Owing to the system's normal frequencies, the first order potential wave theory might not be adequate to catch all the essential results. To cover this weakness uses of airy wave

theory and second order could be well enough. Scientists have developed various time-domain numerical analysis tools to capture the integrated aero-hydro-servo-elastic response of FOWTs. Cordle and Junkman offered a summary of each of these codes [11], for instance, two of the leading codes are FAST and HAWC2[12] (from DTU Wind Energy). Both were designed for land-based turbines and later adapted to offshore turbines. At the time of this thesis, the FAST code was somewhat constrained in its technical, hydrodynamic, and mooring system capacities. Some of these weaknesses are discussed in more current releases of FAST. HAWC2 has improved structural delay, but restricted hydrodynamic force models and longer computational time.

As already said, one of the goals of this thesis is to study a multi-physics numerical model of a spar-buoy platform for 5 MW NREL FOWT in deep water depth (320 m) including connected electrical cable and then estimate lifetime of the electrical cable during the operation phase of the FOWT. Claiming this goal, first it is necessary to model the all FOWT considering rotor, nacelle and the floating spar-buoy platform then attach the electrical cable. Using FEM method, structural parts are modeled. For modeling the turbine as a case study, this thesis uses NREL 5MW regular wind turbine. All aerodynamic responses of the wind turbine in this thesis will simulate using the open-source code, FAST, and for modeling the coupled system of the spar-buoy support platform and wind turbine and connected electrical cable, will use ANSYS Commercial Code.

1.5 Operation Conditions

Having developed a reasonable framework and an analytical method capable of modeling the system, it is important to extend the research to the circumstances that give rise to significant dynamic reactions during the operation phase of the wind farm. In the present thesis, the dynamic response of the SBFOWT in 20 different sea-states are considered, which tries to cover range of operational phase of wind farm. The wind speeds of the simulations depend on the wind turbine design, and in this thesis for 5 MW NREL wind turbine, operational speed starts from 5 m/s to 25 m/s. Selected sea states covers this range with different waves and currents which will explain in the future sections.

1.6 Summary

Reliability has increased since the first inland prototypes were installed, which has led to the deployment of wind turbines in remoter and harsher environments. Experience

from the oil and gas industry in offshore installations and foundations has allowed the wind turbine to go offshore, where the wind is stronger. In technical report of European wind energy association, an analysis shows that offshore wind farms are being built further from the coast and in deeper waters. Since 2011, the average offshore wind farm water depth has increased from 22.8 meters to 25.3 meters, and the distance to shore has increased from 23.4 km to 33.2 km [13]. Today, the wind turbine is a commercial product which is competing against other sources of energy, such as gas and coal. This competition has driven a constantly developing design and optimization process aiming at reducing costs and improving efficiency to reduce the total cost of the energy. Partly as a response to this, the size of wind turbines has increased from kilowatts to multi-megawatts. This trend is supported in another technical report [14], which shows that wind turbines are feasible even at 20 MW with rotor diameters of 252 meters. In Shikha et al [15], the advantages of offshore wind turbines are analyzed. The average offshore wind speed is typically 20% greater than onshore. The ambient turbulence is less, which prolongs the turbine's lifetime. Furthermore, issues related to noise and visual impact are reduced. Depending on the water depth, a variety of foundations have been used. From an economic point of view, the deep-water foundations are the most expensive, however, the expected wind speeds are higher and thus the expected electrical power production is higher. The monopile foundation is a popular example of offshore deployment. However, this foundation is economically limited to shallow water depths below 30 meters. Other concepts of foundations, such as the jacket and tripod, are designed for water depths in the range of 25-50 meters. However, other studies show that the spar-buoy platform has better performance in deep-water (higher than 150m). There are some relevant reasons, to move wind energy production from land to offshore:

- Better wind resources
- Offshore constructions have almost no restrictions concerning noise and visual impact.
- The limited availability of land, especially in Europe, suggests the exploitation of the sea.
- The possible involvement of new competitors, such as Oil and Gas companies (O&G), could bring new values in the market, in terms of both investments and technology.

To solving the problem of complexity of the floating system include supporting platform, wind turbine and electrical cable should consider the different structural parts in the analysis. In this thesis, taking input the NREL 5 MW turbine and spar-buoy support structure in deep-water concept will be investigated. These days a lot of codes and computational programs have been developed for OWTs design, however,

just a very few numerical tools are available for FOWTs design and analyzing fatigue damage on the electrical cable. Therefore, there is a necessity of producing reliable and realistic numerical tools for the preliminary design and analysis of FOWTs (and particularly of spar buoy-supported including electrical cable). This is exactly what is pursued in this thesis, which focuses to model spar-buoy supporting platform using FEM methods in deep water and developing in-house MATLAB routine for calculating fatigue damage of dynamic electrical cable, the novelty of the study will be that it is fully multi-physical modeling of FOWT and then calculating fatigue damage in dynamic electrical cable in the operational phase of FOWT. Fluid-structure interaction (wave loads on spar-buoy support structure) and wind aerodynamic loads on a wind turbine will model to the claim motions of floating support structure motions in the water. Another peculiar aspect of the proposed models is the explicit modelling buoyancy behavior of support structure, which is totally different from fixed support for wind turbine and oil and gas industry support structures because floating support structure must provide enough buoyancy to sustain the wind turbine weight plus its own weight. It also must provide enough rotational stability to prevent the system from capsizing and good wave response motions to prevent the structure from experience large dynamic loads. The aerodynamic response of the wind calculated using FAST and compared with the results of the simulations in ANSYS AQWA to validate the results of the ANSYS AQWA.

Chapter 2

Generalities in FOWTs design and modeling

2.1 Introduction

This chapter starts with giving information of the wind energy system history. In addition, both onshore and offshore wind energy market overview are given, with describing characteristics of the horizontal axis wind turbine. Different floating foundation and their functional conditions are considered. At the end, used software and codes to the modeling and analysis the SBFOWT under different load conditions are introduced.

2.1.1 Wind Energy System History

The sun is the source of wind energy. The sun's light heats various regions of the Earth, which causes temperature variations on the surface of the Earth, resulting in hot air rising and reducing the atmospheric pressure in those areas. Cooler air absorbs rising hot air and produces heat. People have been using wind energy for decades. Windmills were the first form of wind turbine that was used to convert wind energy into mechanical energy. The history goes back to AD 644 with the finds of vertical axis windmills in Sistan (today eastern Iran) [16]. Horizontal axis windmills were used later in 1300-1875 AD in the Netherlands and Mediterranean regions [17]. Towards the end of the 19th century, wind turbines, which were designed to produce electricity instead of mechanical power, were used for the invention of electrical generators. Some of the most important advances in this transition period was the effort by Charles Brush to turn an electrical engine into a rotor windmill in the United States in 1888 and if this effort did not create a new concept, small electrical generators became popular over the next few decades. Such small turbines were the motivation behind the concept of Marcellus Jacobs [16]. The Jacobs turbine had three blades and a real airfoil shape which resembled today's wind turbines and can be seen in Figure 2.1.

Figure 2.1. The Jacob's wind turbine [16]

The design of several larger wind turbines was most prominently seen in Danish wind turbines designed by Poul La Cour in 1891-1918. Approximately 100 wind turbines were installed in the 20-35 kW scale. The La Cour wind turbines were not used in wind farms, but the energy generated by these turbines was used to generate hydrogen which was later used for lighting [16].

The Smith-Putnam wind turbine was the most popular early large-scale wind turbine ever installed. This was installed in the 1930s in Vermont with a rotor diameter of 53.3 m and a nominal capacity of 1.25 MW [16].

Large-scale commercial use of wind turbines was first explored by NASA in the 1970s. In 1980, the world's first 20-turbine wind farm was installed in New Hampshire, United States [18]. While the turbines break down due to unforeseen wind balancing, this project has been a successful experience in the coming years. On the other hand, the last commercial offshore wind farm in the world was built in Denmark in 1991[18].

Wind technology has evolved exponentially in recent years. The size of wind turbines has increased, and the cost of production has declined with recent developments. Countries have been designing plans for transitioning to wind energy.

2.1.2 Market Overview

Wind energy is an increasing renewable source that is projected to meet 20% of US electricity demand by 2030[19]. Other nations have also invested in wind energy in recent years. The total global installed wind power capacity exceeded 591.549 GW by the end of 2019. Figure 2.2 demonstrates how the network power has increased in recent years.

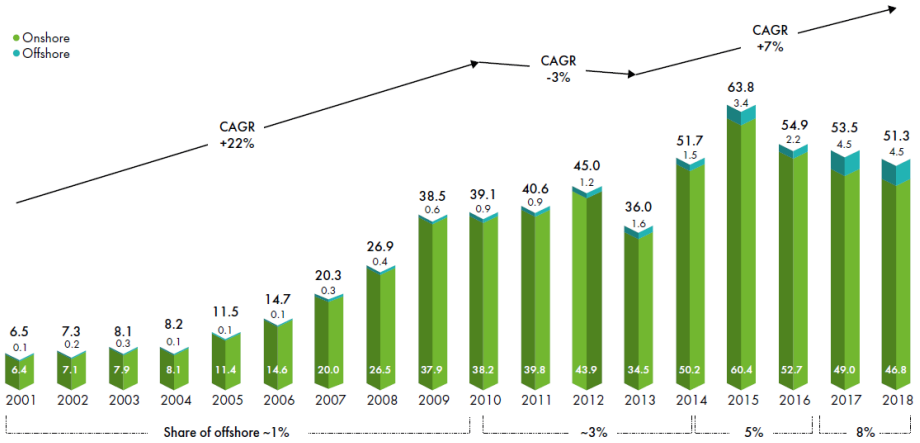

Figure 2.2. Total installed capacity by year [adapted from 20]

Figure 2.3 shows new installation of onshore. Figure 2.4 shows new installation of offshore. Figure 2.5 shows onshore distribution of total installed capacity in the world. Figure 2.6 shows offshore distribution of total installed capacity in the world.

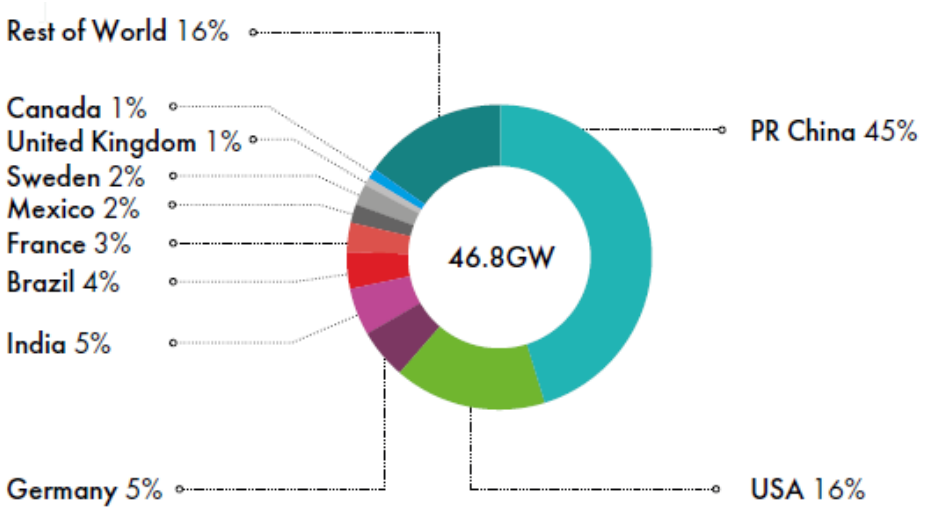

Figure 2.3 New onshore installation [adapted from 20]

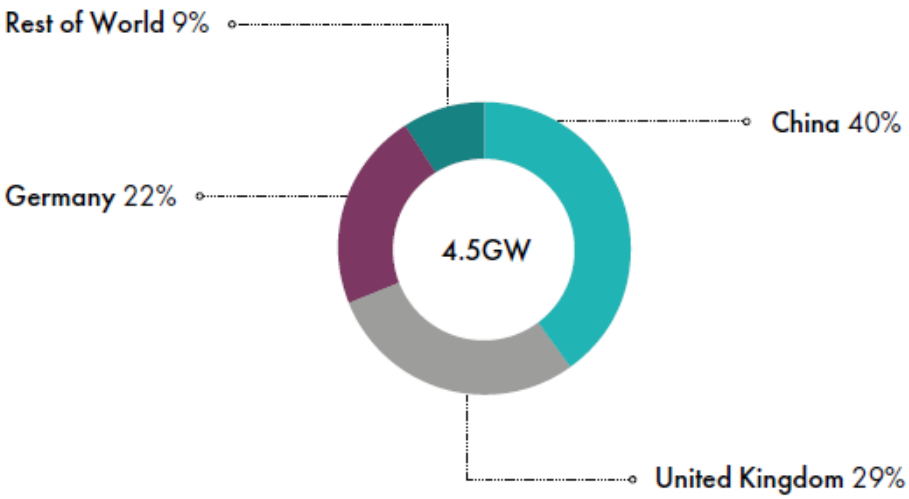

Figure 2.4 New offshore installation [adapted from 20]

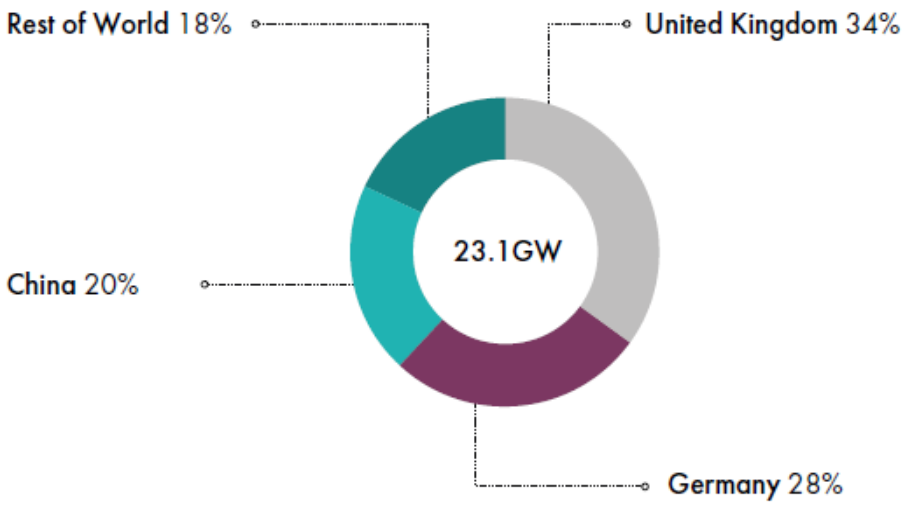

Figure 2.5 onshore distribution of total installed capacity in the world [adapted from 20]

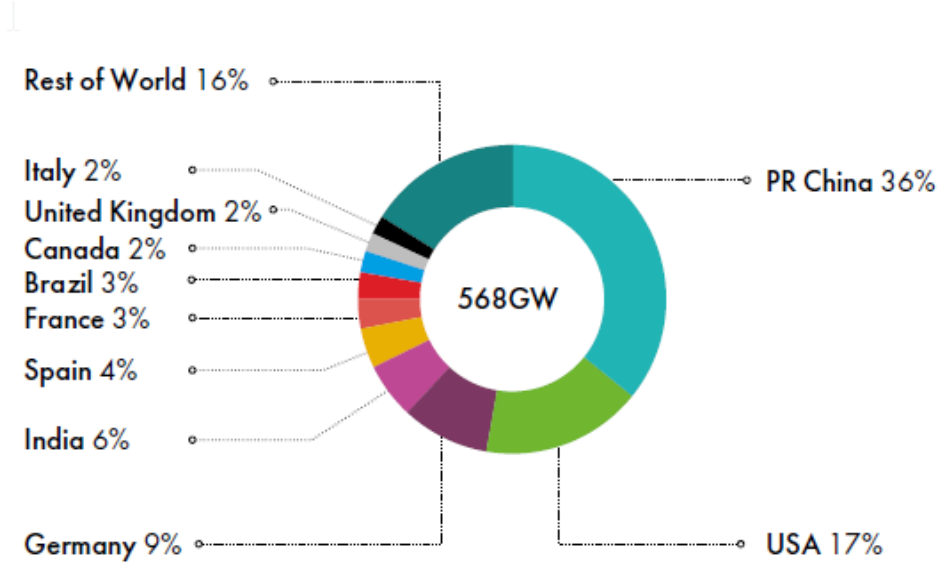

Figure 2.6 onshore distribution of total installed capacity in the world [adapted from 20]

The mature and leading markets in China and North America continued to grow in 2018. Positive developments came from Mexico growing by 500 MW compared to 2017 and reaching 0.9 GW of new installations. Africa/Middle East also grew to 0.9 GW with Egypt and Kenya as leading markets (380 MW and 310 MW of new installations respectively). The decrease in the European onshore market is attributed

to lower volumes in Germany and the United Kingdom. In India, new installations slowed compared to 2017 (4 GW in 2017) as execution challenges need to be solved.[20]

Offshore wind has huge potential in many regions, as the world looks for competitive, zero carbon energy sources that can be deployed at scale and in relatively fast time frames.

For the first time, China installed and connected more offshore capacity (1.8 GW) than any other country. The United Kingdom took the second place with 1.3 GW and Germany third place with 0.9 GW [20].

The second tender for offshore wind in Germany included once again a project bidding for 0.0 EUR/MWh support (repeating the zero-priced bids of the first round in 2017 and meaning that the project will only receive the wholesale price of electricity and no further support/ payment). This proves how offshore costs have come down. It also proves how the structuring of very capital intensive offshore projects (e.g., excluding grid connection cost) can advance projects [20].

Offshore activities in the US market are increasing. Leasing tenders have been executed (Massachusetts) and industry stakeholders have set up offices (MHI Vestas in Boston). The next stage will be the development of on offshore supply chain and projects advancing towards construction and execution timelines [20].

Development in the Asian offshore markets were positive in 2018 – commitments to invest in projects and supply chain have been made. Keeping the momentum requires government commitment and viable levels of support to ensure the growth of the Asian offshore industry.[21]

2.1.3 Characteristics of a wind turbine

A typical onshore wind turbine's component are the blades, nacelle, generator, gear box, tower, and base. Figure 2.7 illustrates a typical onshore wind turbine.

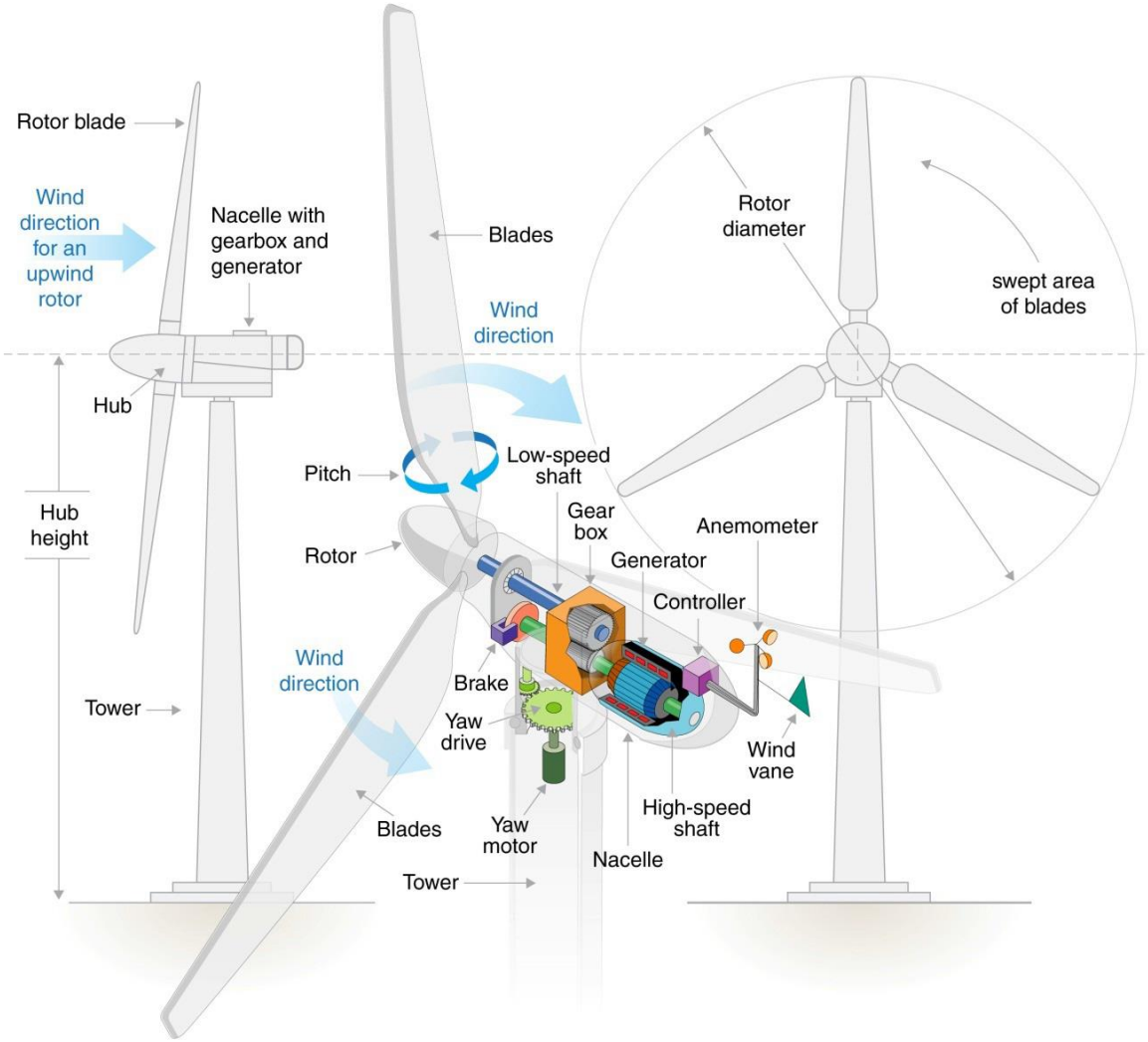

Figure 2.7. Wind turbine components [adapted from 22]

Blades catch the wind with their aerodynamic structure, transferring the kinetic energy of the wind to the rotational kinetic energy of the rotor. The nacelle is the location where the engine, the gearbox and other parts are located. The gearbox increases the spinning speed of the rotor and provides low torque and high speed power to the engine. The tower supports the rotor-nacelle assembly and is built of steel in the shape of a tapered hollow cylinder. It also plays a vital role in bringing the turbine to higher heights.

Conventional wind turbines are three-blade horizontal axis devices with varying diameters. The key parameters that denote the improvements in wind turbine technologies are the rotor diameter and the hub height to access more power from wind turbines, even in areas with lower wind speeds. Larger rotors aid in decreasing specific power, which eventually boosts capacity factors and opens low-wind areas to

more wind. The maximum size of turbines added in 2018 was 4.3 MW, up from 3.3 MW in 2015 [23]. GE is now offering improved onshore turbine technologies rated at 5.3 MW. Siemens-Gamesa presented its 5.8 MW, 170-metre rotor diameter model, which is larger than the largest offshore turbine currently available in the market [23].

Figure 2.8 shows ongoing innovations and technology enhancements towards larger-capacity onshore wind turbines, increased hub heights and rotor diameters would improve energy yields and reduce capital and operation costs per unit of installed capacity [22].

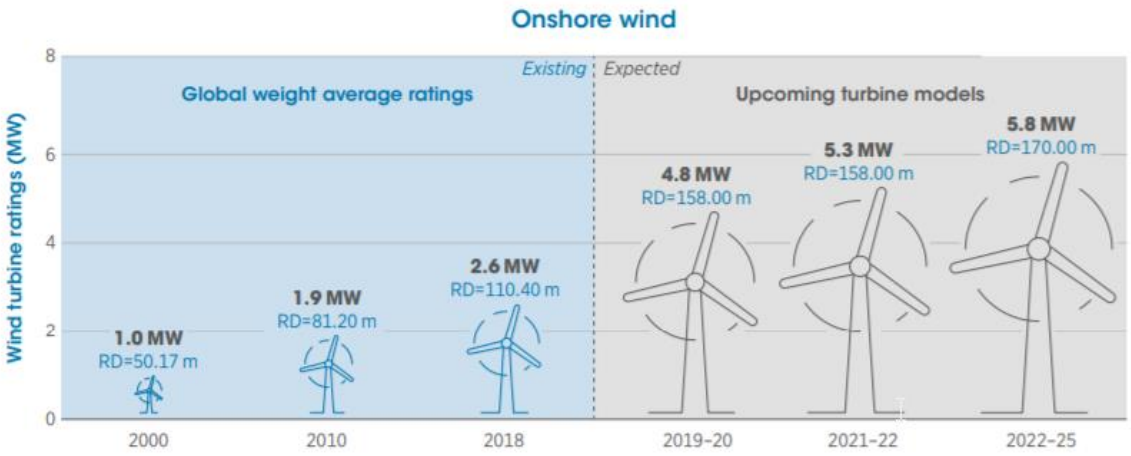

Figure 2.8 Ongoing onshore wind turbine technology [adapted from 22]

Developments in blade, drivetrain and control technologies would enable the development of larger, more reliable turbines with higher capacity ratings. Turbine sizes have increased rapidly in recent decades (Figure 2.9). By 2018, offshore wind turbines with an average rated capacity of 5.5 MW with rotor diameters of around 150 meters were being deployed [23]. Offshore wind farms commissioned in Europe in 2018 used turbines of between 3.5 MW and 8.8 MW capacity [24]. MHI Vestas' turbines of up to 10 MW capacity and 164-metre diameter blades have been commercially available since 2018 (with the first deliveries expected for 2021) [25]. These technology improvements are set to continue beyond 2022, with the largest turbine being developed by GE, the 12 MW Haliade-X turbine for offshore applications, with 107-metre-long blades resulting in blade diameters of over 200 meters. The industry is also working on concepts for even larger turbines of 15 MW by 2030, and up to 20 MW turbines for offshore application can be expected by 2030 [26]. These turbines are likely to have higher capital costs (CAPEX) per MW of rated capacity than existing turbines, but they would allow for a much lower cost of energy through higher energy production and lower CAPEX per MW for the foundations and installation. Further

improved reliability and maintainability would both decrease the operating expenditure (OPEX) and increase energy production, further reducing the cost of energy. With fewer turbines for a wind farm of a given rated capacity, there would be fewer maintenance visits required, improved health and safety, and fewer foundations, reducing the cost and environmental impact. However, blade tip heights would be higher with these turbines, making them more visually intrusive if sited near to shore.

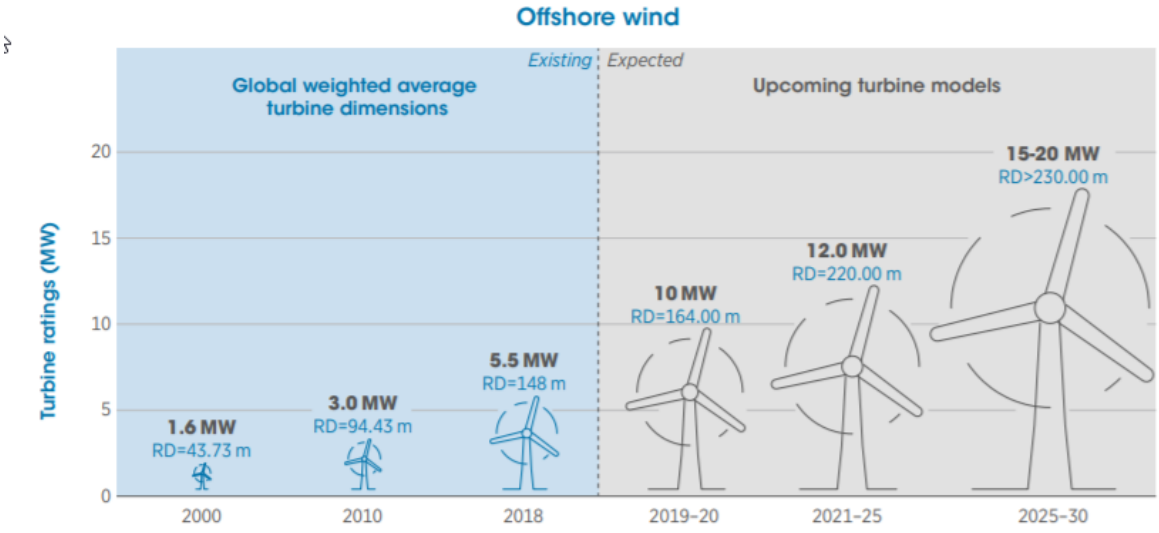

Figure 2.9 The average size of offshore wind turbines grew by a factor of 3 .4 in less than two decades and is expected to grow to output capacity of 15–20 MW by 2030. [adapted from 27]

2.2 Floating Foundations

When the early bottom-fixed foundations moved offshore, a lot of knowledge of how land-based structure concepts might be used, but new problems often emerge from the construction and function of the marine world. There is a natural option to pursue expertise and learn from an older, well-established industry known for its excellence in the construction and design of offshore foundations, namely the O&G market. Foundation options for wind turbines in intermediate (deeper than 45 m) water depth include both fixed and floating structures.

Three primary types of floating wind turbines are under consideration for deep water depth, semi-submersible designs, with multiple widely spaced columns, catenary moored spar designs, which require heavy ballast and a deep keel for stability, and TLP designs, which depend on the mooring system for stability. Examples of these three design types in 320 m water depth are shown in Figure 2.10. This visualization

highlights the deep draft required for the spar platform and the extensive mooring system of the semi-submersible platform. All three types of platforms have been inspired by activities in the onshore oil and gas (O&G) industry.

The offshore wind turbine does not have the same design drivers as the oil rigs. Oil rig construction involves the raising of bulky materials, including oil from the sea floor, thus, oil rigs experience broad vertical loading along with some lateral loading due to water, tides, and wind. In the other side, wind turbines experience high lateral wind loads and gyroscopic loads from the rotor. Such opposing loads make the design of the floating platforms for the two systems (oil rigs and wind turbines) very different. New designs for foundations, towers and platforms are required for use of floating wind turbines in order to make them commercially viable. Offshore wind turbines need to be able to endure intense wave (hydrodynamic) loads as well as high wind (aero-elastic) loads and related tower and floating platform motions.

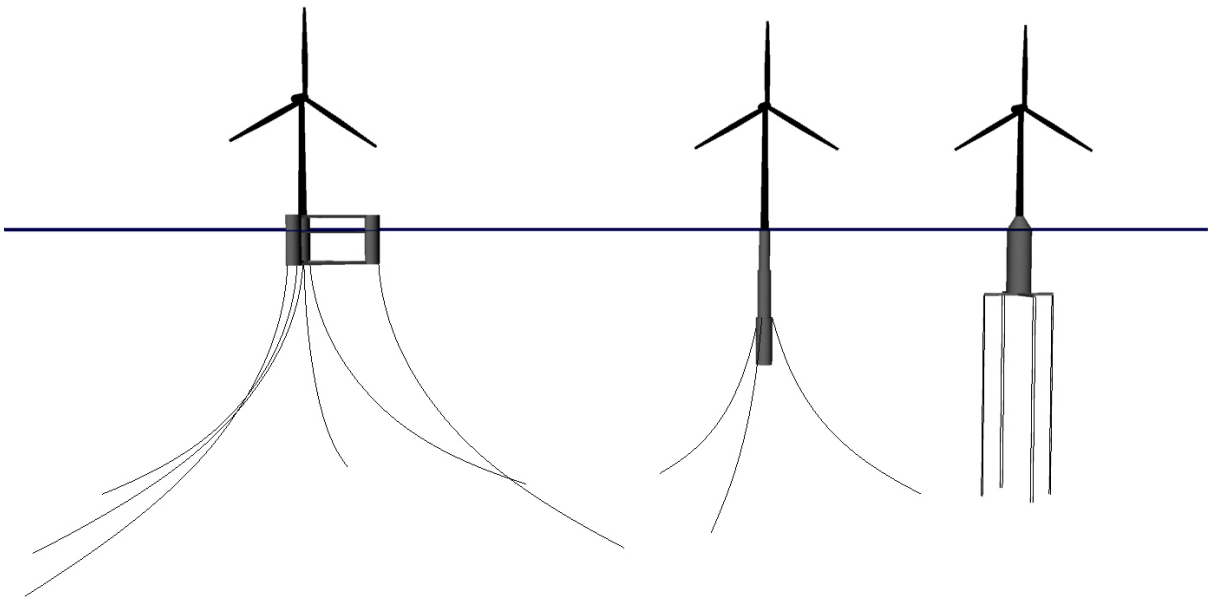

Figure 2.10: Floating support platforms

Semi-submersible (left, based on [adapted from 28]), catenary moored spar (middle, based on [adapted from 29]), and TLP (right, based on [adapted from 30]) wind turbine designs. Horizontal line indicates still water line.

This is clear that there are certain significant variations between the key principles and prototypes and all the resulting pros and cons in the end, though, they all have the same purpose; to provide a safe platform for the operation of the wind turbine.

2.2.1 Spar-Buoy benchmark

In the Phase IV Offshore Code Comparison Collaboration (OC3) report [31] a floating offshore wind turbine based on the spar-buoy model developed by Statoil of Norway was studied. This spar concept was chosen because of the simplicity of its design and ease of modelling. The OC3 spar buoy was based entirely on Statoil's "Hywind" spar, the real configurations used are very different from Statoil's initial concept. The data presented by Statoil on their platform and mooring system have been changed in such a way that the configuration of the platform is suitable for supporting the NREL 5 MW baseline turbine, which in effect has properties that are different from that of the turbine used by Statoil in the production of its Hywind system. This current system is referred to as the "OC3-Hywind" system to differentiate it from the original "Hywind" system of Statoil. The OC3-Hywind device features a deep-drawn, slender spar buoy with catenary mooring lines as seen in Figure 2.11.

The hybrid wind turbine and floating platform system is considered to be subject to regular rigid motion modes that are usually found in every wave-body interaction analysis. Modes 1 to 3 are transnational modes for surge, sway, and heave motion, which define translations along the x, y, z axes, respectively. Similarly, modes 4 to 6 reflect the rotational modes of roll, pitch, and yaw motion and define the rotation of the x, y, and z axes, respectively. To characterize the platform and wind turbine, a coordinate system is described, the origin of which is specified in the x-y coordinates at the middle of the floating platform, also, the z = 0 plane is described to match the still water level (SWL) as seen in figure 2.11.

Modeling wave action on the spar platform accounts for contributions from linear hydrostatics, linear excitation from incident waves, linear radiation from outgoing waves (generated by platform motion) and other nonlinear effects. Hydrodynamic loads due to incident wave excitation and outgoing wave radiation due to surface motion depend on whether or not a flow separation occurs.

In order to achieve realistic rates of hydrodynamic damping under extreme sea conditions, the linear potential flow theory solution has to be combined with the nonlinear viscous drag term resulting from the relative velocity term in Morison's equation. Also, during the OC3 analysis, it was indicated that linear radiation damping, and nonlinear viscous drag did not absorb much of the hydrodynamic damping at Statoil's "Hywind" site. It was also proposed that additional linear damping be applied to the above-mentioned hydrodynamics models for the OC3-Hywind method.[31]

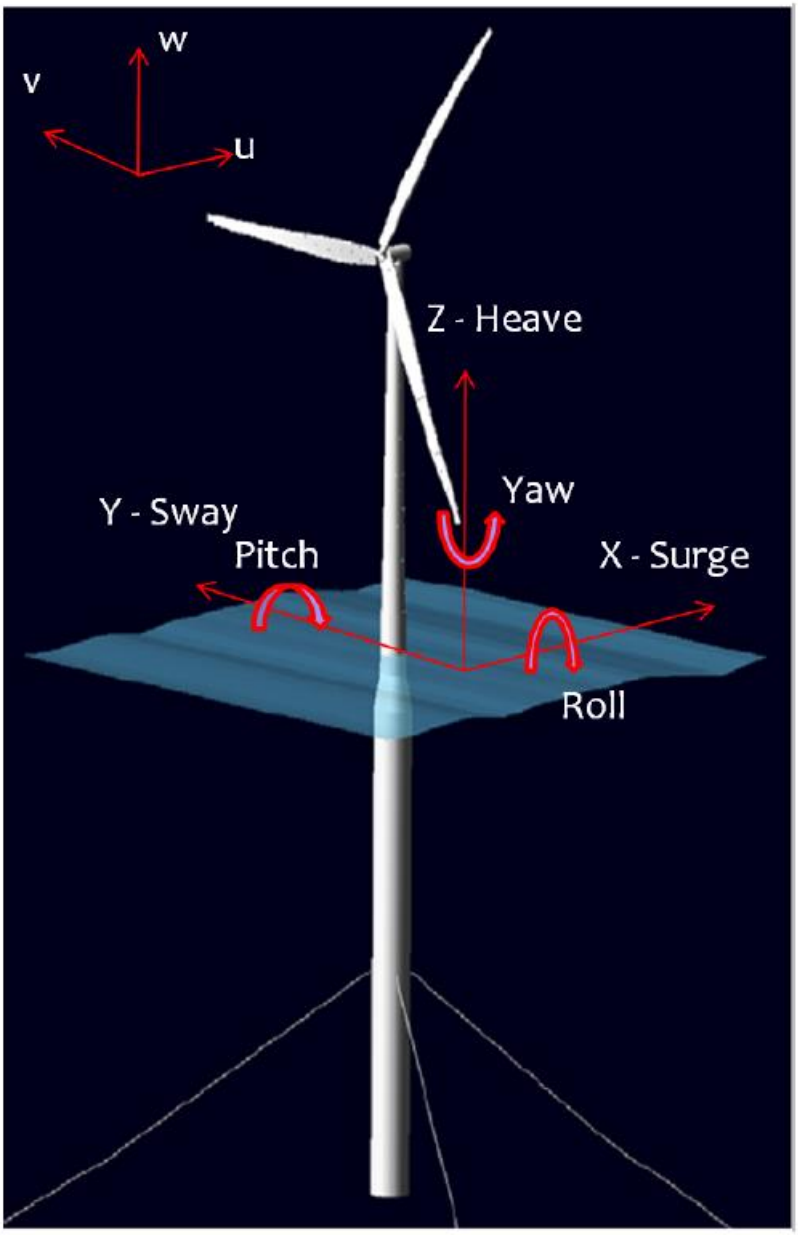

Figure 2.11: The NREL 5 MW wind turbine supported on the OC3-Hywind spar platform. [adapted from 31]

2.3 Floating Wind Turbine Analysis

As mentioned before, wind turbine rotor aerodynamic reactions were carried out using the FAST [32]. In addition, TurbSim [33] was used as a wind (inflow) turbulence simulator in conjunction with FAST. Information on the chosen model of the wind turbine, the support structure, and the mooring lines as well as the reaction of the wind turbine, aerodynamic loads and hydrodynamic loads are given in the following chapter. To add external structures like power cables all floating system is modeled in ANSYS AQWA [33] and the results are compared and validated with FAST results.

The hybrid floating platform and turbine configuration is modeled on a rigid body method, with six degrees of freedom. The non-linear rigidity restoration of the structure is characterized by the contribution of its mooring mechanism and hydrostatics. Hydrodynamic properties of the fluid-structure interaction are modeled in the time domain in ANSYS AQWA for the simulations conducted. Wind and wave loads are covered, taking into account regular wind velocity and wave height. Time of each simulation in ANSYS AQWA is 4000 seconds with time step of 0.5 second. First 400 second of each analysis is neglected due to avoid transitional effect of the motions in the analysis.

2.3.1 Numerical Tools, FAST Vs ANSYS AQWA

The version of FAST code used in this study is OpenFAST. OpenFAST is an open-source wind turbine simulation tool that was established in 2017 with the FAST v8 code as its starting point. OpenFAST is a multi-physics tool for simulating the coupled dynamic response of wind turbines. Practically speaking, OpenFAST is the framework (or glue code) that couples' computational modules for aerodynamics, hydrodynamics for offshore structures, control, and electrical system (servo) dynamics, and structural dynamics to enable coupled nonlinear aero-hydro-servo-elastic simulation in the time domain. OpenFAST enables the analysis of a range of wind turbine configurations, including two- or three-blade horizontal-axis rotor, pitch, or stall regulation, rigid, upwind, or downwind rotor, and lattice or tubular tower. The wind turbine can be modeled on land or offshore on fixed-bottom or floating substructures. OpenFAST and its underlying modules are mostly written in Fortran, but modules can be written in C/C++. OpenFAST was created with the goal of being a community model, with developers and users from research laboratories, academia, and industry.

Turbulent-wind inflow is prescribed by the external computer program TurbSim. FAST with AeroDyn [34] account for the applied aerodynamic and gravitational loads. The latter contribution includes the elasticity of the rotor, drivetrain, and tower, along with the newly added dynamic coupling between the motions of the support platform and the motions of the wind turbine. Nonlinear restoring loads from the mooring system are obtained from a quasi-static mooring line module that accounts for the elastic stretching of an array of homogenous taut or slack catenary lines with seabed interaction. HydroDyn [35] is a module that computes the applied hydrodynamic loads in the time domain. By interfacing these modules as described, fully coupled time-domain aero-hydro-servo-elastic simulation of offshore floating wind turbines is achieved. This capability is crucial for analyzing the dynamic response from combined

wind and wave loading because both can affect the motions, loads, and power production of the system. The generality of each module also ensures that the overall simulation tool is universal enough to analyze a variety of wind turbine, support platform, and mooring system configurations. But to model electrical cable in different configuration and study on fatigue life of the cable it is easier to use ANSYS AQWA. Moreover, the same simulation tools can still be used to model land-based wind turbines by disabling the hydrodynamic and mooring system modules. Figure 2.12 summarizes the modules and their interfaces [33].

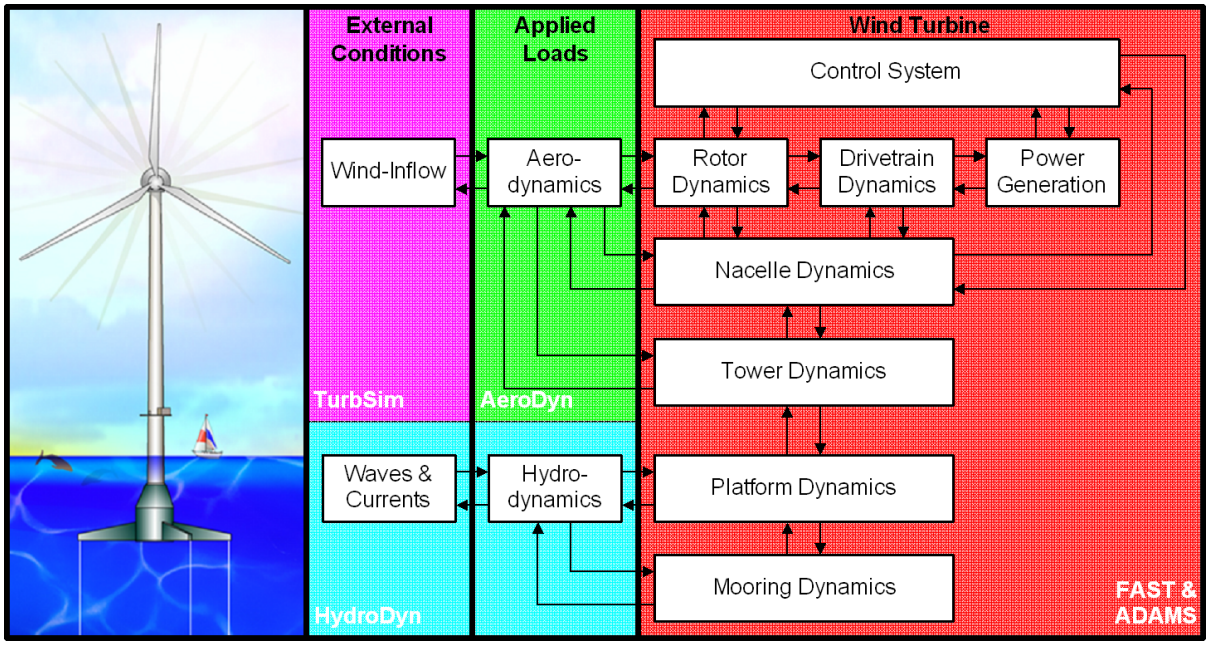

Figure 2.12. Interfacing modules to achieve aero-hydro-servo-elastic simulation [adapted from 33]

ANSYS AQWA provides an engineering toolset for the investigation of the effects of wave, wind and current on floating and fixed offshore and marine structures, including spars, floating structures, storage, semi-submersibles, tension leg platforms ships, renewable energy systems, and breakwater design. ANSYS AQWA provides an integrated environment for developing the primary hydrodynamic parameters required for undertaking complex motions and response analyses. Three-dimensional linear radiation and diffraction analysis may be undertaken with multiple bodies, taking full account of hydrodynamic interaction effects that occur between bodies. Computation of the second-order wave forces via the full quadratic transfer function matrices permits use over a wide range of water depths. ANSYS AQWA provides dynamic analysis capabilities for undertaking global performance assessment of floating structures in the time domain. A wide range of physical connections, such as mooring lines and power cables are provided to model the FOWT in different

electrical layouts. In addition, sea-keeping simulation may be undertaken with the inclusion of forward speed effects. Slow-drift effects and wave conditions may be investigated, and damage conditions, such as power cable fatigue damage, may be included to study any transient effects that may occur. The ANSYS AQWA product provides an integrated environment for developing the primary hydrodynamic parameters required for undertaking complex motions and dynamic response analyses of the floating structure.

As an option, ANSYS AQWA software can include the effects of line dynamics by modeling the mooring lines or electrical cable as a series of rod elements with defined nodes which allow to determine displacement of each elements or nodes to calculate curvature of the cable, which exactly is used in the process of fatigue life estimation in the thesis. The feature is available for both static (drag effects) and dynamic analyses. For the dynamic response, the capability is available within both the frequency and time domains. Frequency domain solutions are very fast and can help determine whether cable dynamics need to be considered as part of the analysis. Time domain solutions can provide much greater accuracy, but they take longer time to run.

2.3.2 FOWT Load Conditions

All through the duration of its lifetime, FOWT can be exposed to a wide variety of environmental load conditions (wind, water, sea, ice), service (tow-out and launch, start-up, shutdown, normal activity, idling, parked and probably defective) and-possibly-accidental service (ship crash, ballast tank breakdown, mooring line loss, re). Extensive DLCs [36-38] should be considered in order to define possible design-driving loads. The issue on which DLCs are designed-in terms of both fatigue and ultimate strength for various types of FOWTs is still open.

In fact, there is a connection between the environmental conditions and the operating condition of the turbine. In the case of very low wind speeds, the engine idles before the operating speed is achieved. The working conditions under which the turbine generates electricity are consistent with a variety of wind speeds from cut-in to cut-out (5 m/s to 25 m/s at hub height for the NREL 5 MW turbine [39]). The blades are feathered for higher wind speeds, and the turbine is either parking or allowed to idle. Many studies have studied the efficiency of FOWTs under operational and idling conditions, including most of the previously cited architecture studies and some comparisons [40]. This study uses 20 sea states to cover the operational range of wind speed of 5 MW NREL wind turbine.

2.4 Energy Yield Calculations

The power that a wind turbine delivers to the grid depends on the wind speed at which it operates. This dependency is captured by the power curve. An example of a power curve of a 5 MW turbine is given in the figure below. At low wind speeds the turbine converts as much wind energy into electricity as possible, while at higher wind speeds the power is limited to the rated power.

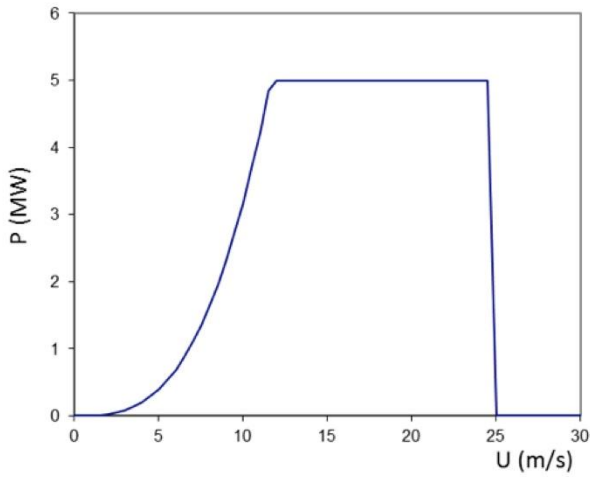

Figure 2.13 example of Power Curve

Because the wind varies over time, the power also varies over time. To determine the amount of electricity that is produced by the wind turbine over a certain period, it is necessary to integrate the variable power. This would require knowledge of the variation of wind speed over time. It is more convenient to use the statistical properties of this variation, particularly the probability density function of wind speeds, $f(U)$. For the calculation of the long-term energy yield probability density function, the average wind speeds for 10-minute periods must be considered.

The probability density function captures how often a 10-minute average wind speed occurs. The probability density function can be used to determine the probability that the wind speed is in a range $d(U)$ around this value. This probability is $f(U)d(U)$. More generally, the probability that the 10-minute average wind speed is between $U1$ and $U2$ equals:

$$F(U1 \leq U \leq U2) = \int_{U1}^{U2} f(U)dU \qquad \text{Eq 2.1}$$

The function is called a density, because with must multiply $f(U)$ with the range $d(U)$ in the integrand. The unit is therefore s/m, because probability F has no unit and $d(U)$ has the unit m/s.

With the power $P(U)$) from the power curve, the probability of occurrence of wind speeds in a range $d(U)$, the energy yield E in a period of duration T can be calculated from:

$$E = T \int_{U_{ci}}^{U_\infty} P(U) f(U) dU \qquad \text{Eq 2.2}$$

If the period of duration is one year, the energy yield is often called AEP, for annual energy production. If the power is expressed in kW and the duration in the number of hours per year, T=8766h, then AEP is expressed in kWh.

2.4.1 Probability density function

The power curve usually provides by the manufacturer of the wind turbine. Then for determining the energy yield, probability density function still needed. For almost every place on earth this statistical property of the 10-minute average wind speeds can be expressed fairly well with a 2-parameter Weibull distribution. This distribution is described by the following function:

$$f(U) = \frac{k}{a}\left(\frac{U}{a}\right)^{k-1} e^{-\left(\frac{u}{a}\right)^k} \qquad \text{Eq 2.3}$$

in which k is the form (or shape) parameter and a is the scale parameter. The figure below gives an example of a Weibull function for form parameter k=2.2 and scale parameter a=10.16(m/s), $Uavg$ being 9 m/s.

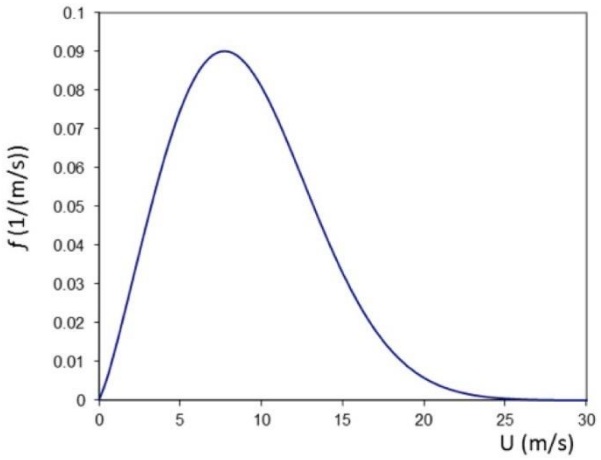

Figure 2.14 Weibull Distribution

The two parameters, k and a, are determined from wind speed data. If these are not known, a reasonable estimate for the north-western European coastal region is $k = 2$. The Weibull parameters are related to the annual average wind speed $Uavg$ through the relation:

$$a = Uavg\Gamma(1 + 1\mathrm{K}) \qquad \text{Eq 2.4}$$

in which $\Gamma(x)$ is the Gamma function. For $k = 2$, $\Gamma\ (1.5)\ \approx 0.886$ and it is possible to estimate the scale factor if the annual average wind speed is known.

2.4.2 Capacity Factor

The capacity factor Cf expresses the ratio between the actual AEP and the amount of energy that would have been obtained if the turbine had operated the entire year at its rated power. This is equivalent to ration between $T_{\text{equivalent}}$ and T_{year}, if $T_{\text{equivalent}}$ is the time that the turbine would have to operate at its rated power to obtain the same energy as it actually does in a year. The capacity factor calculated using the equation 2.5:

$$Cf = \frac{AEP}{P_{rated}T_{Year}} = \frac{T_{equivalent}}{T_{year}} \qquad \text{Eq 2.5}$$

Although the capacity factor is often intuitively interpreted as an efficiency, a high capacity factor is not necessarily good. In the figure 2.15, a turbine shown with a large rotor and a small generator on the left-hand side. The small generator represents a low rated power. Because the rotor easily drives the generator at its rated power, even for low wind speeds, this configuration has a capacity factor close to one. From an economic perspective, the rotor is too large, the rotor is too expensive, and do not tap the amount of wind energy it could convert.

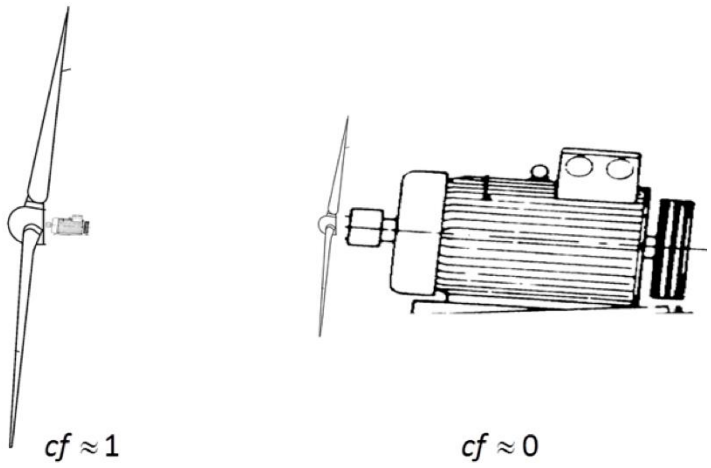

Figure 2.15 Rotor Capacity Factor

2.4.3 Simple energy yield estimation

By flipping the definition of the capacity factor, it is possible to estimate of the annual energy yield without using the wind climate and/or power curve by equation 2.6:

$$AEP = C_f P_{rated} T_{year} \quad \text{Eq 2.6}$$

It is still needed to assume a value for the capacity factor. For a high wind speed site, higher value in the range and for a low wind speed site a lower value must be taken.

This approach is not useful to make design decision in a project development, because it does not include specific information of the turbine or site. However, it can be used to get ball-park figures (e.g., how many households can approximately be serviced with the wind farm) and to check whether to not make a mistake in the detailed energy yield calculations.

2.4.4 Principal of load analysis

The rotor-nacelle assembly may have been designed and certified initially based on a standard wind turbine class. This turbine class specifies external conditions for the design with the expectation that the rotor-nacelle assembly will satisfy the design requirements at locations with similar or milder conditions. The use of a standard class is usually the case, since rotor-nacelle assemblies are not designed site-specific, but are used at many different locations. In this case it shall be demonstrated that the offshore site-specific conditions do not compromise the structural integrity, by comparison of loads and deflections calculated for the specific conditions with those calculated

during initial design. The support structures need to be analyzed and certified for site-specific conditions.

There are various approaches to perform the limit state analysis. DNV-GL distinguishes, [41]

A. design by partial safety factor method
B. design assisted by testing
C. probability-based design

A. Partial safety factor method

The partial safety factor method applies a safety factor to the loads (external forces and dynamic response), a safety factor to the resistance (material properties and geometry) and a safety factor to account for the severity of failure. The analysis of the loads and resistance is performed for specified conditions and the consequential results (e.g., the largest internal moments in the structure) are considered to be representative. This is therefore called a deterministic approach.

The magnitude of the safety factor on loading depends on the expected uncertainty and whether the loading is favorable or unfavorable. E.g., the safety on gravity loading is lower than on aerodynamic loading, because it can be determined with high precision.

Failure of the support structure has large consequences, as other parts of the wind turbine may be damaged or there may even be total loss. Therefore, the safety factor for severity is high for support structure limit state analysis. If a failure only leads to limited component damage and downtime, a lower safety factor is used.

B. Design assisted by testing

For some phenomena, the accuracy of model predictions is low, requiring much conservatism in the design (high safety factors). In such cases tests on a scale model or on a full scale prototype may be used to calibrate models or to demonstrate that design requirements are satisfied.

C. Probabilistic analysis

The starting point for a probabilistic approach is the notion that there is a probability distribution for the loading and for the resistance. The aim of the approach is to

estimate these distributions and to obtain an acceptable probability for the realizations in which the loads exceed the resistance. This is visualized in the figure below. The full analysis of the overlap of the two probability distributions may be cumbersome and imprecise. A practical implementation of the approach is to determine the loading for which the change that this load will be exceeded during the lifetime of the turbine (or other part of the floating system) is below a predefined (low) value.

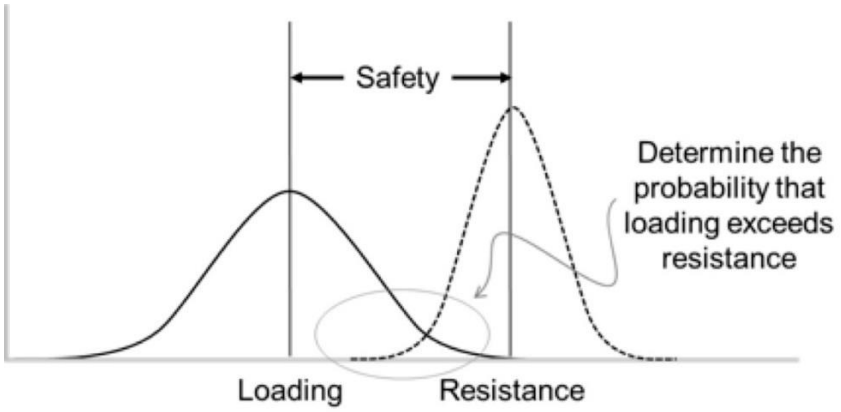

Figure 2.16 Probabilistic analysis

2.4.5 Lifetime Loading

Wind turbines are designed for a lifetime of 20 years or more. The analyses of the limit states must be representative for the conditions that can occur during this entire lifetime. The figure below illustrates the response of the wind turbine to these external conditions to identify several issues for this analysis.

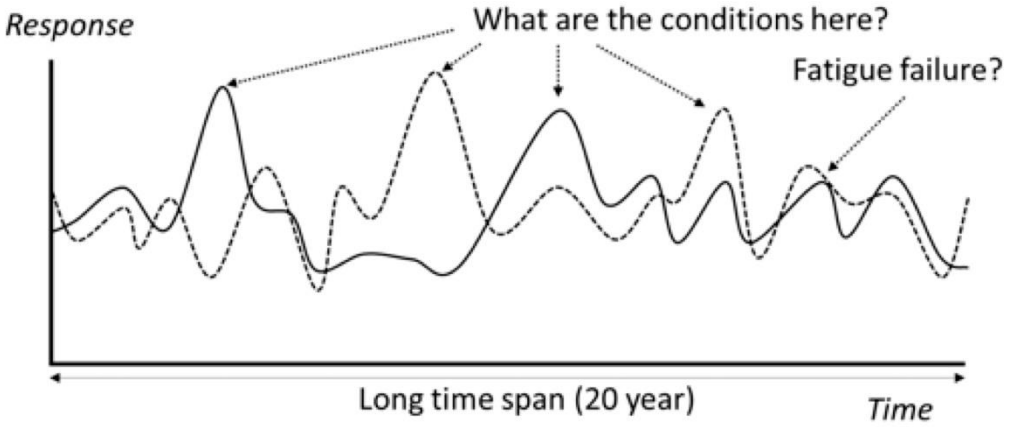

Figure 2.17 Long Life Span

The issues that are illustrated by this figure are:

Simulation of the entire long lifespan would require much computational resources. External conditions are stochastic, and many realizations are possible. The response is a function of external conditions, operation, and dynamics. Therefore, it is unknown what the conditions are that lead to the largest response.

For fatigue assessment the load variation over the entire lifespan needs to be represented, including conditions with lower response.

To deal with these issues, load analysis is performed with load cases. A load case is a combination of external conditions and operational conditions of the turbine that specify a situation that can occur during the lifetime of the turbine. Instead of trying to simulate the lifetime of the turbine sequentially, analyzing a set of load cases. The types of conditions that can be specified by a load case are shown below.

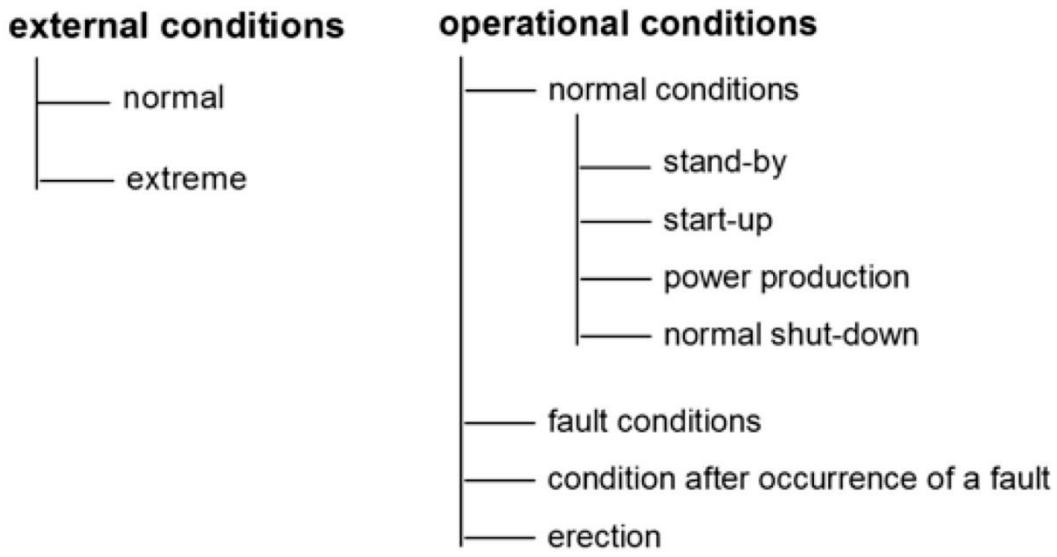

Figure 2.18 Types of Conditions

If study analyze all possible load cases, the design will become unnecessarily conservative. The analysis can be restricted to load cases with a reasonable likelihood of occurrence. For instance, it is not likely that a 50-year extreme wave height and a 50-year extreme gust coincide, let alone that this would happen at the exact moment of failure of the pitch system.

The standards prescribe which load cases should be considered. The rationale used by the developers of the standards is that correlated events are likely to occur

simultaneously, while uncorrelated events are unlikely to occur simultaneously. As an example, the significant wave height in a sea state and the average wind speed are correlated phenomena, as waves are (partly) generated by the wind. Therefore, some load cases consider the simultaneous occurrence of a high significant wave height and a high average wind speed. However, the height of individual waves and individual gusts in that sea state is not correlated. Therefore, these two extreme external conditions are not combined in one load case.

For the analysis of ultimate strength all load cases are considered either separately (in the partial safety factor method) or in a statistical analysis (in the probabilistic approach). For the analysis of fatigue, it is needed to determine a probability of occurrence for each load case(or sea states). With this probability it is possible to determine how often the load case re-appears over the lifetime of the turbine. This is used to determine the cumulative damage of variable loading.

In this study, normal condition considered in both external conditions and operational conditions.

2.5 Floating Wind Farm Design

The planning and design of an offshore wind farm can be divided into two phases, the planning process in which the marine strategic planning is developed and the design phase in which the precise design of the wind farm is carried out. The key challenge in the planning process is to choose the location of the offshore wind farm, determine the capacity limit and designate a particular area that requires wind turbines to be installed. Of course, this preparation must be performed thoroughly and well by acknowledging the marine environment's weakness and the limitations and conditions of all marine uses [42]. In the next chapters, the thesis will explain more information of floating wind farm design.

2.5.1 Shape, orientation, and layout

The majority of wind farm design studies presume that the boundary of a wind farm is given, i.e., with a fixed shape and orientation [42]. In fact, this limit is typically decided by the government's energy or development department, and mostly exists in the planning process and long before the final decision of the configuration of the wind farm. Of course, for a given wind farm site, this may theoretically lead to sub-optimal solutions. For example, well before the tendering process started, the allocated areas for two major offshore wind farms in Denmark were decided and

presented in a public report outlining the tenders and encouraging interested firms to dialogue. The shapes of the designated areas are shown in figure 2.19.[43]

A wide and open outlook against the predominant wind direction is an objective of primary importance. It is very likely to have a speed-up impact in the bargain if there are just a few obstacles to deal with and a low roughness in the same direction when aiming for a rounded hill to position the turbines. The basic configuration of commercial offshore wind farms actually involves a number of wind turbines set up at the chosen location, each linked by a set of cables leading to an adjacent offshore transformer station or directly to the shore. If it is connected to the transformer station, via an external underwater sea cable, the offshore station is connected to an onshore station that enables the onshore station to connect to an existing power grid. The wind turbines are mounted between them, up to a lateral distance of 8 times the rotor diameter.

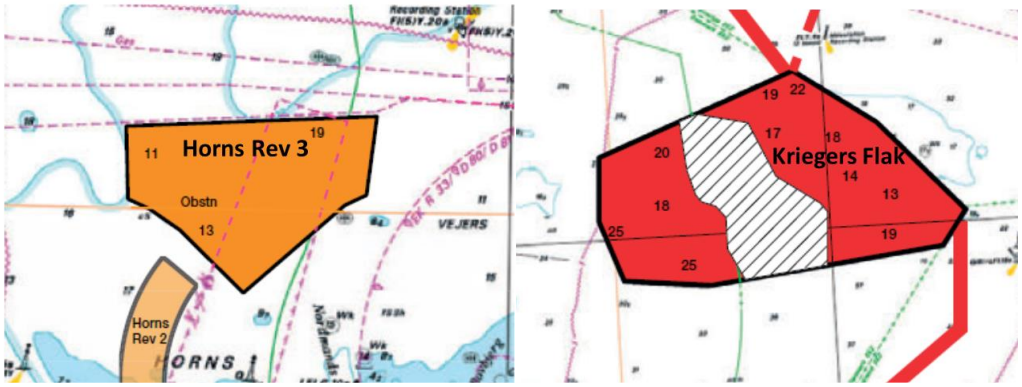

(a) Horns Rev 3 (b) Kriegers Flak

Figure 2.19: Designated areas for two Danish offshore wind farms (adapted from [43])

The designs preferred by wind farm developers typically follow the boundaries established by the designated areas. Researchers may consider a broad range of limits, each with a distinct form and direction, by analyzing the configurations of current wind farms. Five of such wind farms are illustrated in figure 2.20.

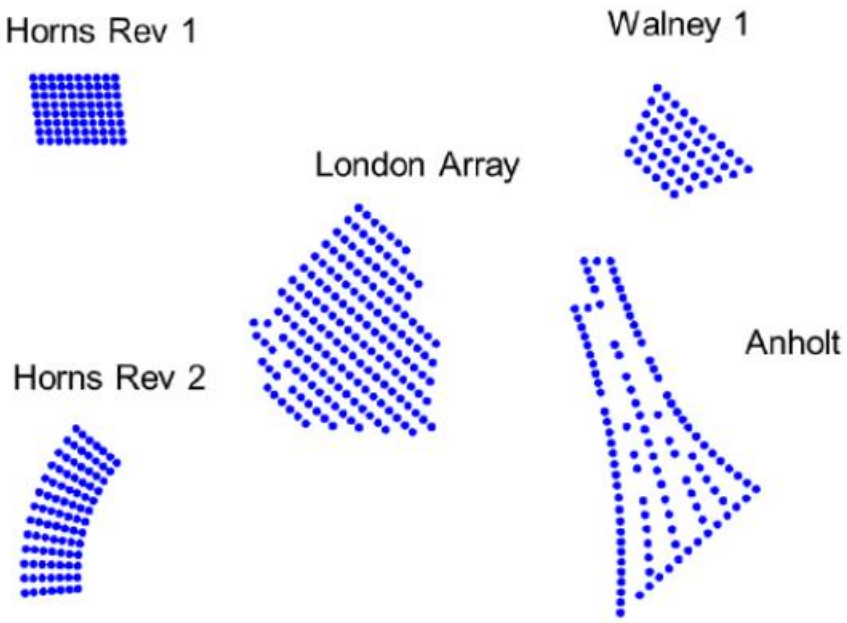

Figure 2.20: Layouts of five offshore wind farms (adapted from [44])

In this situation, the cost of cables will be minimized, but the turbulence and even the wake effects that the turbine can be increased. An architecture consultant will use the gathered site details to carry out a configuration parameterization to arrive at the optimum farm configuration. Using site information study and a mix of simulation methods, the work can be performed. The findings would lead to the measurement of the optimal width of separation between the farms, the size of the space in the middle of the wind farm to be effectively built, the concise quantity of turbines needed for the farm layout, the actual location of each turbine, and the shape of the farm layout.

Chapter 3: Theoretical Background for structural analysis

3.1 Introduction

In the present chapter, a brief mathematical formulation of the SBFOWT motion under waves, wind and current are described. SBFOWTs are dynamic structures to be studied in a multidisciplinary manner, including hydrodynamics, aerodynamics, structural mechanics etc., additional consideration of drivetrain mechanics, but outside the scope of the present work. The general structural force, hydrodynamic force, aerodynamic force, and mooring system are studied. Later, considered coordinate system is explained. At the end operational region of the modeled wind turbine is introduced.

3.2 Structural Mechanics

Global structural dynamic analysis of a floating flexible structure can be performed with various degrees of freedom, such as a linear rigid body approach, modal methods, nonlinear beam models, and more detailed finite element (FE) models considering 2-D or 3-D elements. The present thesis is focused on very common method (finite element method) using 3-D elements and the method can still be solved on a reasonable time scale.

3.2.1 Body Mechanics for Floating Bodies

A single, rigid body is a basic dynamic structural model of a platform, up to six typical global motions on a given inertial reference point can be finely defined. Surge (η 1), sway (η 2), heave (η 3), roll (η 4), pitch (η 5), and yaw (η 6). These global motions can be represented mathematically by the motion vector, ($\eta\ t$):

$$(\eta t) = [\eta 1(t), \eta 2(t), \ldots \eta 6(t)]^T \qquad \text{Eq 3.1}$$

where t represents time. Newton's second law is then applied in an inertial reference frame as:

$$M\vec{\eta} = \vec{F} \qquad \text{Eq 3.2}$$

Where M is a 6x6 matrix containing the entries M_{ij} representing the dry mass of the structure, with the inertia computed about the body reference point; F is a time-dependent vector of all the forces acting on the body, and the double dot represents two differentiations with respect to time.

For a moored floating body subjected to waves, a linear analysis of the global motions can be carried out by separating the force vector into several components: an added mass component which opposes the body acceleration, a linear damping component which is proportional to the body velocity, a linear stiffness due to hydrostatics which is proportional to the body motion, a linear stiffness due to the mooring system, and external wave excitation loads. By collecting the added mass, damping, and stiffness terms on the left hand side, the equation of motion becomes:

$$[M + A]\ddot{\vec{\eta}} + B\dot{\vec{\eta}} + [C + K]\vec{\eta} = \vec{X} \qquad \text{Eq 3.3}$$

Where A represent added mass coefficients, B represents damping coefficients, and C and K represent linear stiffness coefficients due to hydrostatics and the mooring system, respectively. A, B, C and K are 6x6 matrices, including coupling terms, and A and B are frequency-dependent. The 6x1 vector $\vec{X}$ contains the external wave excitation force for each mode of motion.

3.2.2 Loads and Analysis of Offshore Wind Turbines Loads of OWT

Offshore floating wind turbines are designed to work in extreme conditions and are subject to several forms of environmental and unintentional loads. These loads comprise waves, wind, current, ice, tides, and marine growth. Ice, tides and marine growth loads were not taken into account in this thesis.

The following sections will explain the main components of the vector of force given below.

$$F_i^{Platform} = F_i^{Structural} + F_i^{Hydro} + F_i^{Lines} + F_i^{Wind} \qquad \text{Eq 3.4}$$

The index i refers to the platform degrees of freedom (DOF),

3.3 FOWT Kinematics and Coordinate Systems

In order to provide an understanding of the motions and coordinate references used in this thesis, a formal description is given here. A right-handed Cartesian Coordinate Systems (CS) are used, where the counter-clockwise direction of all rotations around the axis is defined as positive.

- A global earth fixed CS (X, Y, Z), where the XY -plane coincides with the sea water level (SWL), and positive Z axis is pointing upwards against gravity.

- A body-fixed CS (x, y, z) is placed at the body center line (CL) at the undisturbed free-surface with the positive z axis pointing upwards.
- A rotor-fixed CS (xRot, yRot, zRot) is placed at the origin of the nacelle, following the body motions. The origin of this rotor fixed CS is located at (0, 0,90), measured from the origin of the body-fixed CS.

The rigid body motions of the floater consist of 6 DOFs. Three of them are translatory, while the other three are rotational. They are defined relative to the body-fixed CS. The translatory DOFs are:

Surge ($\eta 1$) along the x-axis, sway ($\eta 2$) along the y-axis, and heave ($\eta 3$) along the z-axis. The rotational displacements are:

roll ($\eta 4$) about the x-axis, pitch ($\eta 5$) about the y-axis, and yaw ($\eta 6$) about the z-axis.

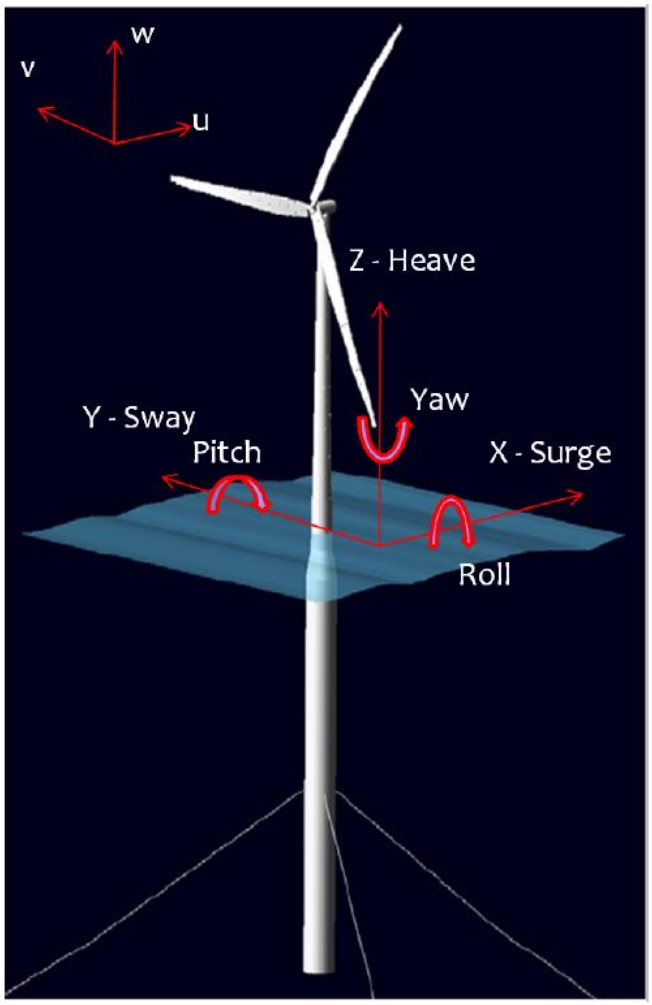

Figure 3.1 - FOWT body motions [adapted from 31]

The motion equation for floater rigid body motions is derived from the laws of Euler (linear momentum), taken on the origin of the body-fixed CS, which is regarded an inertial reference system.

Since a rigid body is being investigated, the translations of points other than the origin have a special relation to the origin, and can be determined directly based on the origin motions [45]:

$$S = [\eta 1 + z\,\eta 5 - y\,\eta 6 \quad \eta 2 - z\,\eta 4 + x\,\eta 6 \quad \eta 3 + t\,\eta 4 - x\,\eta 5] \qquad \text{Eq 3.5}$$

Where η_i is the different rigid body modes described earlier and x, y, z determines the point to which the motions are to be translated. This term can be useful when look at the nacelle's movements and accelerations.

3.4 Structural Loads

The components which define the vector of structural load, $F_i^{Structural}$, are given in Eq. 3.6.

$$F_i^{Structural} = F_i^{Inertia} + F_i^{Restoring} + F_i^{Gyro} \qquad \text{Eq 3.6}$$

The different components of load will be characterized in the following chapters.

In $F_i^{Structural}$, inertia and restore load vectors are not commonly presented in this manner but are the concepts on the left hand side of the motion equation. The purpose here is not to present the completely written equation of motion, but merely to categorize and explain what loads acting on the floater. This specific aspect of presentation has therefore been chosen.

3.4.1 Inertia Loads

The structure of the tower and platform are also assumed to be rigid. The rigid body mass matrix M_{ij} is found from the rigid body dynamics of linear and angular momentum: [46].

$$M_{ij} = \begin{bmatrix} m & 0 & 0 & 0 & mz_G & -mz_G \\ 0 & m & 0 & -mz_G & 0 & mx_G \\ 0 & 0 & m & my_G & -mx_G & 0 \\ 0 & -mz_G & my_G & I_{11} & I_{12} & I_{13} \\ mz_G & 0 & -mx_G & I_{21} & I_{22} & I_{23} \\ -my_G & mx_G & 0 & I_{31} & I_{32} & I_{33} \end{bmatrix} \quad \text{Eq 3.7}$$

m is here the total weight of the platform and tower (X_G, YG, Z_G) are the coordinates of the center of gravity (COG) for the total system taken from the SWL (sea water level) and I_{ij} are the moments of inertia. The inertia load vector can be expressed by,

$$F_i^{Inertia} = -M_{ij}\,\ddot{\eta}_i \quad \text{Eq 3.8}$$

Because of the floater COG 's position all definitions for Y_G will be zero. COG 's location will have a small non-zero X_G term, since the COG turbine is not exactly located at the CL. This also allows the I_{13} and I_{31} cross-terms to be non-zero.

3.4.2 Restoring Forces

The restoring load vector provided here includes both hydrostatic restore forces as well as gravitational forces. The restore forces are proportional to the floater displacement:

$$F_i^{Restoring} = -C_{ij}^{Hydrostatic}\eta_j \quad \text{Eq 3.9}$$

$C_{ij}^{Hydrostatic}$ is hydrostatic restoring coefficient matrix, and η_j represent the DOFs described earlier.

If the platform is disturbed in all of its DOFs, hydrostatic restoration contributions will be provided by dynamic equilibrium considerations, as shown in Eq 3.10 and Eq 3.13 via the assumption of minor angles, the coefficients were linearized. As the platform is symmetrical with the xz and yz planes in the fixed CS body, the final matrix of hydrostatic restoration will take the following form [45]:

$$C_{ij}^{Hydrostatic} = \begin{bmatrix} 0 & 0 & 0 & 0 & 0 & 0 \\ 0 & 0 & 0 & 0 & 0 & 0 \\ 0 & 0 & \rho_w g S_0 & 0 & 0 & 0 \\ 0 & 0 & 0 & \rho_w g \left(\iint_{S_0} y^2 dS + V_W Z_B \right) - mgz_G & 0 & -mgx_G \\ 0 & 0 & 0 & 0 & \rho_w g \left(\iint_{S_0} x^2 dS + V_W Z_B \right) - mgz_G & 0 \\ 0 & 0 & 0 & -mgx_G & 0 & 0 \end{bmatrix}$$

Eq 3.10

Where ρ_w represents the water density, g is the gravitational constant, S_0 is the water plane area at the SWL (sea water level), V_W is the total displace volume in still water, and Z_B is the vertical coordinate to the center of buoyancy (COB).

The $C_{33}^{Hydrostatic}$ entry states that the displaced volume will change if the platform in the vertical direction is disturbed. This will also change the vertical buoyancy force. Since the platform has a radius varying with depth, this term is true only for an area of vertical displacements. The radius at the SWL to calculate S_0 restricts this region to approximately ±4m (neglecting rotations). The vertical excitations are assumed to be small due to the floater's long draft, and $C_{33}^{Hydrostatic}$ is assumed to be true for all of the load case studied. When the platform pitches and/or rolls, $C_{44}^{Hydrostatic}$ and $C_{55}^{Hydrostatic}$ have restoring moments. The integral term captures the stiffness effect and as the platform pitches or rolls, the various parts of the platform will be buried or lifted from the water. The last term in $C_{44}^{Hydrostatic}$ and $C_{55}^{Hydrostatic}$ is that when the platform is disrupted in roll or pitch, the vertical position of the COB will change due to the change in stiffness.

Gravitation and COG terms can include regeneration in roll and pitch. There are also two coupling terms for yaw ($C_{46}^{Hydrostatic}$, $C_{64}^{Hydrostatic}$), as the COG does not correlate with the platform center line (CL). However, because X_G= 0.01m for the whole scheme, the influence of these terms would be minimal.

3.4.3 Gyro Moments

When the turbine is operating, the constant rotor spin at angular velocity ω_r will generate an angular momentum L_x^{Rot} on the x^{Rot} axis as given by:

$$L^{Rot} = [I_{x,r}\ \omega r \quad 0 \quad 0]^T \qquad \text{Eq 3.11}$$

$I_{x,r}$ represent the rotor moment of inertia about the x axis. Both $I_{x,r}$ and ω_r are considered to be constant throughout a simulation.

With an unsteady angular velocity, wind and waves will make the floater spin. This angular velocity will be $\omega_B^{Rot}(t)$ in the rotor-fixed CS. Due to this angular velocity, there will be a transfer in momentum that will cause what is called a gyro moment [47]:

$$M_{Gyro}^{Rot} = \frac{d}{dt}(L^{Rot}) = \omega_B^{Rot}\ L^{Rot} \qquad \text{Eq 3.12}$$

This implies we can usually have a gyro moment in the rotor-fixed device around the $y^{Rot}$and z^{Rot} axis, as the floater experiences rotational motions around the z^{Rot} and y^{Rot}axes, respectively, while the rotor revolves about the x^{Rot}axis.

3.5 Hydrodynamic Loads

The total force vector from hydrodynamic loads and moments on the 6 DOFs of the floater can be expressed by,

$$F_i^{Hydro} = F_i^{Wave(1)} + F_i^{Wave\,(2)} + F_i^{Viscous} \qquad \text{Eq 3.13}$$

Where $F_i^{Wave(1)}$ and $F_i^{Wave(2)}$ are the 1st order and 2nd order wave forces, respectively, and $F_i^{Viscous}$ constitute the contribution from viscous effects on the hull.

3.5.1 Regular Wave Theory

Using the Airy Wave theory, the waves are represented. The waves are defined by this theory as linear long-crested sinusoidal components and are based on potential theory. There are some fundamental assumptions about the fluid that need to be met when applying future flow theory. The fluid shall be inviscid, irrational, and incompressible. According to the Airy wave theory, for these regular waves it is possible to express the velocity potential of $\emptyset_0$ as:

$$\emptyset_0 = \frac{\zeta_0 g \cosh k(z+h)}{\omega \cosh kh} cos\ (-\omega t + kx + \psi_\zeta) \qquad \text{Eq 3.14}$$

Where ζ_0,k, ω and ψ_ζ are the incident wave amplitude, wave number, wave frequency and wave phase angel, respectively. Furthermore, g is the gravitational constant, z and x are the vertical and horizontal coordinates, respectively, h is the water depth taken from SWL, and t is the time.

$\emptyset_0$ satisfies the linearized boundary value problem explained in Faltinsen [45]. The boundary conditions (BC) include fluid particles must stay there on the free surface (kinematic BC), and that the pressure at the free surface (dynamic free-surface BC) should be equal to the ambient pressure.

An expression for the free surface elevation can be found from the free-surface dynamic condition [45]:

$$\zeta = -\frac{1}{g}\left(\frac{\partial \emptyset_0}{\partial \mathrm{t}}\right) = \zeta_a \sin(\omega t - kx + \varphi) \qquad \text{Eq 3.15}$$

$\phi = -\psi_\zeta$ is now what called the phase angel.

Linear theory also leads to a relationship of dispersion that explains the relation between the frequency of the wave and the number of waves. For finite water depths, the dispersion relation is given by,

$$\omega^2 = kg \tanh(kh) \qquad \text{Eq 3.16}$$

Relations for the parcel velocities can be found directly from the definitions of the velocity potential:

$$\frac{\partial \emptyset_0}{\partial \mathrm{x}} = u, \frac{\partial \emptyset_0}{\partial \mathrm{z}} = w \qquad \text{Eq 3.17}$$

In potential theory, all conditions for applying Bernoulli's equation are satisfied. Thus, the Bernoulli's can be used to locate the pressure:

$$p - p_a = \underbrace{-\rho_w g Z}_{\text{static}} \underbrace{- \rho_w \frac{\partial \emptyset}{\partial \mathrm{t}} - \frac{1}{2}\rho_w (\nabla \emptyset)^2}_{\text{Dynamic linear and quadratic}} \qquad \text{Eq 3.18}$$

3.5.2 1st Order Wave Forces

The contribution to the 1st order wave forces acting on the body is split into two terms:

$$F_i^{Waves(1)} = F_i^R + F_i^D \qquad \text{Eq 3.19}$$

where F_i^R and F_i^D are radiation force and diffraction force, respectively.

These two terms constitute the solution of the hydrodynamic linear potential flow problems of diffraction and radiation. An important factor regarding the solution is that it consists of transfer functions that are frequency dependent. Due to the frequency dependence, these functions cannot be used directly in the time domain analysis performed. The two subsequent sections will explain how these forces are implemented in the time domain analysis.

3.5.2.1 Radiation Forces and Moments

Leading to forced oscillations of the body in all of its DOFs, the radiation issue is related to hydrodynamic loads on the body, which radiate outgoing waves, resulting in hydrodynamic forces acting on the body, including additional mass and damping forces. The solution of the radiation problem is the frequency dependent added-mass $A_{ij}(\omega)$ and potential damping $B_{ij}(\omega)$coefficients. The additional mass force is, as the names suggest, proportional to the acceleration of the floater, while the potential damping force is proportional to the velocity.

$A_{ij}(\omega)$ and $B_{ij}(\omega)$ can be split into the summation of their asymptotic values at infinite frequency and their frequency dependent parts ($a_{ij}(\omega)$ and $b_{ij}(\omega)$):

$$Aij\ (\omega) = A_{\infty}ij\ (\omega) + aij\ (\omega), \qquad B_{\infty}ij\ (\omega) + Bij\ (\omega) + bij\ (\omega) \qquad \text{Eq 3.20}$$

It can be seen that the asymptotic value $B_{\infty}ij$ of the potential damping is zero [48]. The total force can be defined in the time domain by taking the inverse Fourier transform of the radiation forces in the frequency domain:

$$F_i^R\ (t) = -A_{\infty}ij\ \ddot{\eta}_j - \int_0^t h_{ij}(t-\tau)\dot{\eta}_j(\tau)d\tau \qquad \text{Eq 3.21}$$

Where $h_{ij}(\tau)$ is the retardation function found from a transform of the frequency-dependent added-mass and damping as shown below.

$$h_{ij}(\tau) = \frac{1}{\pi}\int_0^{\infty}[b_{ij}(\omega)cos\omega\tau - \omega a_{ij}(\omega)sin\omega\tau]d\omega \qquad \text{Eq 3.22}$$

3.5.2.2 Diffraction, Wave Excitation Forces and Moments

Excitation forces and moments of the 1st order wave are related to what it is called the diffraction problem. Presuming that the body is fixed and interacts with incident waves in the diffraction problem. This interaction results in a varying fluid pressure, called wave excitation loads, on the mean wetted surface of the body, which causes hydrodynamic loads. The wave excitation loads are given in terms of force and moment transfer functions:

$$F_i^D(\omega_k, \beta) = H_i^D(\omega_k)\tilde{\zeta}(\omega_k) \quad \text{Eq 3.23}$$

Where H_i^D is the complex first order wave force transfer function and $\tilde{\zeta}(\omega_k)$ is the complex harmonic wave component. With complex it means that e.g., for the harmonic wave component:

$$\tilde{\zeta}(\omega_k) = A_k e^{j(\omega_k t - K_k x + \varphi_k)} \quad \text{Eq 3.24}$$

And the surface elevation, ζ can be found from taking the real part of $\tilde{\zeta}$.

3.5.3 2nd Order Wave Forces

As stated earlier, only terms that are proportional to the wave-amplitude are considered by the 1st order wave forces. When incident waves become steeper $k\zeta_a$ for accurate load and motion estimates, the higher order terms become more significant. The impermeability of the body in its instantaneous configuration will be better applied by adding terms up to the second order, and the pressure at the instantaneous free surface will be considered atmospheric. Moreover, the normal fluid velocity on the free surface would be similar to the normal velocity of the free surface. The forces in the 2nd order are typically much smaller than the forces in the 1st order. They can also be very important for certain structures, since due to differential and sum frequency effects, they can cause resonance excitations. Not all 2nd order forces have been included here, but the slowly varying drift forces have been given by a simplified model. The major reason for including the slowly varying wave forces is that they can cause resonant motion in surge, sway, and yaw for moored platforms. The frequency effects of the 2nd order total are not known to be important to the floater since there are no normal intervals in the frequency spectrum above the wave frequencies.

3.5.3.1 Mean and Slowly Varying Drift Forces

The mean drift forces are the time independent segments of the forces of the 2nd order. There will be 6 average drift forces / moments in general, one for each different DOF. Average loads are due to the capacity of the body to produce waves [45].

The mean drift forces were obtained by momentum conservation. This provides the mean wave drift coefficients $\bar{H}_i^{(2)}(\omega_k)$ in terms of incident wave frequency (ω_k) in surge, sway, and yaw. Then it is possible to find the gross mean drift force $\bar{F}_i^{(2)}$ as:

$$\bar{F}_i^{(2)} = \sum_k^N \bar{H}_i^{(2)}(\omega_k)\, A_k^2 \qquad \text{Eq 3.25}$$

The 2nd order wave force transfer function can be approximated by using only values along the line $\omega_k = \omega_l$ by taking advantage of the Newman approximation [45]. The result of this approximation is that it is possible to measure the slowly changing drift forces based on the mean drift force coefficients and there is no need to find the complete transfer functions of the 2nd order.

3.5.4 Viscous Drag

The potential theory is based on the hypothesis of inviscid fluid. In the actual marine climate, this presumption does not always hold. Viscous effects can lead to large loads in many cases and cause damping of the movements of the platform.

An important viscous load for the floating body is the drag force. In the cross-sectional plane, the drag force acts in-line with the incident wave and current direction. The force is caused by separation of flow and shear stress along the surface of the body. This force will be included in the relative Morrison's equation using the quadratic drag term. Eq. 3.26 defines the drag force in the CS local strip. By incorporation over the wetted body to the mean surface or the free surface, the cumulative drag forces and moments are then discovered.

$$dF_s^{Viscous} = \frac{1}{2}\rho_w C_d D_s dz (V_s - X_s)|V_s - X_s| \qquad \text{Eq 3.26}$$

Where ρ_w is the water density, C_d is a non-dimensional drag coefficient, D_s is the strip diameter, dz is the length of the differential strip, X_s is the strip velocity, and V_s is the water velocity in the local strip CS.

In general, the drag on the strips in surge, sway, pitch, and roll can cause viscous damping forces and moments on the floater ($F_i^{Viscous}$). Due to the floater symmetry, there is no yaw moment, and no vertical force from the Morrison's equation, since it is not true in that direction [49]. Before simulation, the particle velocities are computed. This makes this formulation only for small displacements to be strictly valid.

The drag force will be greater near the free surface, with the assumption of deep water linear incident waves, and it will decrease with depth. This offers an attack point near to the free surface for the result. The application of linear wave theory provides us with an error in the distribution of undisturbed velocity under a wave crest, as there are significant nonlinear effects. When we need to recover the atmospheric pressure at the wave crest [45], the drag force can literally go to zero.

3.6 Morison's Equation

Morison 's equation is also used as an alternative to theoretical flow models for slender systems where the diameter D is small relative to the wavelength λ (approximately,$D < \lambda = 5$)[45]. The transverse force on a cylindrical segment per length (f) is given by Eq 3.27, where the additional mass coefficient is $Ca = Cm - 1$, C_D is the drag coefficient, u is the particle velocity of the transverse wave, and v is the velocity of the local transverse body.

$$f = \rho\pi\frac{D^2}{4}\dot{u} + \rho C_a\pi\frac{D^2}{4}(\dot{u} - \dot{v}) + \frac{1}{2}\rho C_D D(u - v)|u - v| \qquad \text{Eq 3.27}$$

The first expression in Eq. 3.27 reflects the Froude-Krylov force, and the second term includes the mass contributions added, and the viscous drag forces are represented by the final term. According to linear wave theory's deep water limit, the water particle acceleration is given by Eq 3.28 at a position (x; y; z) with z vertically upward from the still water stage. Where ω is the wave angular frequency ζ is the wave amplitude, and $k = 2\pi/\lambda$ is the wavenumber.

$$\dot{u} = \omega^2\zeta e^{kz}\cos(\omega t - kx) \qquad \text{Eq 3.28}$$

A transfer function (H_{Mor}) for the Froude-Krylov and added mass forces on a segment of length dl centered at a vertical position z is given by Eq. 3.29 assuming deep water ($\omega^2 = gk$) and neglecting $\dot{v}$.

$$(H_{\mathrm{Mor}}) = \frac{f}{\zeta} \approx \rho V(1 + C_a)\omega^2 e^{(\frac{\omega^2 z}{g})} \quad \text{Eq 3.29}$$

A combination of Morison 's equation and potential theory formulation can be used in a time-domain dynamic analysis. The complete equation of Morison's is applied for slender elements in addition to the potential flow solution for large volume bodies.

Viscous damping based on the Morison equation can also be applied with reasonable coefficients to the large volume system. Morison 's equation was implemented with linear second-order waves in the present work, with forces incorporated up to the instantaneous free surface.

3.7 Mooring system and Mooring Line Loads

For station keeping purposes, mooring systems are used. If the floating platform is shifted from its place of equilibrium, the mooring lines may have restoring forces and moments, as well as inertia and damping effects due to external forces such as wind and waves. A catenary mooring system is used in the reference model [39], which leads to rigidity by two distinct forms of effects.

When the floating body is displaced, due to the shift in catenary form leading to a restorative force, the stress at the fairlead will change. The second contribution comes from the mooring line elastic deformation. This is highly dependent on the mooring line content, and in most situations, relative to the catenary effect, it is minimal. For taut mooring systems, restoration by elastic deformations is more necessary. Mooring lines also lead to inertia and damping forces on the floating platform, in addition to stiffness. In Faltinsen [45], the catenary equations can be seen.

A finite element method (FEM) approach is used in the implemented numerical codes. 3-D bar elements are modelled on the mooring lines. Such bar elements consist of a node at each end of the element with 3 spatial DOFs (Figure 3.2).

It requires neglecting the bending stiffness of the lines by using bar elements rather than beam elements, which have 3 additional rotational DOFs. For the majority of catenary lines, this is also considered a valid assumption. A complete Lagrangian formulation describes the motion of the nodes, which includes referring the displacements in configuration C_n back to the original undeformed configuration C_0.

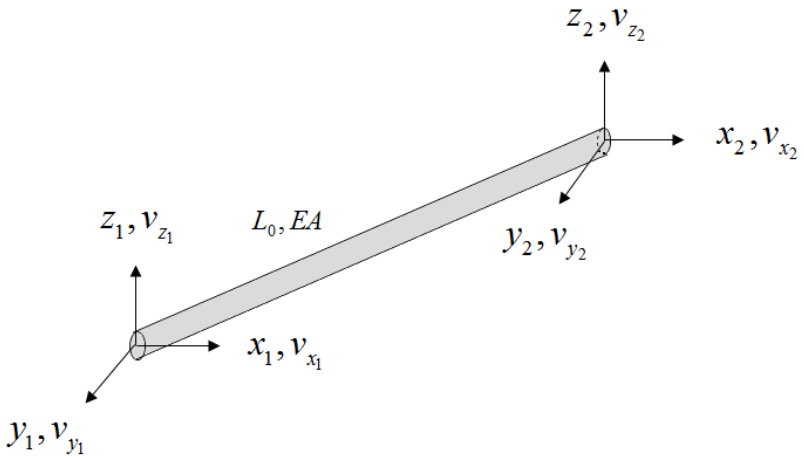

Figure 3.2 Bar Element

The assumption of small strains is introduced in the formulations of strains. Therefore, it is possible to ignore the cross terms in the Lagrangian strain tensor. This provides the approach with the following terms for strain ε and stress σ:

$$\varepsilon = \frac{L-L_0}{L_0}, \sigma = \frac{N}{A_0} \quad \text{Eq 3.30}$$

L_0 is the initial stress free length, and L is the length after deformation. N is the normal force in element, and A_0 is the initial cross-sectional area.

The constitutive law applied is Hook's law for linear elastic materials:

$$\sigma = \varepsilon E \quad \text{Eq 3.31}$$

Where E is the elastic modulus of the material.

Due to weight, buoyancy, sea bed interaction, and structural damping, the mooring lines are subject to loads. Due to vessel movements, they are often susceptible to hydrodynamic loads and forced displacements.

Structural damping is included using Rayleigh mass and stiffness proportional damping:

$$C = \alpha_1 M + \alpha_2 K \quad \text{Eq 3.32}$$

M and K and C are the mass, stiffness, and damping matrices, respectively, of the total mooring line system. α_1 and α_2 are the inertia and stiffness proportional damping coefficients, respectively, that can be specified to approximate the mooring lines' structural damping.

3.8 Aerodynamic Loads

3.8.1 Thrust

A basic expression for the thrust force can be obtained by simplifying a rotor into an ideal permeable disc, as shown in figure 3.3. Frictionless flow over the disk and that there would be no rotational velocity component in the wake are the assumptions behind an ideal disk. Applying the Bernoulli equation from far downstream to the rotor and from just behind the rotor to far downstream in the wake suggests that the wind movement over the rotor induces a discontinuous reduction in pressure on the rotor plane. The thrust force T acting against the flow results in this pressure drop, lowering the wind speed from V_0 upstream to u_1 downstream. The rotor would then sense the force of the momentum driving it downstream. For the thrust power, the resulting expression is given by Eq 3.33 [50].

$$T = \Delta pA = \frac{1}{2}\rho_a A(V_0^2 - u_1^2) \qquad \text{Eq 3.33}$$

Where A represent the disc area, ρ_a is the air density, and the velocities are similar as described above.

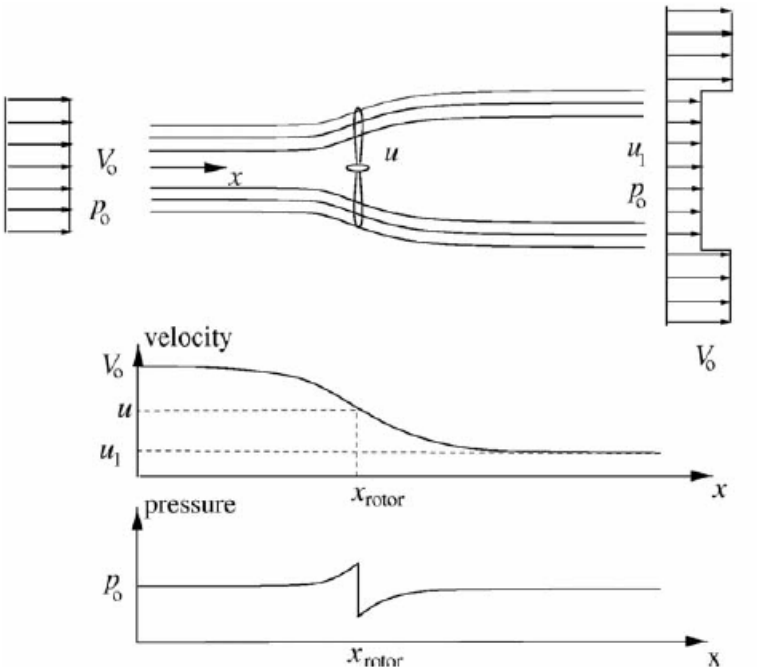

Figure 3.3 simplified rotor [adapted from 50]

Usually, the thrust coefficient C_t is defined when the thrust force T is expressed.

$$T = \frac{1}{2}\rho_a A C_t V_0^2 \qquad \text{Eq 3.34}$$

Via simulations and/or experiments, the thrust coefficient is identified. The thrust coefficients are obtained by the steady state blade element momentum theory (BEM) in this thesis. The BEM theory is essentially an extension of the above explained momentum theory to 2-D, taking into account local events at the actual blades. This theory also has many extensions that correct the assumptions implemented in the BEM theory [51].

C_t can be calculated based on the shapes of specific airfoils when using this procedure and on how it will vary with different attack angles.

As mentioned before, the focuses of this thesis are not on the aerodynamic modeling of the rotor, therefore, there will be not more explanation of behind the rotor aerodynamics equations. The thesis uses aerodynamic forces of the rotor to carry on the motion of the SBFOWT and calculating the fatigue damages on the connected power cables.

3.8.2 Wind Field

The loads on a wind turbine are highly dependent on a practical wind flow explanation. Wind has variations in both space and time, and these variations should be properly defined. Factors such as wind shear, turbulence, obstacles, and wind / tower interactions may be attributed to the variations. Wind shear is related to how, with the height above the sea level, the mean wind speed increases. The surface roughness and atmospheric stability are related to this rise. A standard definition of the variation is generated by a power law profile due to surface roughness. Wind velocity above the sea is given by Eq 3.35. Figure 3.4 shows the wind shear.

$$V_0(z) = V_0(z_0) = (\frac{z}{z_0})^{\alpha} \qquad \text{Eq 3.35}$$

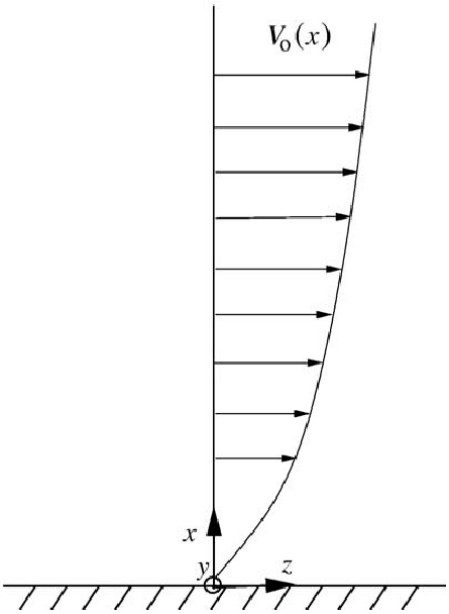

Figure 3.4 Wind Shear [50]

For standard classes of wind turbines, according to IEC61400-1[51], an exponent of $\alpha = 0.2$ for onshore locations and an exponent of $\alpha = 0.14$ for offshore locations should be used. Corrections may also be performed to involve fluctuations in atmospheric stability.

Atmospheric turbulence can cause changes in wind speed that are time dependent. A turbulent wind velocity can be seen as a velocity around a mean value that fluctuates. During the calculation, the turbulence strength is calculated as the ratio between the standard deviation and the mean wind speed. Gusts that cause large loads for a short

period of time, due to a sudden increase in wind speed over a short period of time, are another type of fluctuating phenomenon [52].

The time series of the wind field are generated using a Kaimal wind spectrum:

$$S_w(f) = 4{\sigma_w}^2 \frac{L_k/V_{Hub}}{(1+6f\frac{L_k}{V_{Hub}})^{\frac{5}{3}}} \quad \text{Eq 3.36}$$

where V_{Hub} is the mean wind speed at the hub, f is the frequency, σ_w is the wind speed standard deviation, and L_k is a length scale parameter that depends on the height of the hub. The scale parameter and standard deviation are typically defined as below:

$$\sigma_w = I(0.75V_{Hub} + 5.6), L_k = 8.1\lambda \quad \text{Eq 3.37}$$

λ is normally set to 42 m for hub elevations above 60 m, which is the value used here [46]. Before time domain simulations start, wind time series are made.

3.8.3 Implementation of Thrust

The total load vector induced by the F_W^{Rot} wind in the local rotor CS is first described.

$$F_W^{Rot} = [T \quad 0 \quad 0]^T \quad \text{Eq 3.38}$$

The thrust force is defined as a force that attacks the origin of the local CS rotor in a direction that is always usual for this moving CS.

The thrust force magnitude is determined by substituting V_0 for Eq 27, with the relative velocity component V_{rel}^{Rot} between the wind and the hub. The thrust coefficient C_T will also be determined based on this velocity. The relative velocity is defined as the difference in the local rotor CS between the wind velocity V_w^{Rot} and the hub velocity V_r^{Rot}.

$$V_{rel}^{Rot} = V_w^{Rot} - V_r^{Rot} \quad \text{Eq 3.39}$$

In general, three nonzero components could have V_{rel}^{Rot}. The loads that which occur in the y-and z -directions due to wind flow over the rotor are not considered.

3.9 Control Regions

As earlier mentioned, a NREL 5MW wind turbine is the reference wind turbine type used in this thesis. A total of five separate control regions (1, 1 ½, 2, 2 ½, 3) are used in the control system. Region 1, where the torque is zero, is below the cut-in speed. This is a start-up area, and the rotor is being accelerated by the wind. A transition between 1 and 2 is zone 1 ½. An optimized power capture scheme based on generator torque is used in region 2. This requires adjusting the torque of the motor, such that a steady tip speed ratio is preserved. A peak power coefficient can contribute to this tip speed ratio. The angle of blade pitch in this area is zero. Region 2 ½ is a transition region between 2 and 3 that, at rated capacity, limits tip speed and noise emissions. In region 3, the blade pitch controller is involved. The required blade pitch angle measurements are based on proportional integral (PI) regulation of the velocity error between the filtered velocity and the measured generator velocity. To attain constant generator rpm, this area uses the blade pitch controller, which contributes to constant power.

The resulting steady state output from the NREL 5MW turbine was found in [39] by running a series of simulations with steady uniform wind speeds.

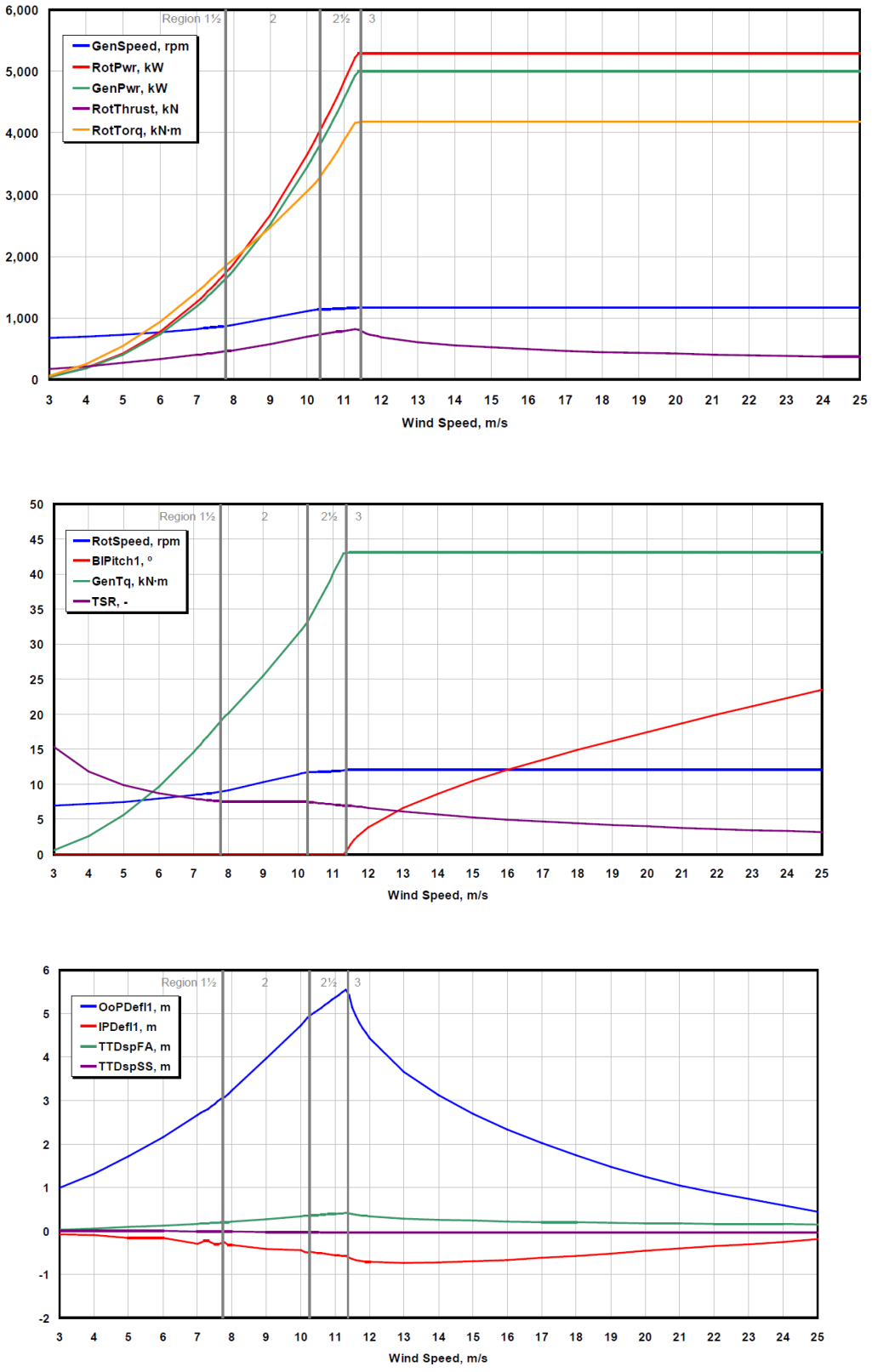

Figure 3.5 Steady state results from the NREL 5MW wind turbine [adapted from 39]

The simulations lengths were long enough to ensure that all transient behavior had died out. The result of only using the thrust curve as input from the steady state simulations and not taking into account the whole dynamics of the wind turbine with the controller is that quasi - static conditions are assumed. Obviously, this assumption cannot hold fully when the turbulent wind modeled. For this comparative analysis, however, the simpler model is deemed satisfactory.

The parameters of the figure 3.5 is defined as the below:

“GenSpeed” represents the rotational speed of the generator (high-speed shaft). “RotPwr” and “GenPwr” represent the mechanical power within the rotor and the electrical output of the generator, respectively. “RotThrust” represents the rotor thrust. “RotTorq” represents the mechanical torque in the low-speed shaft. “RotSpeed” represents the rotational speed of the rotor (low-speed shaft). “BlPitch1” represents the pitch angle of Blade 1. “GenTq” represents the electrical torque of the generator. “TSR” represents the tip-speed ratio. “OoPDefl1” and “IPDefl1” represent the out-of-plane and in-plane tip deflections of Blade 1 relative to the undeflected blade-pitch axis. “TTDspFA” and “TTDspSS” represent the fore-aft and side-to-side deflection of the tower top relative to the centerline of the undeflected tower.

Chapter 4: Fatigue Theory and Dynamic Cables

4.1 Electrical Cable

The current chapter gives a brief information about the development, technologies and different type of the submarine power cables, furthermore, materials and cable structure are discussed. Later, submarine power cable design, and wind farm energy transferring system investigated. At the end of the chapter the fatigue theory, formulation and methods are explained.

4.2 Submarine Power Cables

The first commercial High Voltage Direct Current HVDC submarine cable was built and laid down in 1954 in Sweden by ABB linking the island of Gotland with the mainland. Its voltage was 100 kV and the capacity 20 MW. The length was 90 km. Since then, the technology evolved towards higher capacity and voltage as well as towards optimization of the flow control. More than 70% of the HVDC submarine cables in the world (both in terms of number and length) are located in European adjacent seas shown in figure 4.1[53]. Islands close to the shore and archipelago nations are also places targeted by this technology. The vast majority of submarine power cables have a length of less than 300 km. They usually link countries separated by small to medium width water bodies on the same continent or at its fringes. There are a small number of intercontinental links like Spain-Morocco interconnection and the Red Sea Cable (Egypt-Jordan) but they are HVAC interconnectors and run on short distances (up to 30 km) [53].

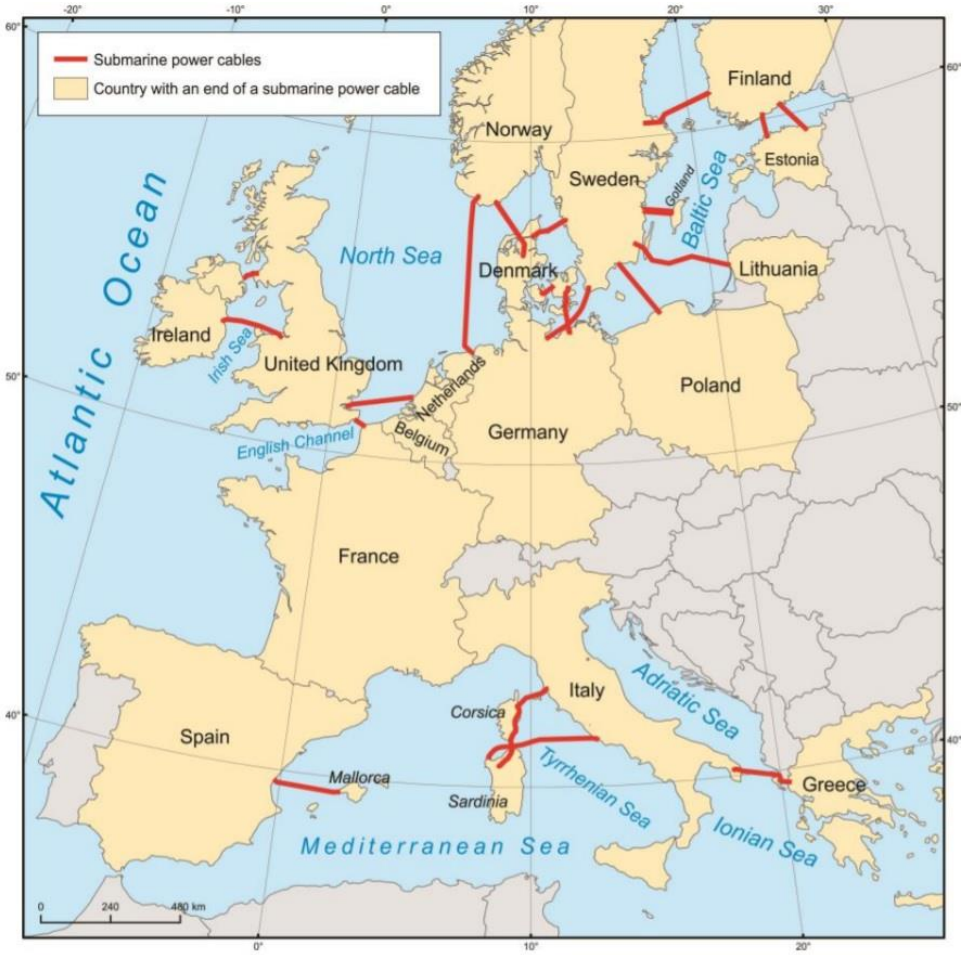

Figure 4.1 Submarine power cables in Europe [adapted from 53]

Most of the transmission power cables at the moment are laid in rather shallow waters, i.e., at less than 500 m depth. Only three cables go beneath this depth: HVDC Italy-Greece (1000 m), Cometa HVDC (1485 m) and SA.PE. I. (1650 m), which is the deepest in the world. The two deepest ones were both produced by Prysmian and are of mass impregnated (MI) paper type. [53]

In water environments special attention must be paid to hydrostatic pressure exerted by the water column, which might become an important factor both in projecting the materials used and in maneuvering methods for laying or repairing the cable. The pressure increases steadily with depth adding around one atmosphere at each 10 m depth (table 4.1) [53]. Although the cable sheath is built to resist to high mechanical stress and maneuvers, special attention is paid when manufacturing segments for deep waters. This is important during cable installation when high tensile forces are applied to cables laid in deep waters. As a recommended in [54] the components in the cable cross section must be able to withstand to a pressure not smaller than 3.5 MPa or the pressure corresponding to the maximum water depth multiplied by a

factor of 1.25. The casings for cable joints must be able to resist at least to 3.5 MPa or to the pressure corresponding to the maximum water depth multiplied by a factor of 1.5.

Depth (m)	Pressure (atm)	Pressure (MPa)
1	1.1	0.11
10	1.99	0.2
100	10.92	1.1
200	20.48	2.11
500	50.6	5.12
1000	100.2	10.15
1500	149.8	15.17
2000	199.4	20.2
3000	298.61	30.25
5000	497.02	50.36
10000	993.04	100.62

Table 4.1 Water column pressure at different depths Depth

4.2.1 Requirements and manufacturers

The submarine environment imposes some basic requirements to power cables that run through it:

- long continuous lengths
- high level of reliability with practical absence of expected faults
- good abrasion and corrosion resistance
- mechanical resistance to withstand all laying and embedment stresses
- minimized environmental impact
- minimized water penetration in case of cable damage

There are many companies producing power cables in the world but just few of them have experience in manufacturing submarine power cables for long distances and high capacity. ABB, Alcatel, Prysmian and Nexans manufactured most of the existing submarine power cables in the world. The latter two have also specialized vessels that allow them to install the cables at sea.

Prysmian is an Italy-based multinational company headquartered in Milan. Its main factory Arco Felice is in Naples, Italy. It holds also the "Giulio Verne" vessel, which was specially built and equipped for laying power cables at sea.

Nexans is a French cable manufacture company headquartered in Paris. The submarine power cable factory is in Halden, Norway. Nexans lays down the cables at sea with its purpose-built vessel Skagerrak.

4.2.2 Voltage and capacity

Electricity transfer over long distances and for high power is made at high or very high voltages. By increasing the voltage, the losses become lower and the capacity of the line increases. Over the years the voltage has gradually increased from 100-250 kV for the first commercial power cables in the '50s-'70s to 300-400 kV ten years later [53]. Most of the newer submarine power cables in the world operate at 450-500 kV. Prysmian and Siemens are currently constructing the first submarine HVDC link with a voltage of 600 kV, i.e., the highest in the world between Wales and Scotland (UK Western Link).

4.2.3 Joints

It is preferable that submarine power cables consist of a minimum number of segments, ideally one. While for shorter cables this is possible, for longer ones more segment must be linked together into a longer piece. The segments are connected by using joints which are pieces of equipment that ensure the conductors, sheaths and armors on both parts are properly in contact. Figure 4.2 shows a sketch of a cable joint.

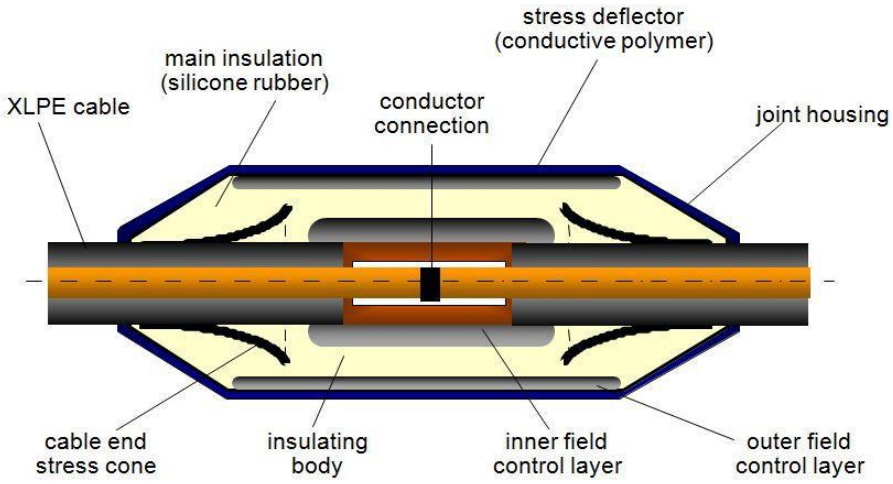

Figure 4.2 Sketch of a cable joint (Source: campbellwhite.com)

Joints can be rigid or flexible depending on the local environmental conditions.

4.2.4 Cable structure, materials, and properties

The structure of the cable must ensure a high efficiency in electrical transmission, a good insulation and magnetic shielding along with a strong mechanical resistance. The structure may differ in materials and layout depending on manufacturers and environmental conditions.

The cables' structure includes a set of layers around the conductor, mainly copper to ensure the physical insulation, impermeability, mechanical strength but also flexibility and electrical and magnetic shielding.

HVDC submarine cables consist of one primary conductor by which the current is transmitted, and a return path represented by another conductor or via seawater using an anode/cathode. In HVAC cables the current is transmitted using three conductors.

The conductors must be insulated against any external contact for the whole length of the cable. There are three main solutions for insulation that are widely used:

- Self-contained fluid-filled cables
    - SCFF/SCOF (self-contained fluid-filled / self-contained oil-filled)
    - HPFF/HPOF (high-pressure fluid-filled / high-pressure oil-filled
    - HPGF (high-pressure gas filled) and GC (gas compression)
- Paper insulated (lapped insulated) cables
    - MI (mass-impregnated) or PILC (paper-insulated lead-covered); it consists of mass
    - PPL (paper polypropylene laminate)
- Extruded cables
    - EPR (ethylene propylene rubber)
    - PE (polyethylene)
    - XLPE (cross-linked polyethylene); it consists of a network molecular structure suited for high temperatures

Self-contained fluid-filled cables which is shown in figure 4.3 are used for very high voltages, usually up to 500 kV. They are suited for conditions where there are no hydraulic limitations and for short distances.

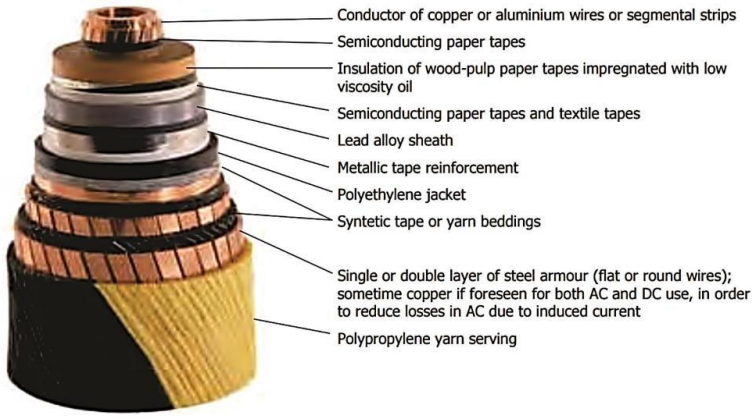

Figure 4.3 The structure of a self-contained fluid-filled cable [adapted from 53]

Mass-impregnated cables which shown in figure 4.4 are the most used since they have proved to be highly reliable for more than 40 years since they are in use. They are used up to 500 kV and operate up to a maximum temperature of 55 °C. With the new PPL insulation, the cable can safely operate at 85° C and a voltage up to 600 kV.

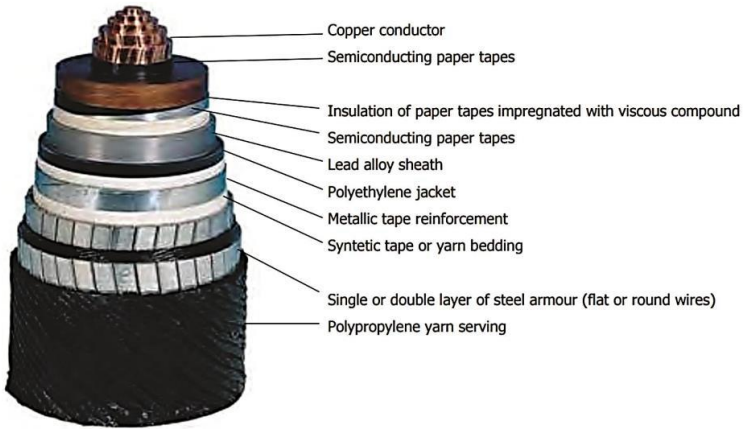

Figure 4.4 The structure of a mass-impregnated cable [adapted from 53]

Extruded cables which shown in figure 4.5 are used for voltages up to 300 kV but the technology improves quickly. They are associated with Voltage Source Converters (VSC), which permit to reverse power flow without reversing the polarity. Tests have demonstrated that for the moment the maximum transmissible power for VSC with extruded cables is up to 800 MW. The drawback is that there are issues with uneven distribution of charges inside the insulation which in the case of rapid polarity reversals can cause localized high stress which results in accelerated ageing of the insulation. Their advantages are related to their weight (20-35 kg/m), which make them very competitive with the other types.

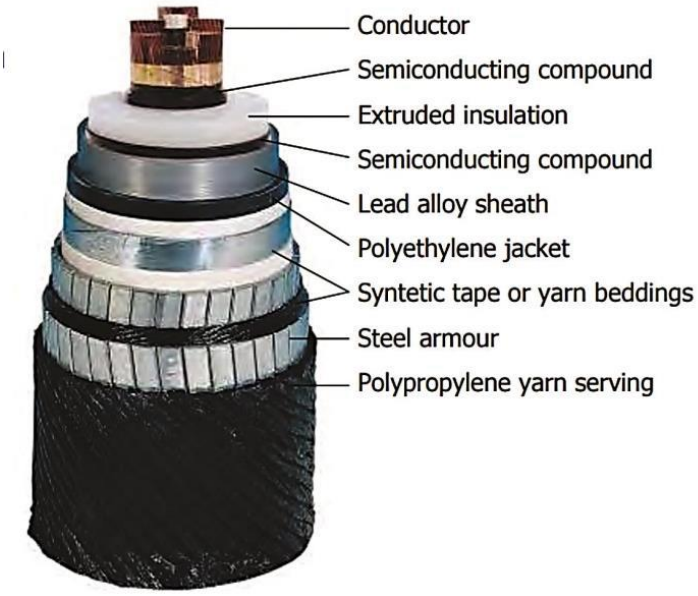

Figure 4.5 The structure of an extruded cable [adapted from 53]

Mass-impregnated and extruded types have been mostly used during last years as cable insulation in space confined environments.

4.3 Marine Power Cable Design Criteria

There are numerous different designs and configurations for subsea power cables, however, a typical marine power cable as shown in figure 4.6 [54] can be considered to consist of the following seven layers.

1. Conductor core:

this consists of wires made from either copper or aluminum that carry the electric current.

2. Electrical insulation:

this is achieved by using three different design/material types: traditional oil-impregnated paper, cross-linked polyethylene (XLPE), or ethylene propylene rubber (EPR). XLPE and EPR have better mechanical/ dielectric characteristics than oil-impregnated paper and are hence the most commonly used.

3. Screen:

this is a semiconducting layer of paper/extruded polymer around the core that minimizes electric field strength and avoids field concentration zones.

4. Sheath:

a metallic sheath is applied around the core that acts as a water barrier and protects the cable against fault currents.

5. Armature:

the entire cable is surrounded by a metallic armature (usually galvanized steel wires) to provide the necessary mechanical strength and impact protection.

6. Optic fiber:

numerous fiber optic cables may be used for data transmission and monitoring purposes.

7. Protecting sheath:

the outer layer consists of polypropylene for abrasion resistance.

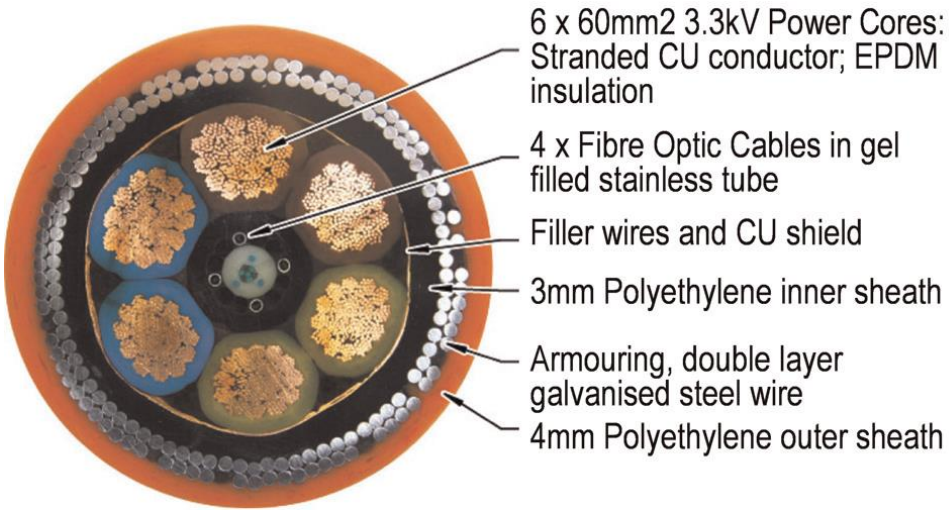

Figure 4.6 Example of HVAC (3.3 kV) subsea power umbilical [adapted from 54].

It is further important to note that manufacturers usually tailor the subsea cable to the application at hand, i.e., there is no such thing as a standardized cable. The subsea geometry of the cable can vary depending on the water depth and loading regimes [55]. Some standard configurations are shown in figure 4.7.

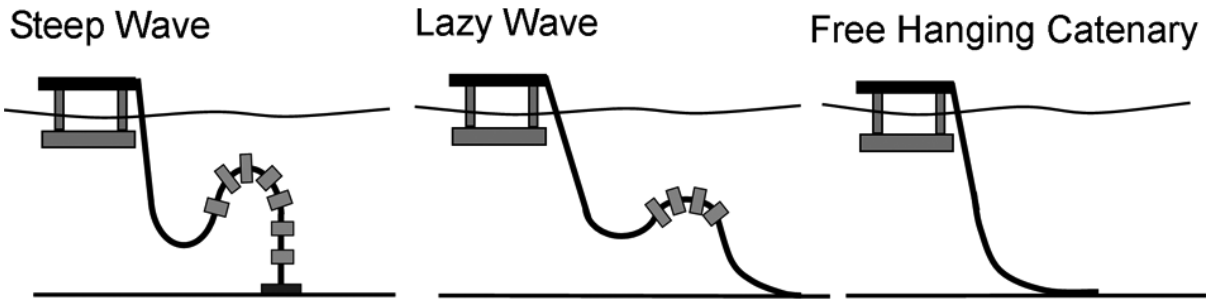

Figure 4.7 Standard flexible riser configurations for floating offshore structures [adapted from 55]

4.4 Offshore Wind Farm Layout

Offshore wind farms consist of arrays of turbines linked together. The energy produced by the farm is collected within this array of turbines and transported to a grid connection point where the electricity is handed over to the integrated public grid in the shore. A typical layout is shown in figure 4.8 [56].

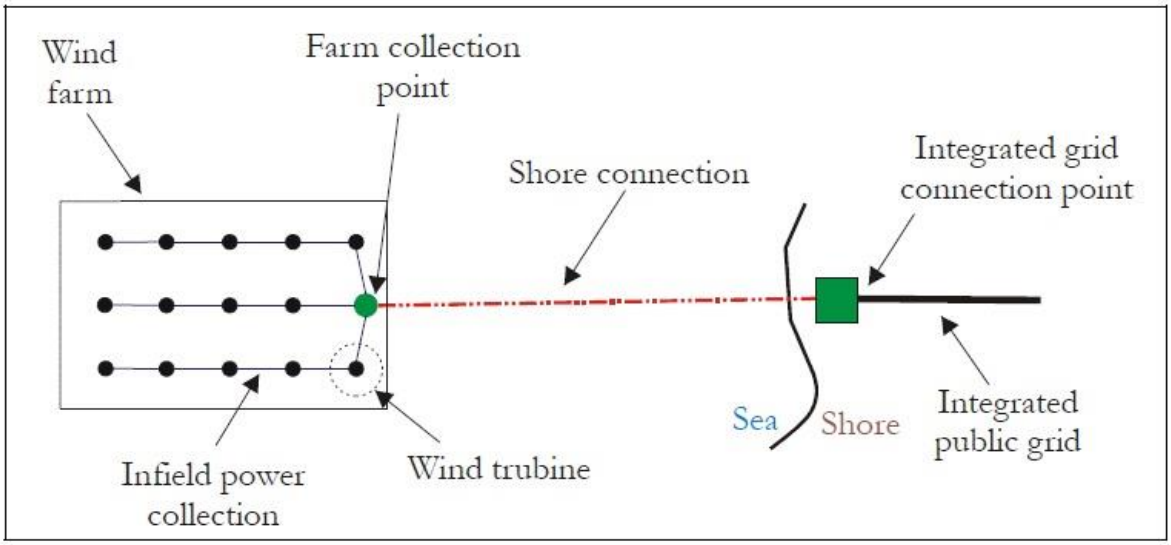

Figure 4.8 Schematic of Offshore Wind Farm [adapted from 56]

An offshore wind farm involves numerous cable connections, most of them for the infield power collection. These connections have impact on the annual produced power, the operation, the reliability, and the installation of the wind farm. The concept of offshore wind farms is relatively new, many of its aspects are yet to be optimized in order to guarantee a successful future. Construction is mostly done with knowledge and expertise of the offshore oil industry but connecting a huge number of single

turbines is a task not similar done in recent offshore operations and therefore only little knowledge about the implications of different set-ups is existent.

4.4.1 Development of a Dynamic Cable System

While conventional submarine cables are installed or secured on the seabed, the cables for floating offshore wind power generation facilities have floating components to enable them to move with the floater, Figure 4.9 shows a typical configuration for FOWT [57]. The cables are continuously subjected to bending and twisting forces, etc., caused by the tidal current and floater behavior, therefore, they are likely to suffer mechanical damage in various sections.

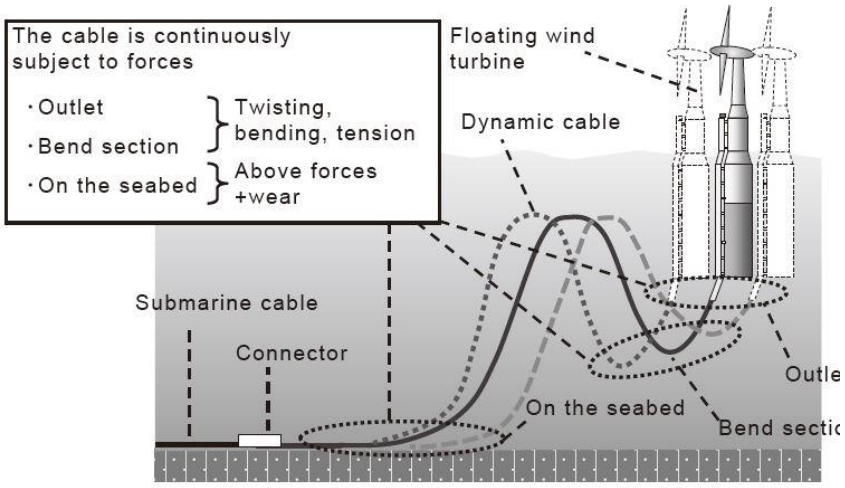

Figure 4.9 Example of cable connection to a floating offshore wind power generation facility [adapted from 57]

4.4.2 Cable Type Used for Modeling

For the simulations of the thesis, a typical array cable with copper conductors has been utilized. The model assumes extruded XLPE isolators and a single layer of galvanized steel armor wires. Values of non-linear bending stiffness has been assumed based on comparable cables. Cross section of the cable is shown on Figure 4.10. The values for the linear and non-linear bend stiffness are plotted in figure 4.11 and the cable layout of the connected power cable is shown in figure 4.12.

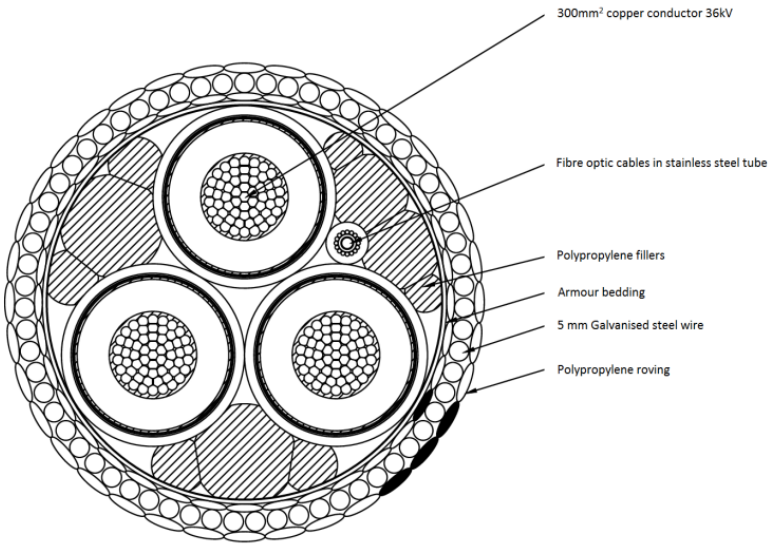

Figure 4.10 Cross section of cable model. [adapted from 58]

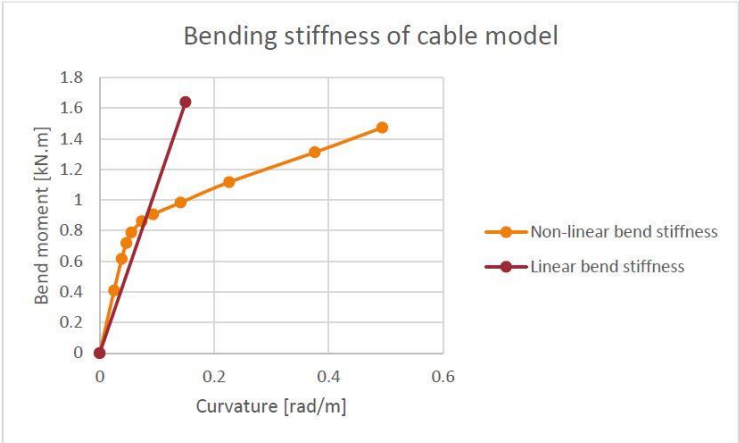

Figure 4.11 Bend stiffness for used cable model [adapted from 58]

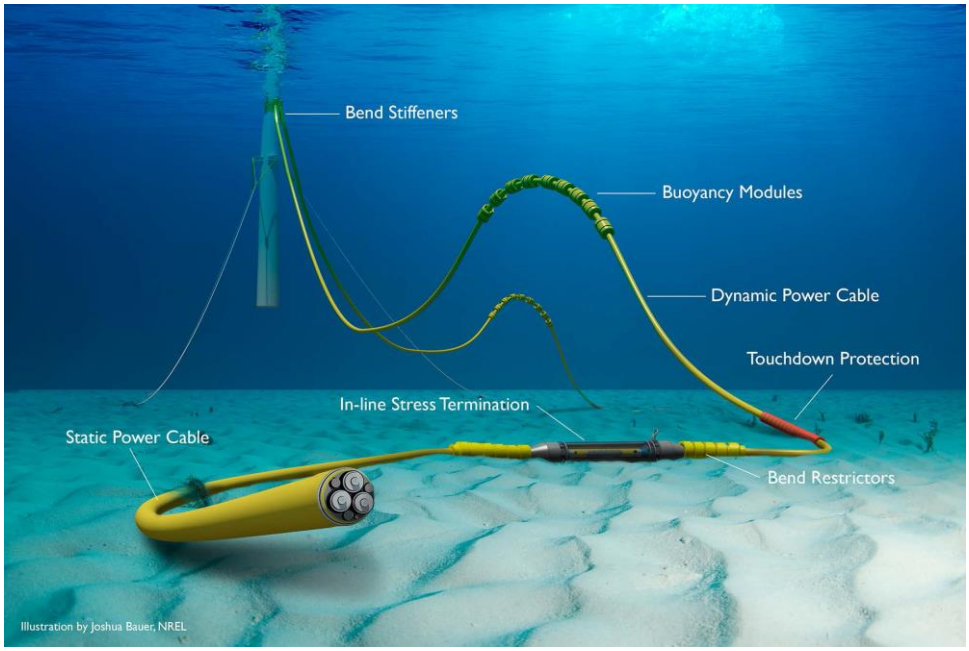

Figure 4.12 connected electrical cable layout

4.5 Fatigue Implementation of Power Cables

As earlier explained, power cables are crucial to a wide variety of applications in both the offshore and onshore industries. They are widely used in electromechanical and communication connections, power transmission lines and electrification of floating oil and gas production systems, where they have to withstand considerable cyclic loads induced by floating body movements in combination with wave and current effects. [58,59]. A relatively new application area for such elements is transmission lines for floating offshore wind turbines (FOWTs) [60]. FOWTs and their mooring systems and connected power cables must withstand various environmental actions. Correlated changes in the wind, current, and wave loads cause variable and uninterrupted dynamic motion and stress in the power cables which are connected to FOWTs each other and/or with the land. The accumulation of variable stress results in cumulative damage to fatigue [61], which for this kind of systems is a weak point in the design panorama, something that, together with other design or operating issues, currently prevent the large-scale installation and diffusion of floating offshore wind farms as a reliable system for energy generation and as an evolution of the currently widely diffused fixed-foundation offshore wind farms.

4.5.1 Fatigue Theory

The increasing demand of safety and reliability brings up the importance of fatigue. Every marine structure built today is designed to last at least 20 – 30 years, so it is self-implied that this subject is thoroughly investigated. For instance, the Hywind Demo is positioned at a location where the weather is not particularly extreme, but it is not necessarily the largest waves produce the highest fatigue-loads. Fatigue is classified on the form in which it occurs: mechanical, creep, thermo mechanical, rolling contact, corrosion, and fretting fatigue. Fatigue can also be classified by the duration of the fatigue life in other words: repeated number of loads. Normally the loads are much lower than the yield stress for the material. These cycles will accumulate and may lead to material failure.

4.5.2 Fatigue Calculation

The relation between the stress Si and number of cycles Ni can be decided from a Stress-Number of Cycles ($S-N$) curve which is defined by Paris's law [62]. The $S-N$ curve is decided with respect to materials and the design of the structure to be analyzed. DNV describes in their rules how much the individual damages can be. Fatigue damage because of varying level of tension bandwidth can be calculated by Miner – Palmgren's hypothesis [62].

$$D = \sum \frac{n_i}{N_i} \qquad \text{Eq 4.1}$$

Where, D is the accumulated fatigue damage on all tension bandwidths, ni is the number of stress ranges with level Si, Ni is the number of stress ranges on level Si which leads to fatigue damage.

For a load scenario with narrow bandwidth the tension bandwidth is almost equal to the double of the tension amplitude. This is a conservative approach which gives bigger calculated fatigue load compared to the actual fatigue.

4.5.2.1 Short Term Fatigue Analysis

Short term fatigue can be calculated from a time domain (TD) analysis or FD (frequency domain). With a stochastic FD analysis, it is possible to calculate the fatigue damage in two different ways, both ways using a stress spectrum found in the actual cross section of the test object. The two different ways are:

- Think of the Gaussian process as a narrow-banded process and then apply the Rayleigh distribution on peaks and stress ranges.

- Generate a stress history from the stress spectrum using FFT (Fast Fourier Transform). This will result in a broad banded Gaussian process. From this the fatigue damage can be calculated by analyzing the stresses by counting the cycles and ranges (normally Rainflow-counting) which will lead to a total fatigue damage result.

From the TD analysis the results can also be analyzed in two different ways:

- Perform a Rainflow-counting, leads to results very fast (advantage of the Rain-flow method is that it does not require too much computational resources).

- Choose a probability distribution where you estimate its parameters based on the load history. Then it is possible to calculate the fatigue damage by integrating the probability density function and the $S-N$ curve.

4.5.2.2 Long Term fatigue Analysis

To perform a long-term fatigue analysis, it is needed to consider all the relevant information connected to environmental and operational conditions, which the structure will experience during its lifetime. It is important to cover the operational aspects such as installation, modification, and repair. The environmental data which the structure is to be designed for is usually based on wave and current statistics. These data can be presented as a frequency distribution of significant wave heights (Hs) and zero up-crossing, peak or average periods.

If the long-term fatigue analysis is performed in the FD (and stochastic linearization is carried out), the transfer function for the response on the structure will be depending on the wave condition. In other words, the transfer function must be established for each wave condition. A way to solve this is to divide all the sea states into blocks. The advantage of this is fewer sea states to iterate, and the computation time will depend on how many blocks the sea states are divided into. When the long-term fatigue analysis is performed this way, it becomes important to select the right size of the iteration blocks [63].

This study performs short term fatigue analysis to get the fatigue damage for each sea states, because long term sea states is composed of short term sea states and it

considering short term fatigue analysis is adequate to follow the purpose of the study in current stage.

4.5.3 Cumulative Damage

As mentioned before, data from a fatigue analysis is normally presented in an $S-N$ diagram. The stress/strain ($\Delta S/\Delta\varepsilon$) range is plotted versus cycles to failure (N). differentiating between low cycle fatigue life and high cycle fatigue life, low cycle range and high cycle range is categorized by:

- Low cycle range is below 105 cycles
- High cycle range is above 105 cycles

The $S-N$ data in the high cycle range tend to follow a log-linear relationship:

$$N(\Delta S)^m = Const \qquad \text{Eq 4.2}$$

When the load cycles occur with constant amplitudes, the $S-N$ diagram will look like this:

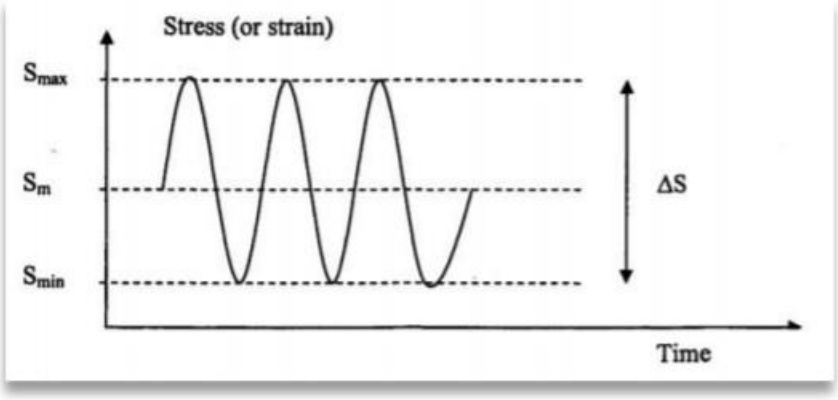

Figure 4.13 Constant amplitude loading [adapted from 64]

4.5.3.1 Characterization of Fatigue Loading

Fatigue is a cumulative process made from a load history. As before mentioned, normal design life time for a typical offshore structure spans up to a period of 20-30 years. When it comes to fatigue loading, typically differentiate the load history to the loading characteristics must applied. In addition to the constant amplitude loading mention it exists [64]:

- Variable amplitude loading/spectrum loading or irregular loading. These three names are used on any type of loading that have non-constant amplitude (most common).
- Block loading; composed of blocks of constant amplitude cycles.
- Random loading/stochastic loading; a variable amplitude loading from a random process

This is an example on how the $S-N$ curve may look like with variable loading:

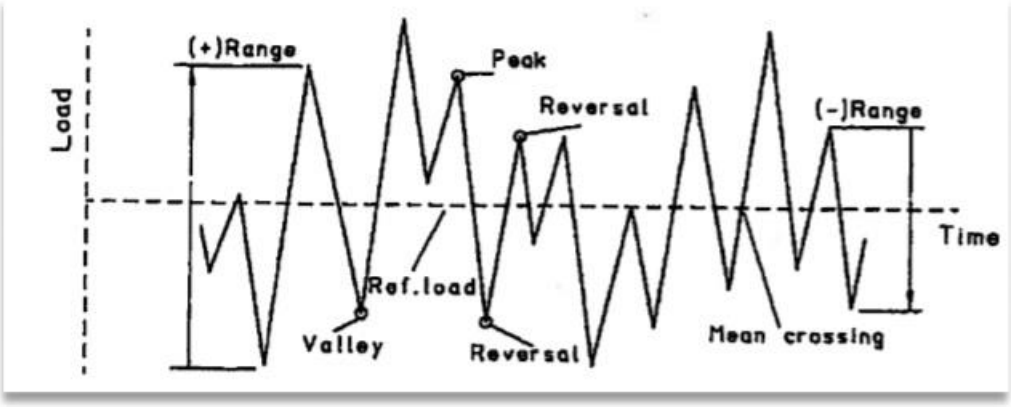

Figure 4.14 Varying loading amplitudes [adapted from 64]

Explanation:

- Peak is the point where the first derivative of the loading/time history changes from positive to negative sign.
- Reversal is the point where the first derivative of the loading/time history changes sign.
- Valley is the point where the first derivative of the loading/time history changes from negative to positive sign.
- Range is the difference between the valley and the peak loading or between a successive peak and valley. Ranges can vary in terms of the definition applied. Overall range is the difference between the highest peak point and the lowest valley point.
- Mean crossings is where the number of times the loading history crosses the mean load level.

Irregularity factor is a measurement of the irregularity on the data, in other words the bandwidth (stress range) of the signal. The bandwidth is defined as the ratio between the positive mean crossings to the number of valleys or peaks in that given load

history. In a fatigue analysis, the mean stresses can normally be neglected, so the mean-crossings are defined as the zero-crossings [64].

4.5.3.2 Cycle Counting

In cumulative damage analysis the stress-time history is broken down into individual cycles, which are summed up to a distribution of the different stress ranges. Various methods of cycle counting exist, each with their own cons and pros. In many cases it is important to use a counting method that physically represents the fatigue process most correct. Cycle counting can be represented by different spectra's:

- Occurrences spectrum is a representation of a variable amplitude loading, by the number of times a specific loading parameter (range, peak, level, etc.) occurs within a set interval. In statistics this is called frequency functions or probability density functions (PDF).
- Exceedances spectrum is a presentation of a spectrum loading situation by the number of times the value equals or exceeds a loading parameter.

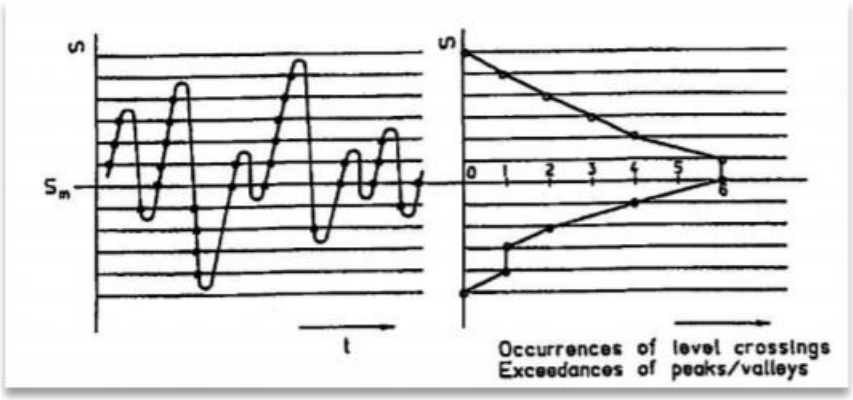

Figure 4.14 Exceedances spectrum [adapted from 64]

Next section describes how it is possible to count the cycles and amplitudes and the different counting methods can achieve different results, at the end by choosing best method, regarding to the modeling how this thesis claims most accurate results for the fatigue analysis.

4.5.3.3 Level Crossing Counting, Peak Counting and Simple Range Counting

Level Crossing Counting

This counting method counts when the value crosses/reaches different levels of load. How many levels the counting is divided into is crucial for this methods accuracy. In order to reduce the counting events by a factor of two, positive-going level-crossings are recorded at and above the mean load and negative-going crossings below the main load. The difference between the counts for two neighboring levels on the positive side of the mean level is equal to the number of peaks in the corresponding interval of stress. But regardless, the occurrences spectrum of the stress levels is the same as the exceedance's spectrum of the peak levels. The main flaw with the level crossing counting method is that there is no information obtained about the irregularity of the load.

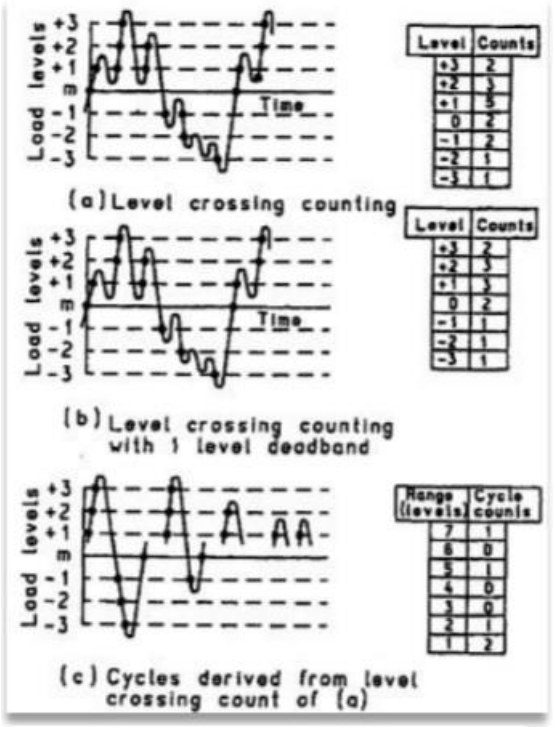

Figure 4.15 Level crossing counting [adapted from 64]

Explanation of the figure:

(a) represents a broad-banded load history. The result from the counting (of (a), without dead band) is presented in (c), while in (b) a dead band has been introduced.

The reason the dead band is introduced is that for many cases the small stresses may be assumed to be non-damaging, so they can be neglected in the counting procedure. A normal method of counting cycles is to construct the largest possible cycle followed by the second largest and so forth until all the level crossings are demonstrated. The reversal points are normally assumed to occur halfway between the levels, and with this method a narrow-band process is represented in a realistic way. However, for a broad banded loading the stress ranges with mean values different from the mean level from the loading will be combined in an unrealistic way. For this process the level count method tends to be a bit conservative.

Peak Counting

All the values above the mean level are counted as a peak, and all values below the mean level are counted as a valley. The peaks and valleys are usually separated from each other in the results. A regular variation of this method is to count all the peaks and valleys without respect to the mean level. The two different peak counting methods are presented below.

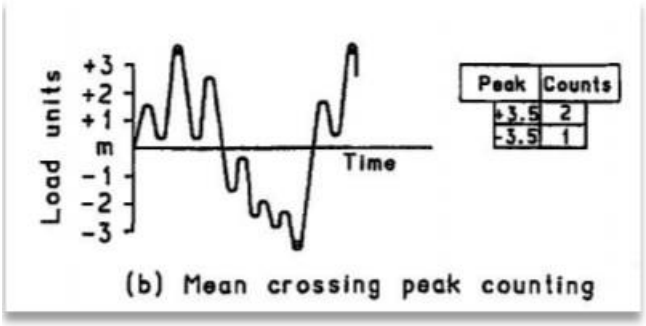

Figure 4.16 Mean crossing peak counting [adapted from 64]

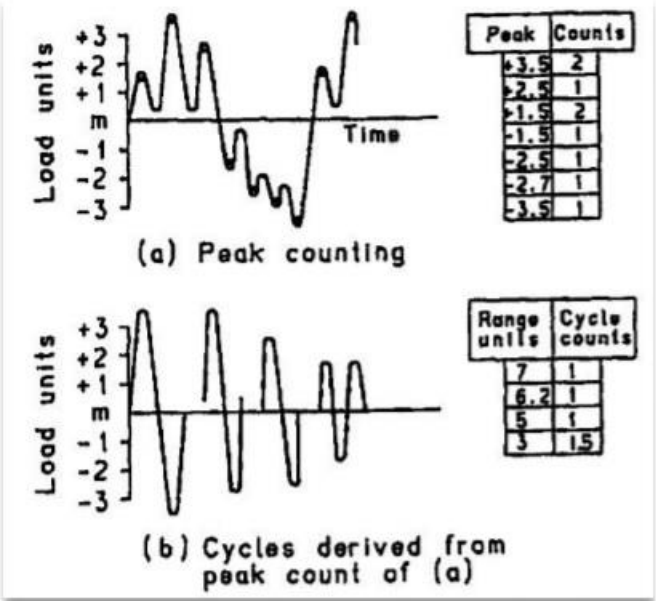

Figure 4.17 Peak counting [adapted from 64]

As with the level counting, the peak counts are combined by constructing the largest possible cycle then then second largest cycle and so forth. This is, as mentioned above a conservative counting method. An alternative to this is to combine pairs of peaks and valleys in a random way.

Simple Range Counting

In this method a range is defined as the stress difference between two reversals. It distinguishes between positive and negative ranges. If the mean of each range is counted the method is called range-mean counting. If only positive ranges are counted, each range is counted as a cycle. When both positive and negative ranges are counted each range is counted as a half-cycle.

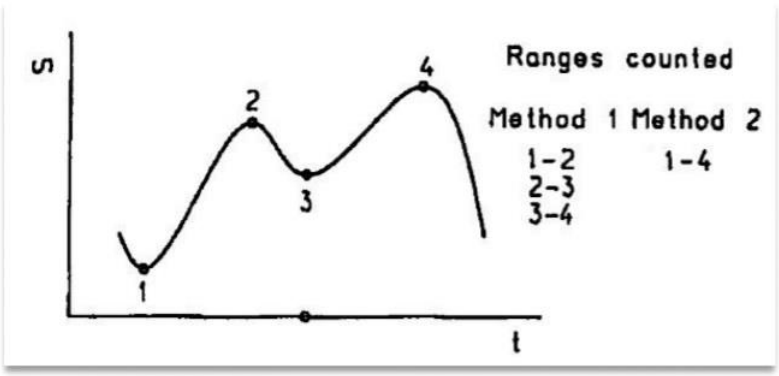

Figure 4.18 Simple range counting [adapted from 64]

A problem with this method is how to take care of the small cycle's in-between the larger cycles. The sequence above can be counted as three individual half cycles or one large half cycle. The final damage summation will depend significantly on the choice of the threshold level for counting small cycles.

4.5.4 Rainflow Counting Algorithm

Rain flow counting itself is used as a common name for a large class of counting methods, such as, range-pair counting, the Hayes method, the original rain-flow method, ordered overall range counting, racetrack counting and hysteresis loop counting. If the load history begins and ends with its maximum peak or minimum valley point, these methods give identical results (number of counts). The original method is used in the analysis of fatigue data in order to reduce the measured statistics into a smaller set of stress reversals. There are multiple methods and algorithms which give the same results, but this is the most popular one.

It is important that this algorithm allows the Miner's rule, in order to evaluate the fatigue life of the structure. The algorithm was created by Tatsou Endo and M. Matsuishi in 1968. [65] For simple periodic loadings rainflow counting is unnecessary, since it can easily be modeled and estimated by a simple application of the $S - N$ curve (given that the stress amplitude is known). This method is well suited for a broad banded load history. The way of performing algorithm is:

- Reduce the time history to a sequence of tensile peaks and compressive troughs.
- Imagining that the time history is a template for a rigid sheet
- Turning the sheet clockwise 90 degrees (earliest time on top)
- Each tensile peak is imagined as a source of water that drips down to the "ground underneath"
- Count the number of half-cycles by looking for terminations in the flow occurring when either:
- It reaches the end of the time history
- It merges with a flow that started at an earlier tensile peak
- It flows opposite a tensile peak of greater magnitude.
- Repeats step 5 for compressive troughs
- Assigns a magnitude to each half-cycle equal to the stress difference between its start and termination time.
- Pair up all the half-cycles of identical magnitude (but opposite sign) to count the number of complete cycles. Typically, there will exist some residual half-cycles

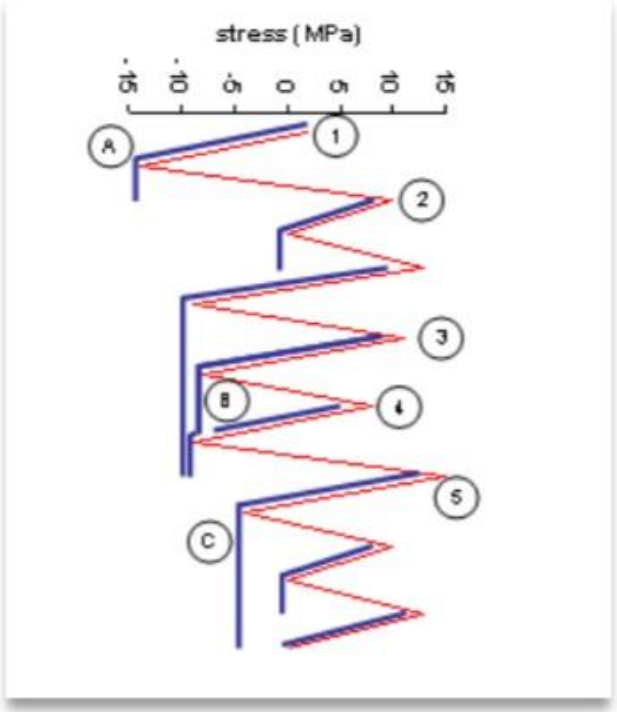

Figure 4.19 Rainflow analysis for tensile peaks [adapted from 64]

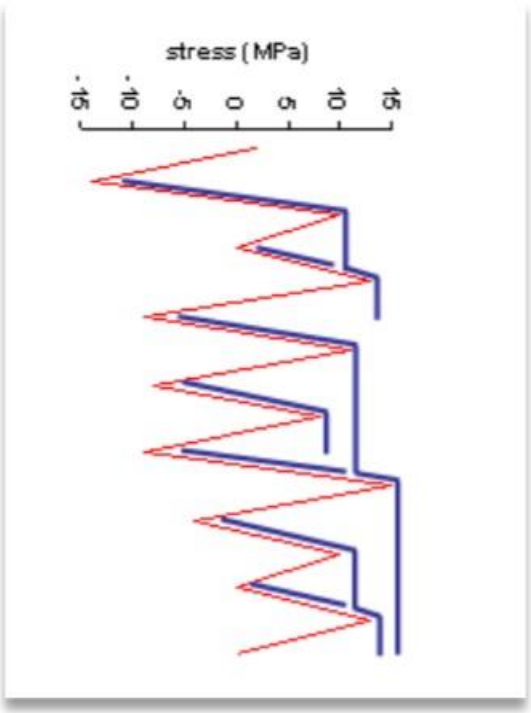

Figure 4.20 Rainflow analysis for compressive troughs [adapted from 64]

The result from using this algorithm will give the user number of cycles at the different amplitudes, as shown on the figure below.

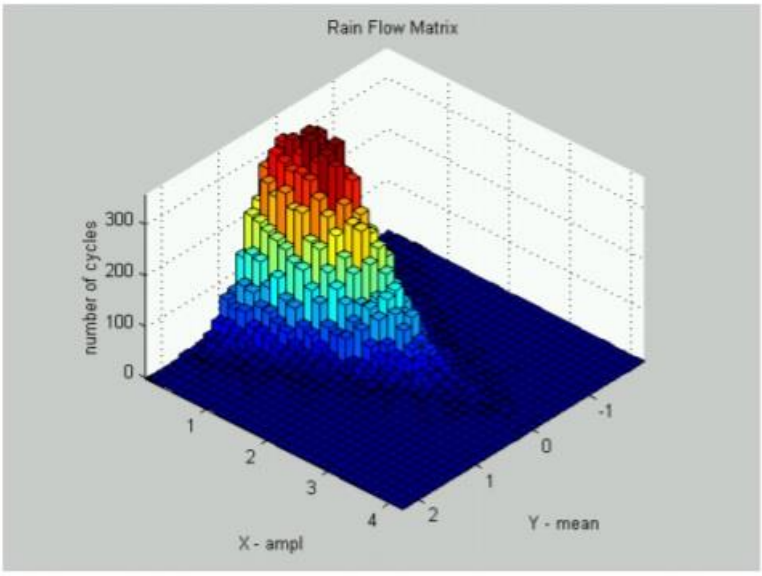

Figure 4.21 Rainflow matrix example result [adapted from 64]

4.6 Analytical Fatigue Damage Calculation

It is possible to perform an analytical fatigue damage assessment, but it requires certain prerequisites. However, when these are met this method is way faster than counting methods discussed previously in this thesis. The analytical formula is derived as follows: As described earlier the total damage can be calculated with the Miner – Palmgren's hypothesis:

$$D = \sum \frac{n_i}{N_i} \qquad \text{Eq 4.1}$$

If the size of each block is reduced the expression can be written as:

$$D = \int_0^\infty \frac{d_n}{N} \qquad \text{Eq 4.3}$$

Expected damage can be found by the integral:

$$E(D) = \int_0^\infty \frac{1}{N} E d_n \qquad \text{Eq 4.4}$$

Where E dn is expected number of stress ranges given by:

$$Ed_n = f_s(s)d_s * N_{tot} \quad \text{Eq 4.5}$$

Where:

$f_s(s)$ is the probability density function for specific stress range. If the long term distribution can be described as a Weibull distribution (2-parameter), the closed form expression for fatigue damage can be written as:

$$E(D) = \frac{N_{tot}}{K}\lambda^m \tau\,(\frac{m}{\beta} + 1) \quad \text{Eq 4.6}$$

Where:

- $Ntot$ is total number of stress cycles in the time history
- τ is the gamma function
- λ, β are parameters in the Weibull distribution
- K, m are parameters from $S - N$ curve

If the stress ranges are Rayleigh distributed, the closed form solution for expected damage:

$$E(D) = \frac{N_{tot}}{K}(2\sqrt{2} * \sigma)^m \tau\,(\frac{m}{\beta} + 1) \quad \text{Eq 4.6}$$

Where:

- Σ is the standard deviation to the stress process
- σ is the stress

The main criteria for using these two formulas are that the stress process is narrow-banded. Furthermore, the two expressions can only be used if the $S - N$ curve has a constant slope and no fatigue limit. In other words, the $S - N$ curves equation is valid for all positive values of the stress range.

If the $S - N$ curve has a fatigue limit, all the stress ranges below this limit will not contribute to the fatigue damage.

4.6.1 Fatigue Limit States

The basis of the DNV fatigue [61] design is the $S - N$ curve and cumulative damage. The $S - N$ curve is usually based on fatigue tests in the laboratory. For best interpretation of the $S - N$ curves from the fatigue tests, the fatigue failure is defined

to have occurred when a fatigue crack has grown through the thickness of the structure or structural component. The characteristic $S-N$ curve shall in general be taken as the curve that corresponds to 2.3% quantile of N given S, for example the $S-N$ curve that provides 97.7% probability of survival. The design fatigue life for all the structural components (like the anchor pin joints and all the connection parts for the mooring line system, also for the electrical cables) should be based on the specified service life of the structure. As earlier mentioned, common rule is to design it for 20 years. The fatigue analysis shall be carried out for each individual member subjected fatigue load. Critical parts are to be analyzed more detailed to ensure correct data.

Chapter 5: Modeling

5.1 Introduction

The current chapter presents procedure of the modeling the FOWT and connected power cable using both codes by investigating their advantages and disadvantages, furthermore, the procedure presented by a flowchart, which step by step explains modeling phase. In addition, fatigue life assessment of the power cable using in-house developed code has been studied. Furthermore, the current chapter provides properties of used baseline FOWT.

5.2 Modeling

In the modeling iteration, a variety of different types of software were used, as well as some self-made post-processing code and support code for the generation of the necessary input files for the simulations. The flowchart shown in figure 5.1 provides a description of the method of the modeling section step by step.

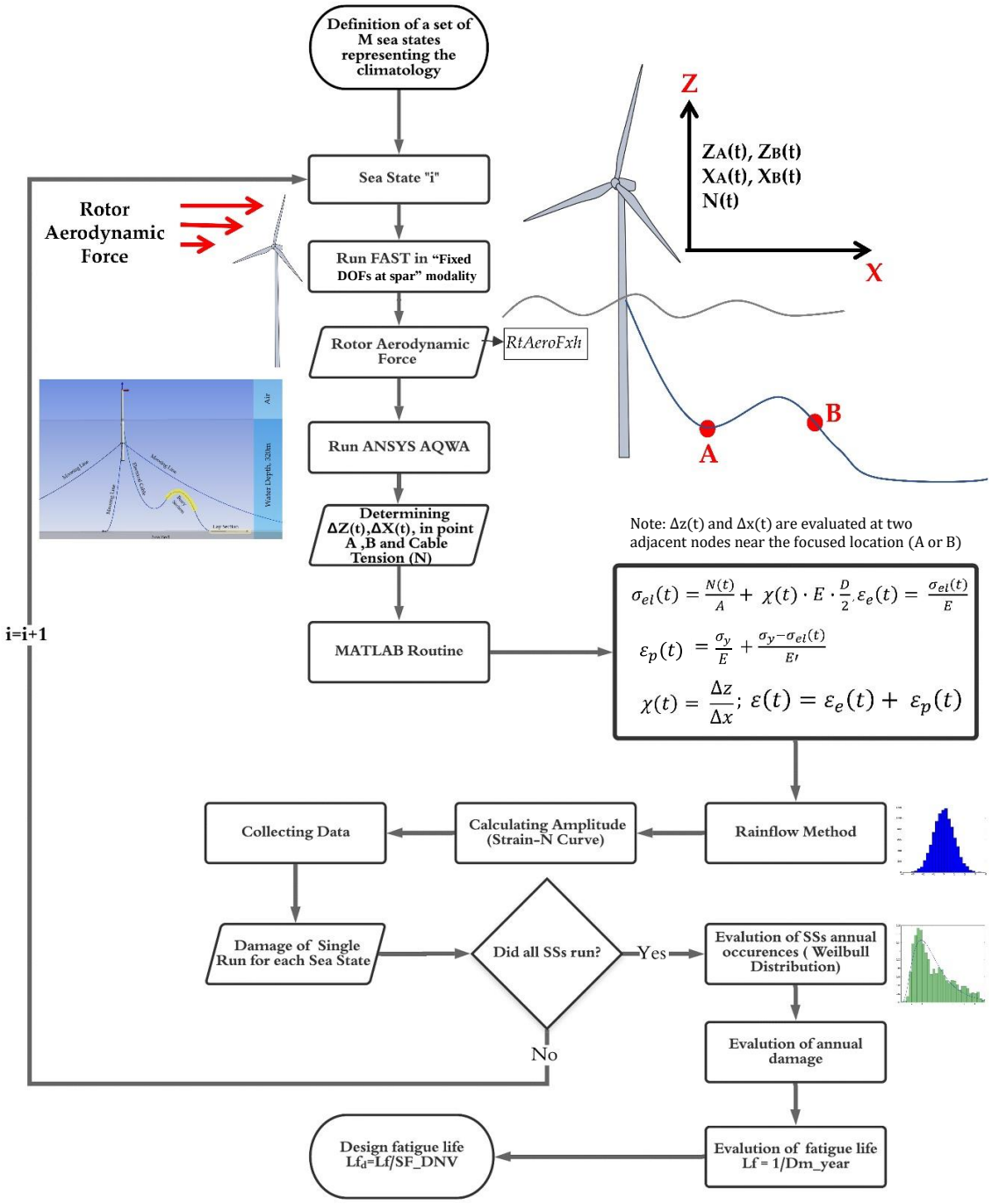

Figure 5.1 Analysis Flowchart

The NREL 5 MW wind turbine on the OC3-Hywind spar-buoy FOWT was chosen as a case study for modeling dynamic response of the floating platform and evaluation of the fatigue life of an inter-array turbine (umbilical) cable. This case study was chosen for its simplicity in design, sustainability for modeling and the existence of numerical results in the literature.

For dynamic modeling of NREL 5 MW FOWT, OpenFAST open-source code is used to find dynamic response of the floating platform in 6 degrees of freedom (sway, surge, heave, pitch, roll and yaw) and then floating platform including electrical cable is modeled using ANSYS AQWA (academic version) and dynamic response of the platform and connected electrical cable is calculated. At the end fatigue life of the electrical cable in several sea states is estimated.

5.2.1 NREL Offshore 5 MW Wind Turbine Properties

The requirements of the offshore 5-MW baseline wind turbine of NREL are described in this section and the justification behind its design. As earlier explained, to have a cost-effective wind system in deep-water environment, because of the significant portion of system costs in the support structure of a deep-water wind system, it is necessary that each individual wind turbine must be rated at 5 MW or higher.

Figure 5.2 shows NREL 5-MW spar buoy floating offshore wind turbine schematic, which is modelled to analysis of the aerodynamic, hydrodynamic, and structural response of the FOWT both OpenFAST and ANSYS AQWA software.

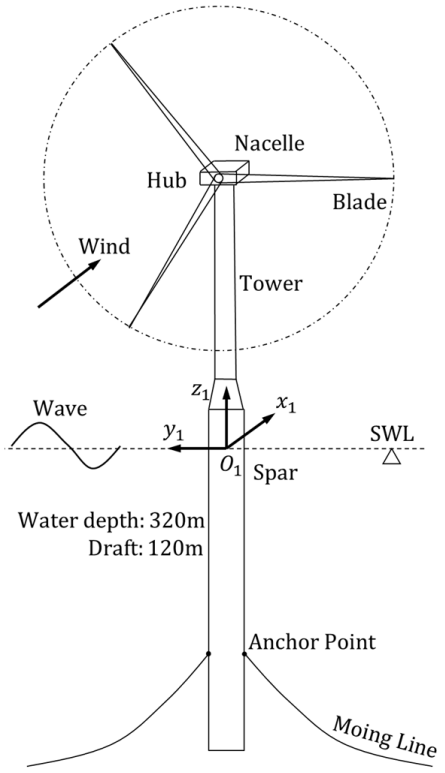

Figure 5.2 Spar Buoy FOWT scheme

The gross properties of NREL 5-MW baseline wind turbine are given at the table 5.1 [49]. The (x, y, z) coordinates of the wind turbine 's overall center of mass (CM) location are indicated in the tower-base coordinate system, which originates at ground or mean sea level (MSL) along the centerline of the tower. The x-axis is oriented nominally downwind from this coordinate scheme, the y-axis is oriented transverse to the nominal wind direction, and the z-axis is directed vertically from the base of the tower to the yaw bearing.

Rating	5 MW
Rotor Orientation, Configuration	Upwind, 3 Blades
Control	Variable Speed, Collective Pitch
Drivetrain	High Speed, Multiple-Stage Gearbox
Rotor, Hub Diameter	126 m, 3 m
Hub Height	90 m
Cut-In, Rated, Cut-Out Wind Speed	3 m/s, 11.4 m/s, 25 m/s
Cut-In, Rated Rotor Speed	6.9 rpm, 12.1 rpm
Rated Tip Speed	80 m/s
Overhang, Shaft Tilt, Precone	5 m, 5º, 2.5º
Rotor Mass	110,000 kg
Nacelle Mass	240,000 kg
Tower Mass	347,460 kg
Coordinate Location of Overall CM	(-0.2 m, 0.0 m, 64.0 m)

Table 5.1 Gross Properties Chosen for the NREL 5-MW Baseline Wind Turbine

5.2.2 Floating Structure

To carry on the analysis, the Hywind platform that was developed to support a 5-MW wind turbine, as analyzed in [49,66,67] was chosen. The NREL 5-MW turbine 's rotor-nacelle assembly, including aerodynamic and structural properties, remained the same as in [49], but the support structure (tower and substructure) and properties of the control system were altered. The new system is known as the 'OC3-Hywind' system.[49]

As seen in figure 5.3, the OC3-Hywind device features a strongly drafted, slender spar buoy with catenary mooring lines.

Figure 5.2 OC3 Hywind FOWT [adapted from 49]

Structural properties, hydrodynamic properties and mooring line properties of the system are shown at the tables 2,3,4.; the concept is documented in much greater detail in [49].

Description	Unit
Gravitational acceleration (m/s^2)	9.80665
Hub mass (kg)	56780
Hub inertia about rotor axis [3 blades] or teeter axis [2 blades] (kg m^2)	115926
Generator inertia about HSS (kg m^2)	534.116
Nacelle mass (kg)	240000
Nacelle inertia about yaw axis (kg m^2)	2.60789E+06
Yaw bearing mass (kg)	0
Platform mass (kg)	7.46633E+06
Platform inertia for roll tilt rotation about the platform CM (kg m^2)	4.22923E+09
Platform inertia for pitch tilt rotation about the platform CM (kg m^2)	4.22923E+09

Platform inertia for yaw rotation about the platform CM (kg m^2)	1.6423E+08

Table 5.2 Structural properties

Description	Unit
Water density (kg/m^3)	1025
Water depth (meters)	320
Displaced volume of water when the platform is in its undisplaced position (m^3)	8029.21
Incident wave kinematics model	Regular
Analysis time for incident wave calculations (s)	3630
Time step for incident wave calculations	0.25
Significant wave height of incident waves (meters)	6
Peak-spectral period of incident waves	10
Range of wave directions(degrees)	90
Wave Type	Stokes 2nd-order wave theory
Low frequency cutoff used in the summation-frequencies (rad/s)	0.1
High frequency cutoff used in the summation-frequencies (rad/s)	1.9132
Current profile model	No Current
Analysis time for wave (s)	2000
Time step for wave (s)	0.0125
Additional Linear Damping in Surge N/(m/s)	100,000
Additional Linear Damping in Sway N/(m/s)	100,000
Additional Linear Damping in Heave N/(m/s)	130,000
Additional Linear Damping in Yaw Nm(rad/s)	13,000,000

Table 5.3 Hydrodynamic properties

Description	Unit
the mass per unit length of the line (kg/m)	77.7066
the line stiffness, product of elasticity modulus and cross-sectional area (N)	384.243E6
Diameter (m)	0.09

Table 5.4 Mooring system properties

5.3 Modeling in FAST

The modules of FAST (AeroDyn, HydroDyn, etc.) correspond to different physical domains of the coupled aero-hydro-servo-elastic solution, most of which are separated by spatial boundaries.

Figure 5.3 shows the control volumes associated with each module for floating offshore wind turbines [3].

All simulation in this thesis carried out by considering the aerodynamics, hydrodynamics and structural part of the analysis, regarding this matter, power generation and all electrical parts of the rotor and other modules (which are shown at figure 5.3) are not considered in the modeling, nor in the calculation.

As shown in the figure 5.3, first part of the modeling is investigating of the external condition, for implementing this issue, InflowWind [68] module was used for wind-inflow calculation. For claiming hydrodynamic response of the structure, Hydrodyn [69] module was used to model waves and currents effects.

Second part of the modeling is investigating of the applied loads. To get aerodynamic response of the structure, AeroDyn [70] was used to get aerodynamic response of the structure. Again, using HydroDyn, hydrodynamic responses of the structure were calculated.

At the end MoorDyn [71] was used to get mooring lines dynamic responses.

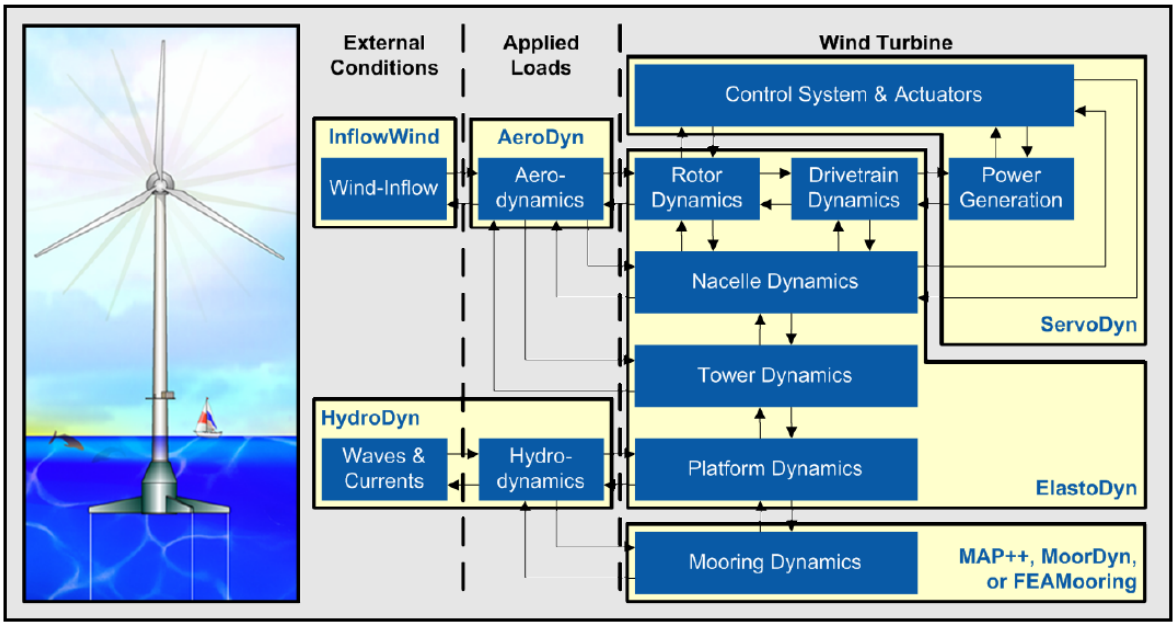

Figure 5.3 control volumes for FAST [adapted from 3]

5.3.1 Modules of FAST

As before mentioned, this thesis claims different modules of FAST to model the FOWT and run analysis to get dynamic responses of the structure. First of all, using InflowWind module, wind data are generated for different environmental conditions.

InflowWind is a wind-inflow processing module that has been combined with the multi-physics engineering tool FAST to enable aero-elastic simulation of horizontal-axis wind turbines.

InflowWind derives the coordinate location of multiple points at each time step from the driver code (either the standalone driver or the FAST glue code) and InflowWind returns the undisturbed wind-inflow velocities at these positions. In the module, there are no states, each part of the wind velocity is determined as a function of the positions of the input coordinates and internal time-varying parameters, unaffected by the wind turbine interaction.

AeroDyn is a time-domain aerodynamics module for wind turbines that has been coupled to the FAST to enable aero-elastic simulation of horizontal-axis wind turbines. When coupled to FAST, AeroDyn can also be linearized as part of the linearization of the full coupled solution.

AeroDyn 's aerodynamic equations are based on the principles of actuator lines, where local two-dimensional (2D) flow at cross sections approximates the three-dimensional (3D) flow around a structure, and the transmitted pressure and shear stresses are approximated by lift forces, drag forces, and pitching moments lumped in a 2D cross-section at a node. The analysis nodes are distributed along the length of each blade and tower, the 2D forces and moment are measured as distributed loads per unit length at each node, and the overall aerodynamic loads of 3D are identified by combining the distributed loads of 2D along the length.

The discretization of the blade and tower analysis nodes can be separate from the discretization of the nodes of the structural modules when AeroDyn is coupled to FAST. The actuator line approximations limit the model's relevance to slender structures and 3D behavior is either ignored or captured by model-inherent corrections. AeroDyn assumes that atop a single tower, the wind turbine geometry consists of a one-, two-, or three-bladed rotor. If the undeflected tower is considered to be straight and vertical, out-of-plane curvature and in-plane sweep can be taken into account by an undeflected blade. For blades, the out-of-plane curvature may be accompanied by the 2D cross sections where the aerodynamic study takes place, but in-plane sweep is believed to be done by shearing rather than rotating the 2D cross section. Using geometrical variations between each blade, aerodynamic imbalances are possible.

HydroDyn is a hydrodynamics time-domain module that has been coupled to the FAST to allow aero-hydro-servo-elastic simulation of offshore wind turbines. For both fixed-bottom and floating offshore substructures, HydroDyn is applicable.

To measure the hydrodynamic loads on a structure, HydroDyn allows several approaches: a potential-flow theory solution, a strip theory solution, or a hybrid combination of the two. Internally generated waves can be regular (periodic) or irregular (stochastic) and long-crested (unidirectional) or short-crested (with wave energy distributed across a number of directions) within HydroDyn. In HydroDyn, wave elevations or full wave kinematics may also be generated externally and used. Internally, using first-order (linear Airy) or first-plus second-order wave theory. HydroDyn produces waves analytically for finite depth with the option to incorporate lateral spreading, but wave kinematics are only computed in the domain between the flat seabed and still-water level and no wave stretching or higher order wave theories are used. Time-domain calculations of difference- (mean- and slow-drift-) and sum-frequency terms provide the second-order hydrodynamic implementations. Fast

Fourier Transforms (FFTs) are used in the summation of all wave frequency components to minimize computing cost.

HydroDyn receives the position, direction, velocities, and accelerations of the (rigid or flexible) substructure at each coupling time stage when HydroDyn is coupled to FAST, and then calculates the hydrodynamic loads and returns them to FAST. At this stage, for a floating platform, FAST's ElastoDyn structural-dynamics module assumes that the substructure (floating platform) is a rigid body of six degrees of freedom.

Internal axial stiffness and damping forces, weight and buoyancy forces, Morison equation hydrodynamic forces, and vertical spring-damper forces from interaction with the seabed are accounted for in the model. The formulation supports the use of wave kinematics in hydrodynamic force measurements, but in the absence of a consistent procedure for obtaining wave kinematics data in coupled simulations, the feature is currently disabled. Hydrodynamic loads can ultimately be controlled externally in the FAST by combining with HydroDyn.

5.3.2 Environmental conditions and considered sea states

As earlier mentioned, because of covering the operational range of 5 MW NREL wind turbine the sea states (SS) conditions are selected from the South China Sea S4 area, which wind velocities are between 5 m/s to 25 m/s. Table 5.5 shows selected sea states properties for the analysis.

As described before, wind turbines are typically designed for 20-25 years [72], Under average wind conditions, the wind turbine can generate 4,000-7,000 hours of electricity per year, equivalent to 70-80% of the total hours of the year. [73] On the above basis an average number of 15 windy hours each day for a total of 365 days during the year (5475 hours per year) is considered in evaluating the occurrences of the SSs.

SS	U_{10} (m/s)	U(H) (m/s)	Hs (m)	T (s)	Cv (m/s)	P (%)
1	5.6	7.279722555	0.675	4	0.168	2.24096
2	6	7.799702738	0.675	5	0.180	8.68372
3	7	9.099653194	1.050	4	0.210	1.96084
4	7.80	10.13961356	1.050	6	0.234	14.006
5	8.5	11.04957888	1.550	4	0.255	1.4006
6	9	11.69955411	1.550	5	0.270	10.36444
7	9.40	12.21953429	1.550	7	0.282	20.16864
8	10.8	14.03946493	2.175	5	0.324	5.32228
9	11.2	14.55944511	2.175	7	0.336	15.4066
10	12	15.59940548	2.875	6	0.360	8.96384

11	13.2	17.15934602	3.625	6	0.396	3.08132
12	14.5	18.84928162	4.000	6	0.432	0.56024
13	15.0	19.49925684	4.500	7	0.450	3.64156
14	16.1	20.92920235	5.000	7	0.483	0.84036
15	16.7	21.70917262	4.500	10	0.501	0.84036
16	17.2	22.35914785	4.500	11	0.516	0.28012
17	17.4	22.61913794	5.500	10	0.522	0.56024
18	18	23.39910821	5.500	11	0.540	0.56024
19	19.1	24.82905372	6.750	10	0.573	0.84020
20	20	25.99900913	3.625	12	0.600	0.280
		Sum of Probability				100

Table 5.5 shows environmental conditions used for simulations.

5.4 ANSYS AQWA

As mentioned earlier, ANSYS AQWA software is a suite of tools for engineering analysis to investigate the effects of waves, winds and currents on floating and stationary offshore and underwater installations, including spars, semi-submersibles, and tension leg platforms (TLPs). An integrated environment is given by the ANSYS AQWA diffraction product for the design of the primary hydrodynamic parameters needed for complex motion and response analyses. Three-dimensional analysis of linear radiation and diffraction can be performed with multiple bodies, taking full account of the effects of hydrodynamic interaction between bodies. Computation of second-order wave forces using complete quadratic transfer function matrices allows for a wide variety of water depths to be used.

AQWA Hydrodynamic Time Response provides dynamic analysis capabilities for floating structures in the time domain to undertake global performance evaluation. In order to model the restraining conditions on the floating structures, a broad range of physical connections, such as mooring lines and electrical cables, are provided. Furthermore, with the inclusion of forward speed effects, sea-keeping simulation may be undertaken. Slow-drift and extreme-wave conditions may be investigated, and disruption conditions can be used to research any effects that may occur.

5.4.1 Coupled Cable Dynamics

As an alternative, via the simulation of the mooring lines and electrical cables as a collection of rod components, Ansys AQWA may provide the effects of line dynamics. This has the added advantage of including drag loads and added line mass effects, which can be critical in deep-water applications for the long line lengths encountered. For both static and dynamic analyses, the feature is available. The functionality is

available both within the frequency and time domains for the complex response. As mentioned before, frequency domain solutions are very quick and can help decide if the research requires consideration of cable dynamics. Time domain solutions can have much higher precision but running them takes longer. All analysis in this thesis carried out using time-domain analysis to get more precious results.

Using this feature, it is possible to model connected electrical cable to floating wind turbine, while modeling electrical cable using FAST is not suggested by the developer of the code.

For the simulations in this thesis, a typical XLPE with copper conductors has been utilized for the electrical cable. The model assumes extruded XLPE isolators and a single layer of galvanized steel armor wires. The mechanical characteristics of the cable have been assumed from the literature [74-76]. The values for the diameter, weight and strength are shown in figure 5.4, with reference to figure 4.11, the linear and nonlinear elastic module E and E′ and the yielding stress (σy) are equal to 128 GPa, 6.4 GPa and 350 MPa, respectively. Figure 5.4 shows cable specifications which is used in the simulations.

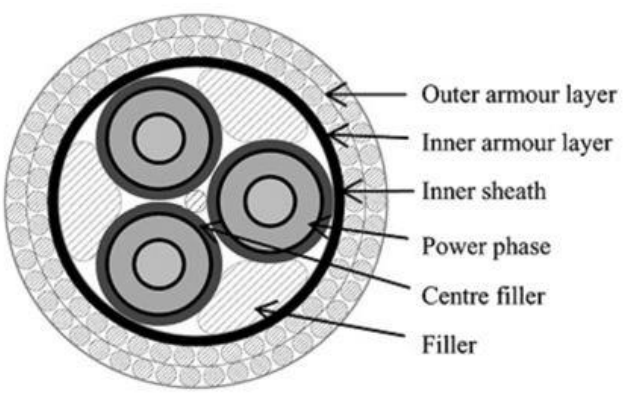

Cable Specification	
Nominal Diameter	0.2 m
Nominal weight in seawater	39 Kg
Bending Stiffness	10 kNm²
Axial stiffness	700 MN
Minimum Breaking Load	100 kN

Figure 5.4 Cable specifications [adapted from 76]

5.5 Simulation in ANSYS AQWA

As mentioned before, to model the electrical cable this study performs ANSYS AQWA, and modeling procedure starts with modeling the geometry of the wind turbine. In the present thesis, same 5MW NREL wind turbine is modeled with the same material properties, structural properties, hydrodynamic properties, etc.

Because of the difficulty of modeling the rotor and blades in ANSYS AQWA, the floating structure modeled as shown in the figure 5.5, then aerodynamic loads extracted from FAST applied to the rotor (top of the structure) in the analysis.

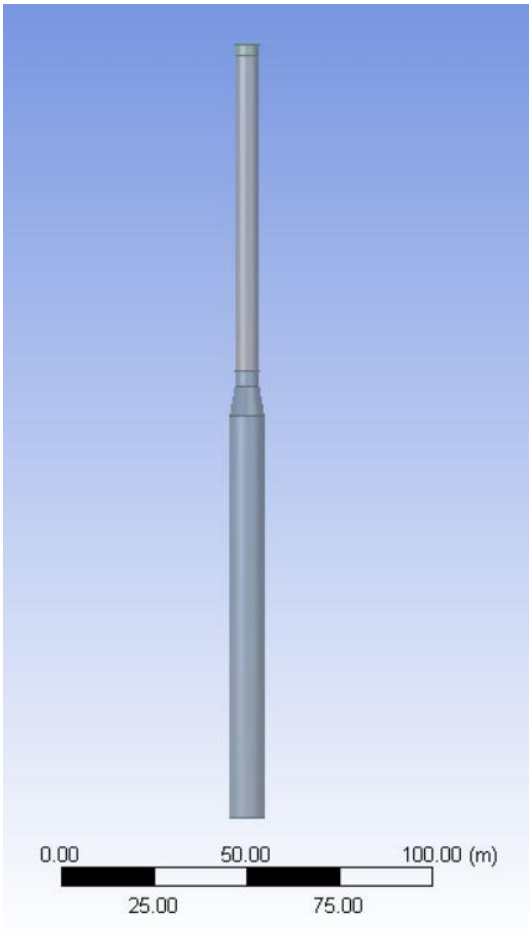

Figure 5.5 Geometry of spar-buoy platform in ANSYS AQWA

5.5.1 System Setup

After attaching the geometry to hydrodynamic system in ANSYS AQWA, mooring lines and connected electrical cable in the simple configuration is added to the floating wind turbine, figure 5.6 shows final setup of the floating structure in ANSYS AQWA.

The status of a wind turbine depends on wind speed and environmental conditions: between the cut-in and the cut-out wind speed, the wind turbine produces electricity, and the blades rotate, while the wind turbine is parked for the wind speeds higher than the cut-out value, with blades parallel to the wind [77]. Time history analyses are conducted for 4000 seconds for different environmental conditions, and the first 400

seconds are removed to neglect transitory effects of the simulation and waiting for to the model to reach the stationary operation state.

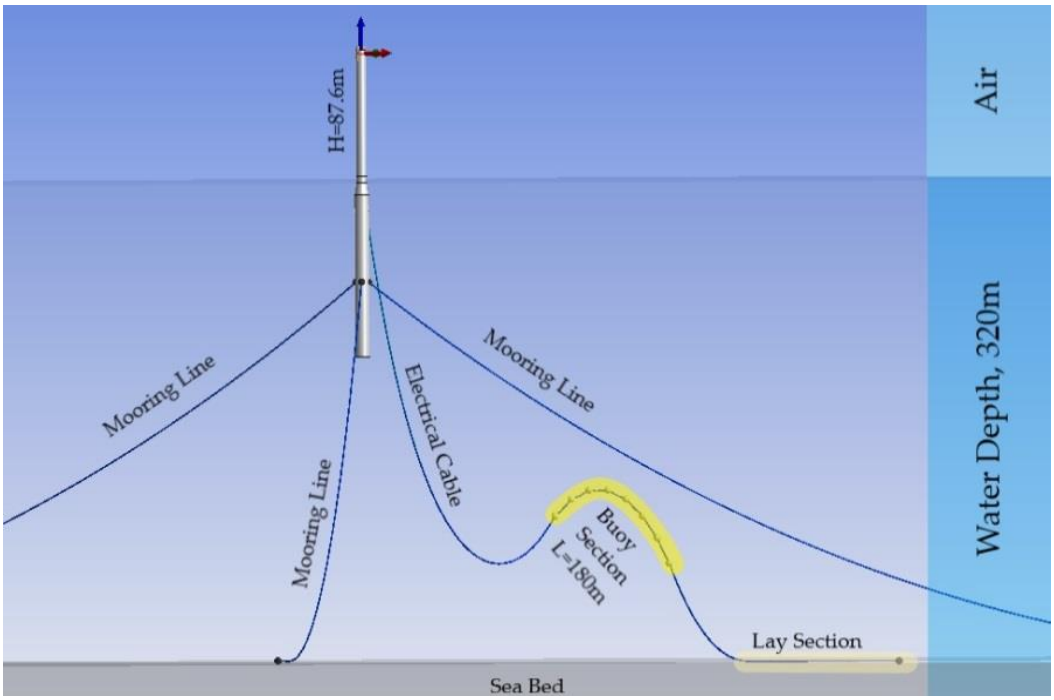

Figure 5.6 FOWT configuration included electrical cable in ANSYS AQWA

As mentioned earlier, the used version of the FAST Code does not allow to add extra structural elements (like power cable, etc.), but it is easily possible to add extra structural parts in ANSYS AQWA, this is the motivation why the electrical cable and the fatigue analyses have been conducted in ANSYS AQWA on the current thesis. On the other side, one of the issues faced in the used version of ANSYS AQWA (version 18.2) is the difficulty and time consuming procedure of modelling and analysis of the rotating blades in operating conditions, for covering weakness of the both codes and having most accurate results the rotor-nacelle assembly is modelled in ANSYS AQWA as a concentrated mass at the hub height. In addition, The total rotor aerodynamic load time history (force in the x-direction) called "RtAeroFxh" output [3] derived from the FAST initial simulation (where the electrical cable is not modeled) is successively added to the hub in the ANSYS AQWA model (where the electrical cable is now modelled and meshed by 100 finite elements).Since hydrodynamic loads are evaluated in ANSYS AQWA based on the implemented wave theory and by making use of the Morrison's equation, to avoid double-counting of hydrodynamic effects during the simulation in ANSYS AQWA, the "RtAeroFxh" aerodynamic force should be evaluated by not taking into account the three following effects:

i) presence of waves.

ii) action of a sea current.
iii) inertial effect of water volumes moving with the platform.

Since results can be taken into consideration in the ensuing ANSYS AQWA simulation.

One of the techniques that can be introduced to prevent double-counting is by performing a tentative FAST analysis by thoroughly limiting the bottom DOFs of the platform and preserving the overwater dynamics (named "Fixed DOFs at spar"). This procedure would totally disregard the double-counting of all three results, however, but at the other hand, this option would also neglect certain fluid-structure interaction (FSI) effects that have a non-negligible impact on RtAeroFxh (e.g. the wind incoming velocities and angles of attack are not combined with the correct translational velocities and rotational displacements experimented by the rotor during the large pitch, thrust and heave displacements of the floating platform when relative wind-rotor velocities and rotational angles are obtained for aerodynamic load calculation purposes). The second technique for solving the double-counting problem is to perform an analysis in FAST code by assuming "still water" (no sea current and no waves) and allowing the DOFs to move. By adopting this strategy, the FSI effects are mostly taken into account (the relative velocities between the wind and the rotor and tower will correctly take into account the large displacements of the floating platform induced by the wind itself) also if the impact on the relative velocities of the hydrodynamic forces (less important than that of wind) is not considered and, at the end of the process, there will also be a (partial) double-counting of the inertial effect of water volumes moving with the platform. A contrast can then be made to run the analysis with the combined use of the two computational codes. In order to show the differences found in the RtAeroFxh by running the preliminary analysis with three different strategies: the above mentioned “Fixed DOFs at spar” and “Still Water” options, and the analysis carried out by considering all the loads in FAST (“wave and current” mode, something that would cause the above-mentioned double-counting effect if the extracted RtAeroFxh is successively applied to ANSYS AQWA), the time histories of the RtAeroFxh obtained for the three cases are compared in figure 5.7 for one of the sea states considered in the following fatigue analysis: sea state 15 as identified in table 5.5 by grey highlighting (wind velocity at the hub height equal to 21.7m/s, current velocity equal to 0.5m/s, wave height equal to 4.5m with period of 10s).

From Figure 5.7 (b), it is clear that the “Fixed DOFs at spar” option provides conservative results with respect to the "Still Water" option, although it is also clear

that the inclusion of waves and current would result in an additional contribution (which, if included, would be doubled in the ANSYS AQWA) that is applicable to the load case being examined. Figure 5.7(c) shows that the frequency content varies significantly between the three alternatives (with different frequency contents for the "Wave and Current" case relative to the other two). On the basis of this analysis, the final option was made by opting for the "Fixed DOFs at spar" strategy in the subsequent fatigue calculation, as this is conservative in relation to the "Still Water" model.

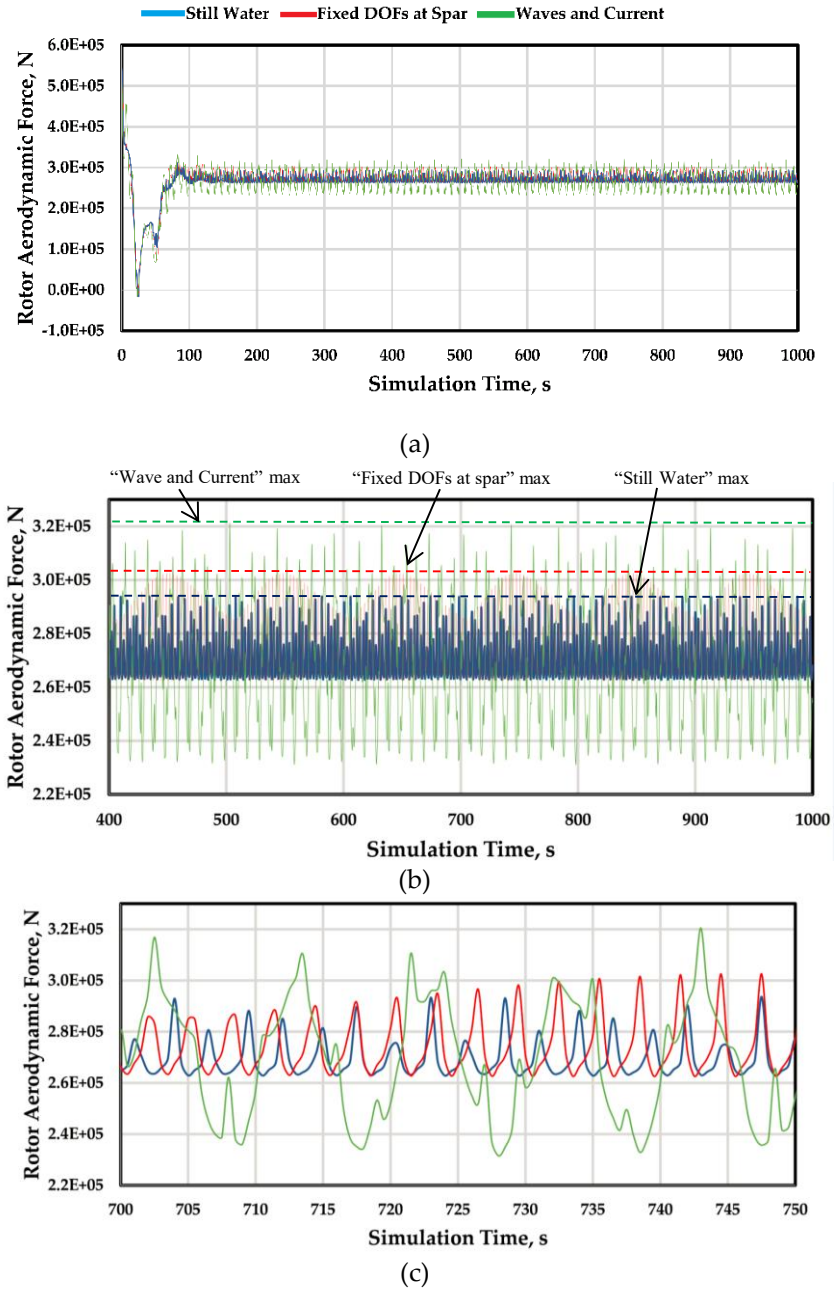

Figure 5.7 Rotor Aerodynamic Force RtAeroFx as extracted from FAST for the sea state 15 and the three strategies that would be adapted for neglecting the double-

counting of the hydrodynamic effects. 0-100 sec scale (a); 400-1000 sec scale (b); 700-750 sec time interval (c).

5.6 Model Verification

Having a vision of the above mentioned joint use of the two codes, the method needs to be validated, in particular with regard to the evaluation of the hydrodynamic loads obtained by the two codes: having the same response of the model under hydrodynamic loads is a primary requirement in order to conclude that the results obtained are reliable and that the above-mentioned procedure for the extraction of aerodynamic loads. For this reason, a series of validation analyzes (comparison of the dynamic platform obtained by FAST and ANSYS AQWA and comparison with the results of the literature for the same problem under different load conditions) are carried out and are based on the reported results of Phase IV of the NREL 5 MW FOWT [78]. Fully nonlinear analysis in ANSYS AQWA and FAST are performed with all wind turbine DOF's (surge, sway, heave, pitch, roll, yaw). Environmental condition for validation simulation is shown in table 5.8 [78]. Hydrodynamic, structural and mooring line properties considered the same as in [78] while the electrical cable is not modelled in this validation phase.

Enabled DOFs	Platform, Tower
Wind Condition	None
Wave Condition	Regular Airy: H=6 m and T= 10s
Analysis Type	Time-series solution

Table 5.8 Validation sea state

Figure 5.8 shows time histories of the platform surge, heave and pitch displacement considering load case shown in Table 5.8 as obtained in the present thesis by ANSYS AQWA and FAST and compared with results published in [78] as obtained with FAST ("OC3" in the Figure) for validation purposes. The simulation shows there is a good agreement between the results of FAST and ANSYS AQWA.

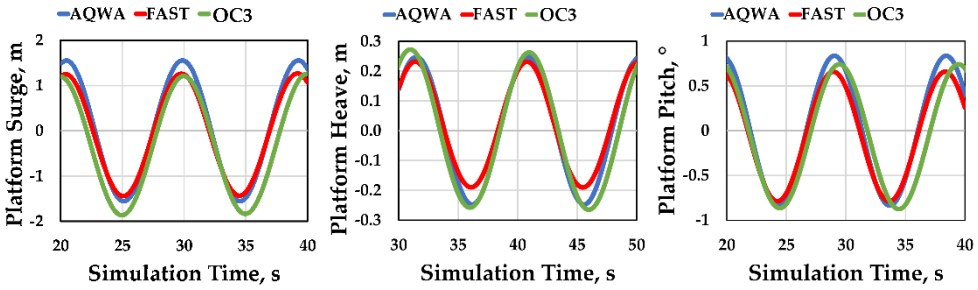

Figure 5.8 Comparison of the time histories of the platform main DOFs under the load case shown in table 1, as obtained by FAST an ANSYS AQWA models. Surge (a), Heave (b), Pitch (c).

In the fatigue analysis presented in the next section, the motion responses of the spar-buoy platform were calculated in ANSYS AQWA under the combination of wind, current, and wave loads. As far as the wind is concerned, in each analysis, in addition to the time history of the total force acting on the rotor (RtAeroFxh) as derived from FAST, the mean wind is applied to the tower above the sea. Airy's theory of regular waves is applicable to wave mechanics computation, while Morrison's equations are used to evaluate hydrodynamic forces. Regular sea states are assumed to model the environmental situation.

5.7 Fatigue analysis of the connected power cable

The above-mentioned general procedure for fatigue life evaluation has been applied to the case study by using the validated numerical models as described above. The complete flowchart of the fatigue analysis procedure adapted in this thesis is shown in figure 5.1, the goal is to determine the fatigue life in the cross-section of the cable that is located at a critical position along with the cable development for fatigue analysis.

As has been stated, for each considered loading condition (sea state “SS” in what follows) the aerodynamic forces time histories are extracted from FAST (in “Fixed DOFs at spar” conditions and without modelling the electrical cable) and applied to the top of the tower in the ANSYS AQWA model. Further, the structural response is evaluated in ANSYS AQWA by a fully non-linear time-domain analysis considering also the model provided by the electrical cable. Outputs that are applicable to the assessment of fatigue damage in the electrical cable using the method mentioned above (axial force and bending curvature in the cross-section of the cable at the fatigue-relevant location) are then extracted to feed the in-house MATLAB routine that performs the assessment of the total strain time history. The bending curvature of the cable is obtained step-by-step as spatial first derivative of the bending deflection starting from the time histories of the displacements of the two nodes adjacent to the focused location.

As an alternative to the $\sigma - N$ plane, the fatigue curves can also be represented by the total strain (ε) versus the number of cycles (N) as described below. Equation 5.1 is functional for both stress versus number of cycles curve and strain versus number of cycles ($\varepsilon - N$). A non-linear numerical analysis of the coupled FOWT-electrical cable system is carried out in the assessment of the total strain time history in the critical fatigue-prone position of the cable and corresponding to a particular sea state, and ε accounts for both the elastic (ε_e) and the plastic strain (ε_e) and can then be expressed as follows.

$$\varepsilon(t) = \varepsilon_e(t) + \varepsilon_p(t) = \frac{\sigma_{el}(t)}{E} + \varepsilon_p(t) \qquad \text{Eq 5.1}$$

where E is the Young's elastic modulus assigned to the equivalent homogenous material modelling the cable, and σ_{el} is the elastic tension stress of the electrical cable, evaluated step-by-step as the maximum cross-section tensile stiffness in the homogeneous material cross-section by considering both the axial and bending contributions:

$$\sigma_{el}(t) = \frac{N(t)}{A} + \chi(t) \cdot E \cdot \frac{D}{2} \qquad \text{Eq 5.2}$$

in which, by referring to the circular cross-section of the cable, N is the axial force, A is the area, χ is the bending curvature, and D is the diameter.
The plastic strain contribution (ε_p) enters in the game only when the total stress, evaluated by the equation 5.2, is larger than the yielding stress σ_y of the cable, which can be evaluated from the strain-stress constitutive law assumed for the equivalent homogeneous material used for modelling the cable (figure 5.9) as detailed in equation 5.3.

$$\varepsilon_p(t) = \frac{\sigma_y}{E} + \frac{\sigma_y - \sigma_{el}(t)}{E'} \qquad \text{Eq 5.3}$$

where E′ is the material plastic modulus.

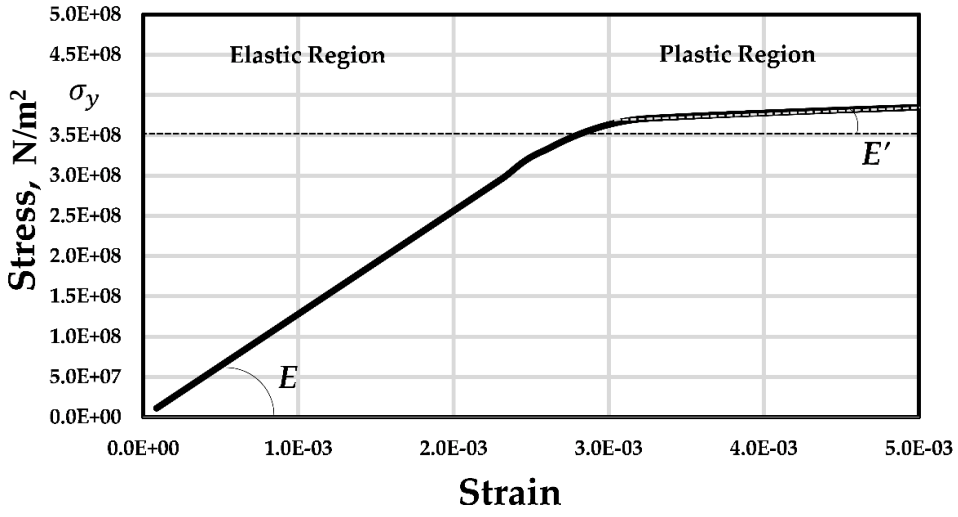

Figure 5.9 Stress-strain constitutive relationship of the cable

The impact of both plastic and elastic strain on the fatigue curve can be described by the Coffin-Manson relation [79] providing the ε-N curve:

$$\varepsilon(N_{cycles}) = \varepsilon_e(N_{cycles}) + \varepsilon_p(N_{cycles}) = = C_1 \cdot N_{cycles}^{-\beta_1} + C_2 \cdot N_{cycles}^{-\beta_2} \qquad \text{Eq 5.3}$$

where $\varepsilon(N_{cycles})$ are the strain amplitudes leading to failure at N_{cycles} number of cycles, Ci and βi (with i=1,2) are appropriate material constants, provided at [80] for a typical FOWT umbilical cable as C1 = 0.7692, β1 = 0.5879, C2 = 0.0219, β2 = 0.1745, which results in the highly non-linear graph in figure 5.10. This curve forms the basis of the present fatigue analyses.

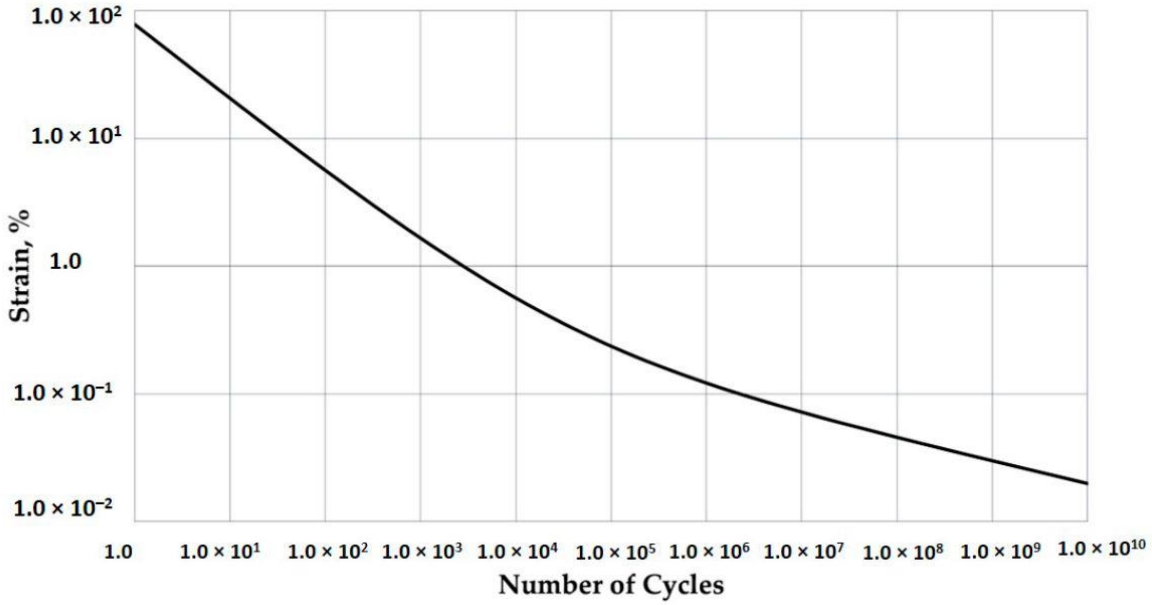

Figure 5.10 Strain cycle ($\varepsilon - N$) fatigue curve for ETP copper [adapted from 82]

According to the above estimation, the total strain time history of the critical cross-section of the cable must be evaluated and then processed by cycle counting, leading to a collection of amplitudes-number of cycle histograms that are compared to the fatigue curve of the cable in order to determine the fatigue damage (Dm) associated with each single time history

Once the time history of the total strain at the given position of the cable for a certain SS is acquired, the MATLAB routine for the rain cycle counting method [81] is used and the fatigue damage for the SS considered is evaluated at the point of interest by comparing the cycle-counting histogram with the $\varepsilon - N$ fatigue curve shown in figure 5.10.

The procedure is repeated for all the relevant SSs. Finally, the damages obtained are multiplied by their pertinent annual occurrences evaluated by a fitted Weibull distribution indicating the climate of the FOWT location. The total annual fatigue damage (Dm_{year}) is then evaluated as the sum of the annual fatigue damages induced by the single SSs and the fatigue life of the cable (Lf) is evaluated as the inverse of the annual fatigue damage, while the design fatigue life (Lf_d) is obtained by considering a safety factor (SF_DNV) equal to 10 as indicated in DNV standards [54].

Figure 5.11 shows the electrical cable configuration. The electrical cable configuration provided in [83] is used in the simulations. The cable is hanging off a fixed point on the spar-buoy platform at the sea surface, and the electrical cable modelled by 100 elements. The fatigue of the cable is calculated at different locations along the cable to individuate the most critical cross-section for fatigue. The fatigue damage is highly influenced by the position of the cross-section along the cable. For demonstration purposes, in the following the fatigue life is evaluated for locations A and B along the cable as shown in Figure 5.11.

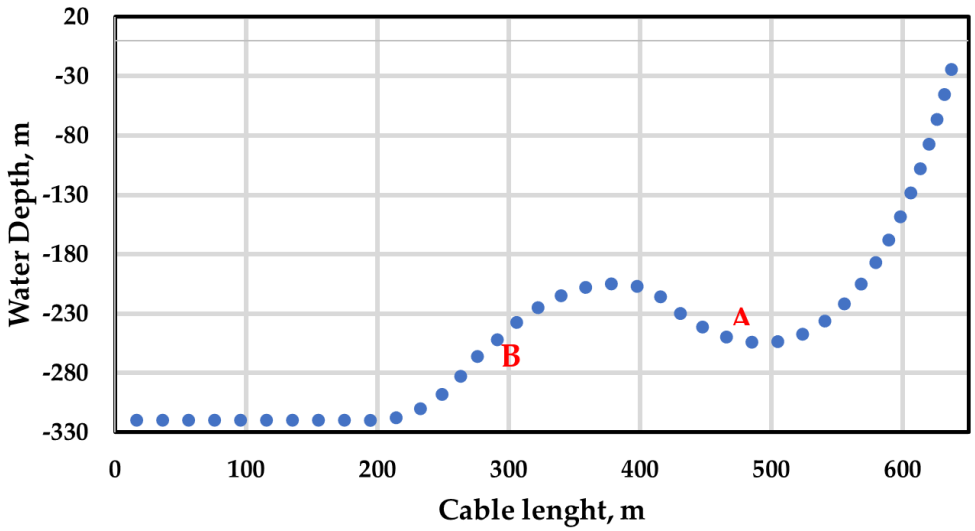

Figure 5.11 Electrical Cable layout

5.7.1 Environmental conditions and considered SSs

As before mentioned, the SS conditions for fatigue life evaluations are selected from the South China Sea S4 area, the angle of incidence of wind and waves is fixed to the direction coinciding with to the X-axis, that is orthogonal to the cable longitudinal extension, since this is recognized to be the most critical configuration for fatigue in umbilical cables. According to the wave scatter diagram of South China Sea S4 in one

year, the chosen sea states are listed in table 5.5. The wind speed profile representing the variation of the mean wind with the height above the still water level $U(z)$, is evaluated by the power-law model shown in equation 5.4, where $U10$ is 10 mins average wind speed at 10m height above the sea still water level, α is power-law profile:

$$U(z) = U_{10} \cdot \left(\frac{z}{10}\right)^{\alpha} \quad \text{Eq 5.4}$$

Also, in Table 5.5, Hs is the waves height and T is the waves period, Cv is the current velocity, and P is the annual probability of each sea state as evaluated by a Weibull probability distribution function adopted in fitting the number of occurrences of the sea states. Equation 5.5 describes Weibull probability density function. Figure 5.12 shows Weibull probability distribution function.

$$PDF_{weibull} = \frac{\beta}{V}\left(\frac{U_{10}}{\gamma}\right)^{\beta} e^{-\left(\frac{U_{10}}{\gamma}\right)^{\beta}} \quad \text{Eq 5.5}$$

Where, $\beta = 2.49$ and $\gamma = 10.4\ m/s$ are the values assumed for the shape parameter and scale parameter [84] in order to fit the available SSs data.

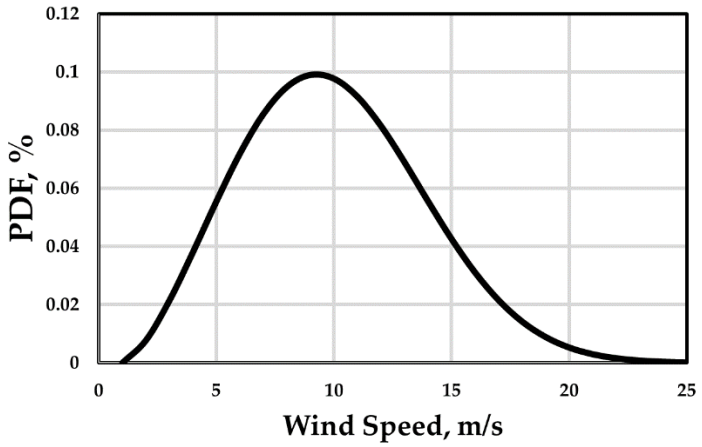

Figure 5.12 Weibull distribution adopted for U_{10}

As earlier described, wind turbines are typically designed for 20-25 years, under average wind conditions, an onshore wind turbine can produce electricity for 4,000-7,000 hours a year, corresponding to 70-80% of the total hours in the year on the above basis an average number of 15 windy hours each day for a total of 365 days during the year (5475 hours per year) is considered in evaluating the occurrences of the SSs.

5.7.2 Fatigue Life Estimation

As already described, in order to avoid transitory effects of the simulation in rainflow method calculations, first 400 seconds are removed from the ANSYS AQWA analysis output before feeding the cycle-counting MATLAB routine. As an instance, figure 5.7 shows time histories of the cable axial force as obtained at location *A* from the *SS* 10 simulation in Table 5.13. The results obtained for the annual fatigue damage at location *A* for the 20 SSs are shown in figure 5.14, while figure 5.15 shows the percentage of the contribution of each SS to the annual fatigue damage. As mentioned above, the annual fatigue damage due to a particular SS is evaluated by multiplying the fatigue damage obtained by the non-linear time history analysis conducted in ANSYS AQWA by the number of annual occurrences of that SS.

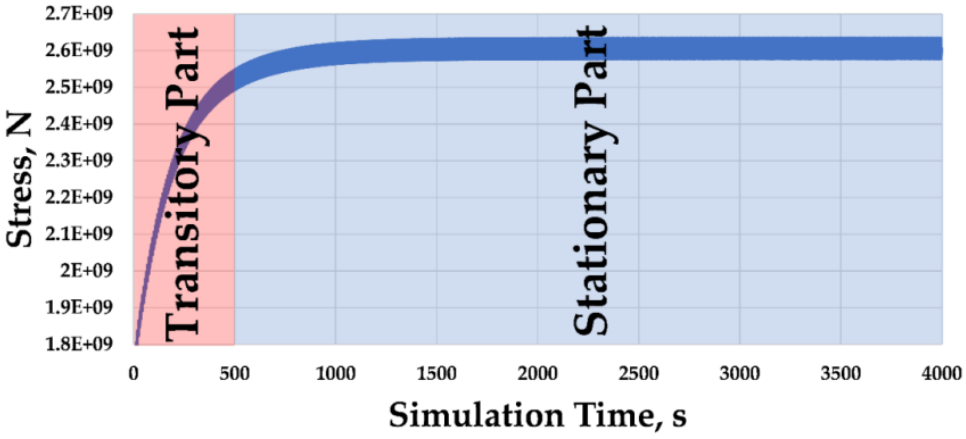

(a)

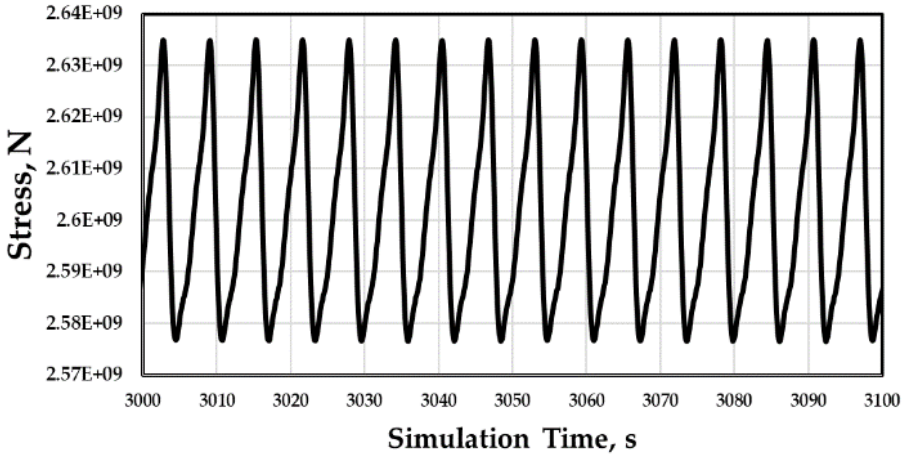

(b)

Figure 5.13 Example of axial stress time history in the cable at location A and for the SS no. 10. Whole (a); focus (b)

Finally, the Table 5.6 represents the evaluation of the annual fatigue damage (*Dm_year*) due to all the 20 SSs considered with their occurrences. From these results, it is evident how the location A is critical point for fatigue and that it suffers important

damage who quantifies the fatigue life (Lf) of the umbilical cable to about 10 years, if scaled by the safety factor (SF_DNV) reduces to 1 year. This result confirms that fatigue in electrical cables is a weak point for this kind of structures.

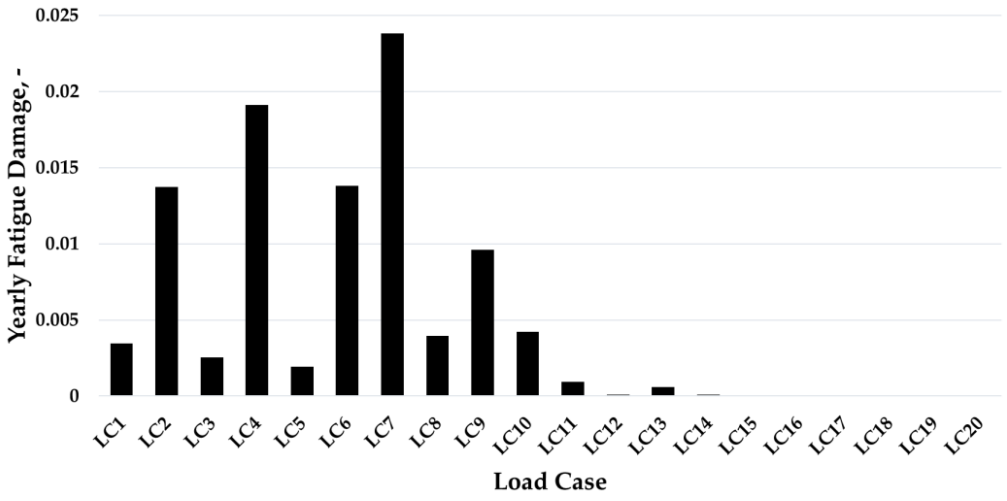

Figure 5.14 Annual fatigue damage induced at location A for all considered SSs

Sea State	Annual Fatigue Damage. Location A	Annual Fatigue Damage. Location B
1	3.442737E-03	2.68358E-04
2	1.3747238E-02	9.76374E-04
3	2.526371E-03	2.0901E-04
4	1.9108678E-02	1.10222E-03
5	1.923422E-03	1.13001E-04
6	1.37916E-02	8.4595E-04
7	2.380188E-02	1.44312E-03
8	3.962855E-03	2.18672E-04
9	9.60747E-03	3.96218E-04
10	4.204048E-03	1.88023E-04
11	9.2328E-04	3.25774E-05
12	1.00209E-04	3.50426E-06
13	5.72823E-04	1.28245E-05
14	8.0497E-05	1.65752E-06
15	6.27443E-05	1.28641E-06
16	1.97191E-05	3.1258E-07
17	3.50939E-05	5.99213E-07

18	2.66189E-05	5.45779E-07
19	2.54863E-05	9.23608E-07
20	5.53736E-06	4.84702E-07
Sum of the annual damage for all SSs	9.796831E-02	5.81566E-03
Fatigue life of the cable Lf (years)	10.2074	171.9495
Fatigue design life of the cable Lfd (with the application of the SF_DNV Safety Factor (years)	1.02074	17.19495

Table 5.6 Annual fatigue damage and fatigue life estimation

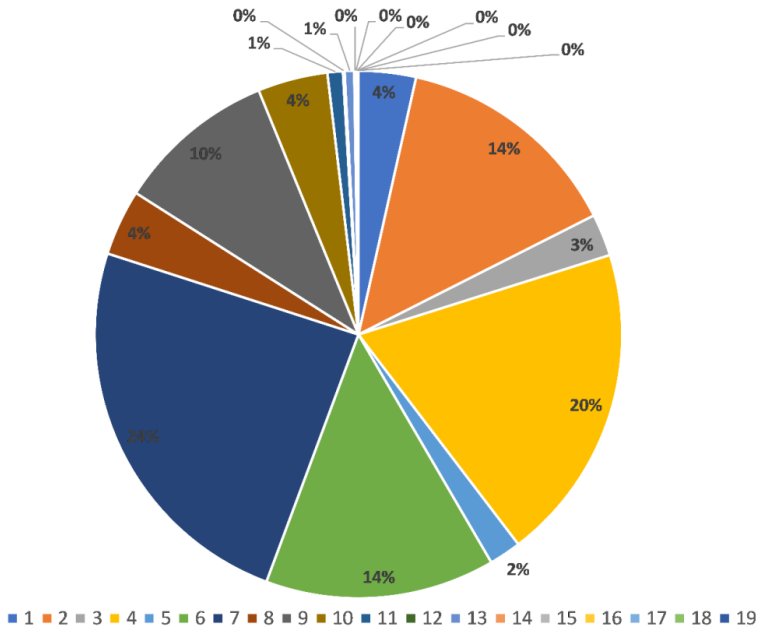

Figure 5.15. Relative contribution at location A to the annual fatigue damage of all considered SSs

From Table 5.6 it is also evident how the evaluated fatigue damage is strongly dependent from the location along the cable: location B experiments much less damage (more than 10 times lower) than location A. This was expected in advantage, because the experimented oscillations and bending deformations of the cable decrease from *A* to *B* due to the presence of the buoy section of the cable development, being the cable stabilized by the buoyancy.

Fatigue life assessment is highly dependent on the cable diameter and the location of the calculation point for the fatigue analysis. As already mentioned above, two

different points are used in fatigue analysis in this research to calculate strain amplitude of the points (figure 5.11). The suggested safety factor (SF) of 10 based on recommendations [84] is applied in the present study to assess the fatigue life.

Chapter 6: Optimal Layout of Electrical Cables in an Offshore Wind Farm for Fatigue Strength improvements

6.1 Introduction

Many offshore wind farms are planned near to each other and in regions where it is necessary to consider the connection of the wind farm grid in parallel with power exchange connections between different countries. With long transmission distances to onshore connection points and expensive subsea cables, it is possible that the sharing of grid resources would achieve substantial reductions in energy costs. A solution that combines the expense of the infrastructure with the capacity of the system to utilize the cheapest means of generation is the most advantageous grid design.

For the first projects in Northern Europe, various solutions for wind farm connection to the onshore grid have been adopted. Developed in 2002 and with a capacity of 160 MW, Denmark's Horns Rev wind farm, the main European offshore pilot project, was the first plant to use an offshore transformer substation to connect to the shore through the use of a 15 km long three-core ac cable with a rated voltage of 150 kV [85]. The 165.6-MW Nysted wind farm in Denmark, also installed with an offshore transformer station in 2004, linked to the shore via an approximately 10-km 132-kV ac submarine cable. The 90-MW Barrow wind farm in the United Kingdom, built in May 2006 and like commissioning, also adopts an offshore 33/132-kV substation with a 132-kV ac cable that connects 7 km to the shore. In addition, the U.K. The offshore wind farms, Kentish Flats (90 MW, 8.5 km offshore as of December 2005) and Scroby Sands (60 MW, 2.5 km offshore since about 2004) do not have an offshore substation. Via three three-core medium voltage cables, their wind turbine generators (WTG) are connected to the power grid. In the Netherlands' Egmond aan Zee offshore wind farm, this grid topology was also adopted (108 MW, since 2006). North Hoyle, the first offshore wind farm in the UK (60 MW, since 2003) [85].

As in the previous chapters mentioned, the cables for floating offshore wind power generation facilities have floating components to allow them to move with the floater while standard submarine cables are installed or secured on the seabed. Bending and twisting forces, etc., caused by the tidal current and floater action, are constantly subjected to the cables; thus, they are likely to sustain mechanical damage in different part, which is the main reason of reducing lifetime of the cables regarding to fatigue damage.

After a brief overview of the installed, under construction and future offshore wind farms, this chapter focuses on the grid system and electrical cables layout inside the farm (i.e. inter-turbines geometrical layout and diameters of different cable parts) in

order to assess optimal electrical cable layout in terms of fatigue strength. This is made by conducting the fatigue analysis presented in the previous chapter with the avail of a model of a group of three FOWTs with different cables layouts

6.2 Recent trends for cable layouts in worldwide offshore wind farm projects

As well as better wind regimes, public rejection of onshore wind farms makes offshore wind power an enticing option. With the first experimental project, Vindeby, which installed 11 bonus 450 kW turbines in 1991, Denmark become the beginnings of the industry. Just 10 years later, twenty 2 MW turbines were used by Middlegrunden, also in Denmark. Offshore wind power is currently one of the fastest growing electricity generation technologies [86]. For example, an impressive surge in nominal turbine power has occurred in recent years. The average offshore turbine size installed in 2009 was 2.9 MW, however the Siemens 3.6 MW turbines (Siemens, Munich, Germany) are now being used as a benchmark for planned projects. Also, bigger alternatives are available, such as the REpower 5 MW (REpower Systems, Hamburg, Germany) machines to be used at the Ormonde farm in the UK3 and the newly unveiled 7 MW Vestas colossal new turbine (Vestas, Aarhus, Denmark). The farms are also growing, the average of plant size is 72 MW in 2009 after the first offshore project in Denmark with a capacity of 40 MW [86]. There are now much larger plants being constructed, such as the 1000 MW London Array or the 504 MW Greater Gabbard in the UK. In addition, the projects planned would be much larger. Dogger Bank is expected to accommodate 9000 MW of power generation in the North Sea [86], and there are over 10 more projects in the UK and Ireland with over 1000 MW. The major projects in progress, under construction and planned as of March 2011 are summarized in Tables 6.1, 6.2 and 6.3, respectively.

There is a perception that wind energy, and in particular offshore wind farms (OWFs), will be a key element in the future energy ecosystem of Europe and a key instrument for achieving the goal of reducing carbon emissions by 20% by 2010 and 80% by 2050 [86], while, as seen in recent years, improvements can be offset by rising commodity prices. The North, Baltic and Irish Seas are ideal settings for this type of plant because of particularly favorable conditions, such as calm winds and shallow waters. As can be seen in Tables 6.1 to 6.3, the UK and Denmark are now delivering the first of a remarkable pipeline of projects.

OWF	Capacity (MW)	Country	Turbines
Thanet	300	UK	100 x Vestas (3MW)
Horns Rev II	209	Denmark	91 x Siemens 2.3
Rodsand II	207	Denmark	90 x Siemens 2.3

Table 6.1 Largest offshore wind farms in operation.

OWF	Capacity (MW)	Country	Turbines
London Array	1000	UK	175 x Siemens 3.6
Greater Gabbard	504	UK	140 x Siemens 3.6
Bard 1	400	Germany	80 x BARD 5.0

Table 6.2 Largest offshore wind farms under construction.

OWF	Capacity (MW)	Country	Turbines
Dogger Bank	9000	UK	Not decided
Norfolk Bank	7200	UK	Not decided
Irish Sea	4200	UK	Not decided

Table 6.3 Largest offshore wind farms proposed.

However, in order to achieve the full potential of this energy, there are still some engineering problems that should be solved, Specially, submarine cables need some refinement due to high fatigue damages. The lead coating tends not to withstand mechanical wear as needed, plus the industry would be very welcome to have higher quality XLPE cables.

Simpler multi-terminal high-voltage direct current (HVDC) will allow the proposed big wind farms to be transmitted and run more efficiently. As earlier mentioned, floating foundations will enable OWFs to be built even in deep waters, allowing wind harvesting in areas where such technologies are now prohibitively costly.

6.3 OWT cable array

As stated earlier, the electrical system of an OWF is about 20% of the total cost and has a profound effect on the efficiency and reliability of the farm. Therefore, finding a good design solution is critical. The electrical characteristics of the turbines installed should be taken into account in the solution, fatigue failure as one of major issues in the system should be addressed. Regarding the issue, in this section analysis carrying out cable lifetime by considering fatigue damage.

The OWF array cable layout issue usually introduce by the cable installation contractor as follows: given the location of the turbine and transformer and the capacity of the cable in the number of turbines, find a set of cable lines that reduce the total cost of the cable, connect each turbine to the transformer, not exceeding the capacity of the cable and so that cables do not cross the others.

While it could be possible to let cables cross, the problem was posed to this in principle, including the restriction of not letting cables cross for two reasons: first, heat produced by high voltage power cables, meaning that two crossing cables will have to be isolated against each other. Second, for their safety, the cables are buried in the sea bed. One of two crossing cables will have to be hidden below the other at the crossing for a cable crossing. If the lowest buried cable fails and has to be substituted, all cables will have to be dug up, resulting in much higher costs [87].

6.4 Electrical layout options

The next designing task once the turbine locations have been identified is to transfer the generated energy to shore in the most cost-efficient way. In practical applications, via small/medium voltage inter-array cables, the energy of the offshore turbines is first collected at an offshore collection point, called an offshore substation. The electricity current then transported to shore by a single high-voltage export cable. In certain practical applications, the case of multiple substations may also occur.

The energy from the turbines is collected by the collector system, so that it can be transferred to shore. Current generators operate in AC, so the collector system is built to work in AC as well. In the design of collector systems, several standard configurations were proposed and used. Furthermore, in the following section most commonly used electrical design described.

6.4.1 Radial

The most basic of the possible assortments is the radial collection system. In a string arrangement, a number of turbines are attached to the same feeder. Because of its lower cost and simple control, it was the most commonly used. The lack of redundancy, however, means that its efficiency is low, as any fault would theoretically prevent power from being provided by offshore turbines. It is, however, the design with the most losses [88]. Figure 6.1 shows the radial collection system.

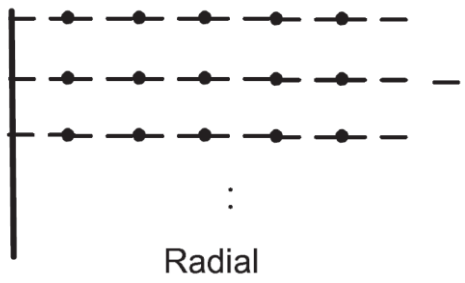

Figure 6.1 Radial connection system [adapted from 86]

6.4.2 Single-sided ring

The single-sided ring is given with an additional cable back to the collection hub from the last turbine in a row. The total power generated by the string should be able to support this cable. It is the most costly of the standard ranges, doubling the cost of a radial layout. It is also the most efficient, however, and one with the least losses [88]. Figure 6.2 shows single-sided ring collection system.

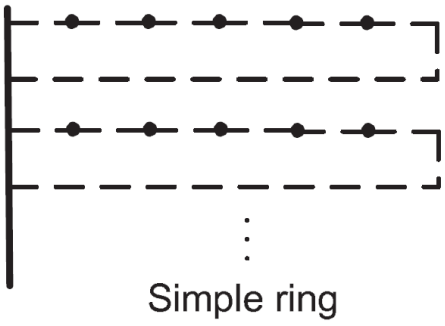

Figure 6.2 Single-sided connection system [adapted from 86]

6.4.3 Double-sided ring

By using the neighbor string's cable as the redundant circuit, the double-sided ring aims to solve the cost disadvantages of the single-sided ring. Any string will have to deliver the maximum power of two strings if a fault occurs. They should therefore be rated at twice the power of a chain. This alternative is thought to be approximately 60% more costly than a radial design [88]. Figure 6.3 shows double-sided ring collection system.

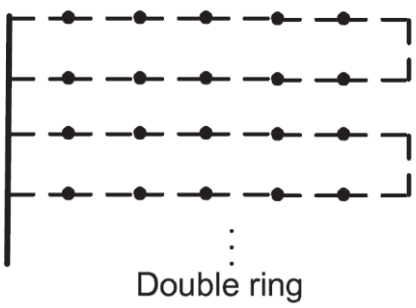

Figure 6.3 double-sided ring collection system [adapted from 86]

6.4.4 Star

As an effort to minimize cable ratings, the star design was suggested as a (as all the cables from its center to the arms would just need to bear the power coming from one turbine). Cables can however be longer and the switchgear more complicated, so the cost advantage relies on the particular case under analysis. This design also provides a high degree of security, with more than one turbine affecting only the cable failures that link the center to the collector core [88]. Figure 6.4 shows star collection system.

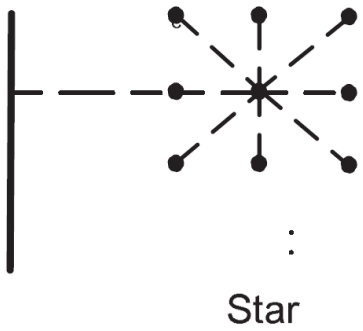

Figure 6.4 star collection system [adapted from 86]

6.4.5 Multi ring

The multi-ring was built as a way to divide the power produced between the remaining rows in a defective string so that the capacity does not need to be updated as in the double-sided ring. This range has about 25% lower losses than a standard radial array; it is more efficient and only about 20% higher in cost [88]. Figure 6.5 shows multi-ring collection system.

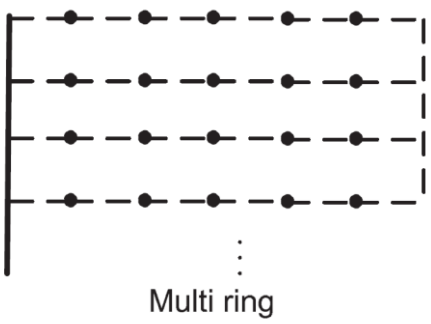

Figure 6.5 multi-ring collection system [adapted from 86]

Although preliminary studies of standard designs are useful, both cost and reliability are so dependent on the specific geometry that a combination of these architectures is typically the optimal solution. What is more, the optimal layout can be asymmetric despite symmetry in the geometry.

The optimal layout for three installed OWFs are discussed in [87]. Wind turbines position and cable layout of the three OWFs are shown in figure 6.6 [87]. Configuration of OWFs showed in figure 6.6 proves that cable layout of a common wind farm is a combination of above-mentioned collection system in a much possible simplest way.

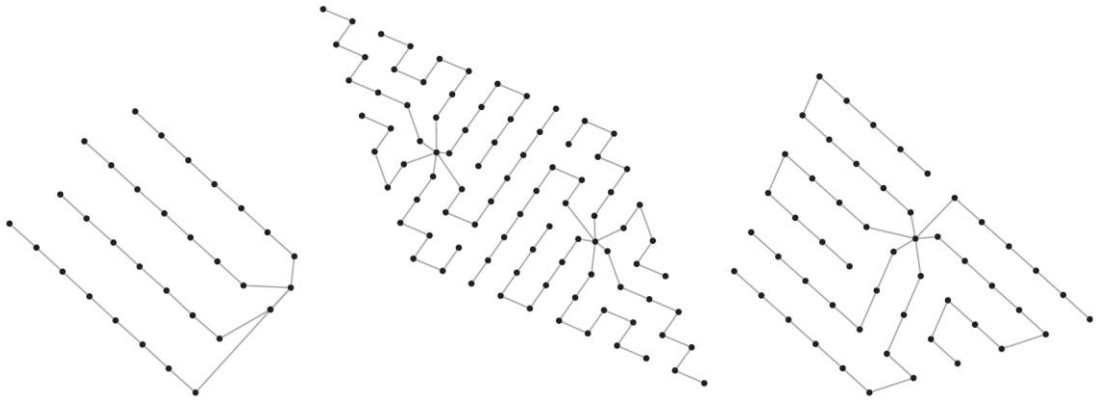

Figure 6.6 Optimal layouts for actually installed cable capacities: (a) Barrow OWF; (b) Sheringham Shoal OWF; (c) Walney 1 OWF. [adapted from 87]

The clustering and grid connection architecture of offshore wind farms are interlinked and involve a common approach. How the offshore grid should be built, of course depends on where there are wind farm clusters or other offshore hubs. On the other hand, the optimum clustering depends on the configuration of the offshore grid as well.

6.5 Three-element offshore wind farm electrical connection system

For an offshore wind farm, the electrical communication system may be divided into an offshore collection system and a transmission link to the shore.

The offshore collection system collects the power output of the wind turbine and carries it to a central collection point that then connects to the main grid. A string or star cluster configuration is typically the collection method. A number of WTGs inject power into a feeder for string clusters whose voltage level must be sufficiently high to hold the total power produced in the string (several tens of kilovolts).

What is understandable from the literature, connections between turbines can have different configuration based on the design, environmental conditions, distance to the shore, etc., and, from the literature and installed WFs (figure 6.6), it is clear that position of wind turbines and cable connection between them is a pattern mostly included 2 or 3 wind turbines, in the cases more than 3 turbines the pattern is usually repeated. In this thesis, efforts made to model 3 FOWT connected with 3 different electrical cables to each other in 2 different cable configurations. Figure 6.7 shows configuration of the FOWTs and electrical cables.

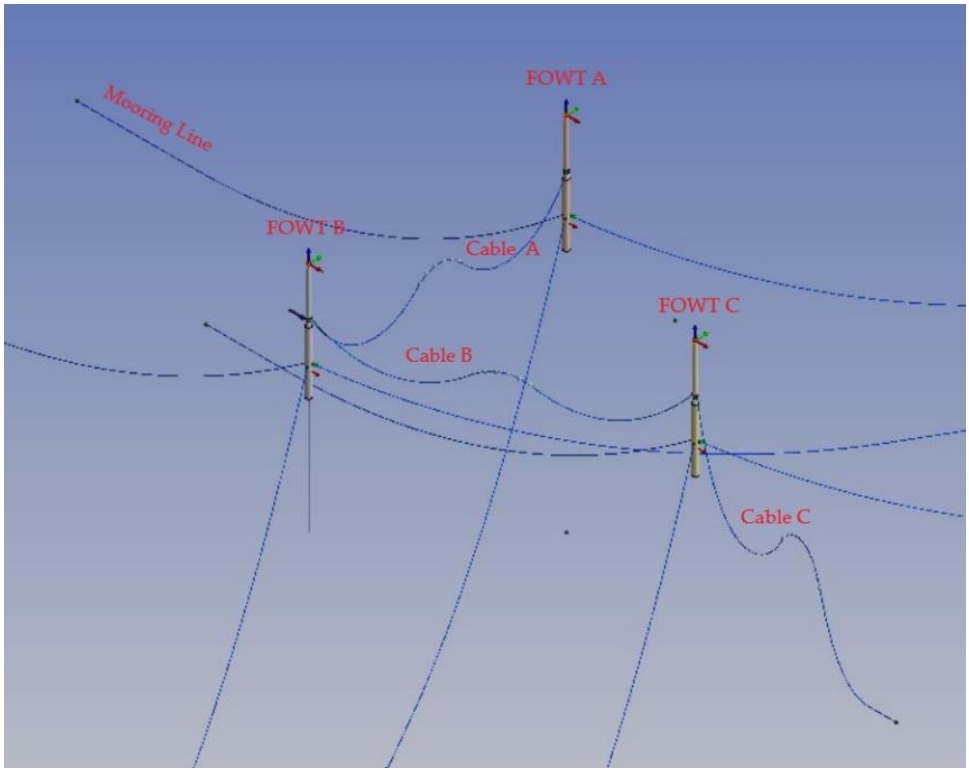

Figure 6.7a three FOWT configuration

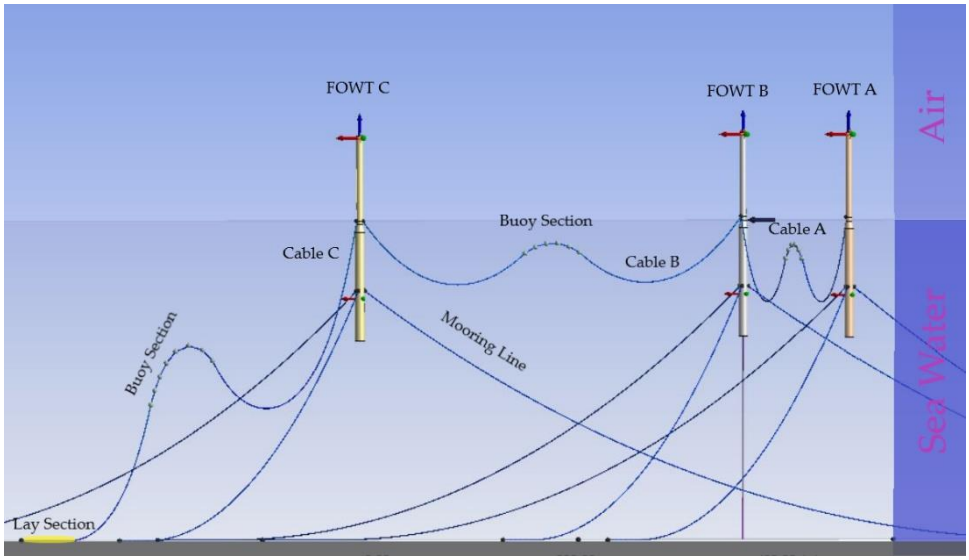

Figure 6.7b three FOWT configuration

6.5.1 Modeling of 3 FOWT and power cables

As the main goal of this thesis, study of the fatigue damage in the dynamic cables, electrical aspects are neglected, then three FOWT with connected electrical cable connected with different cross section and material properties are modeled.

As discussed in the previous chapters, different scenarios are possible in the design and modeling phase, however, this study considered one of the most simple configuration for the position of the wind turbines and connected electrical cables.

In the current chapter of this thesis, 3 FOWT are modeled in ANSYS AQWA, each wind turbine has a connected electrical cable with different diameters. Figure 6.7 shows the model in ANSYS AQWA. All FOWT are considered 5 MW NREL baseline wind turbine and as shown in the figure 6.7, generated power of FOWT A is ready to transfer to FOWT B through the cable A, and then, generated power of FOWT B transfers to FOWT C through cable B, and at the end all generated power by three FOWT will transfer to the substation or directly to the shore through cable C. by above mentioned consideration, diameter of the cable A is less than cable B, and the diameter of cable B is less than cable C, because cable C has to transfer all three FOWT generated powers and FOWT B has to transfer two wind turbine generated power.

Based on installed cables [87], for Barrow OWF two type of the cables used with the diameters of 120 mm and 300 mm. The cables installed at Sheringham Shoal OWF

have diameters 185 mm and 400 mm. The cables installed at Walney 1 OWF have diameters 150 mm and 500 mm (figure 6.6 shows mentioned OWFs cable layout).

Based on the mentioned facts, diameters of the cables are considered 200, 300 and 400 mm for the modeling the 3 FOWTs and cables are called A, B and C, respectively.

Attention must be paid to the development, design, and optimization of a flexible dynamic power cable for offshore floating wind turbines, requiring a high degree of durability, compatibility with floater motion and fatigue resistance in dynamic environments. The combined effects of waves, winds, seabed touchdown interactions and top-of-the-range floater motions on the cable attached to the float are important. As earlier mentioned, the electrical cables are modeled in two different configurations, for connection between two FOWT w-shaped configuration is used, and for export connection lazy-wave configuration is used. Figure 6.8 shows electrical cable in two different configurations.

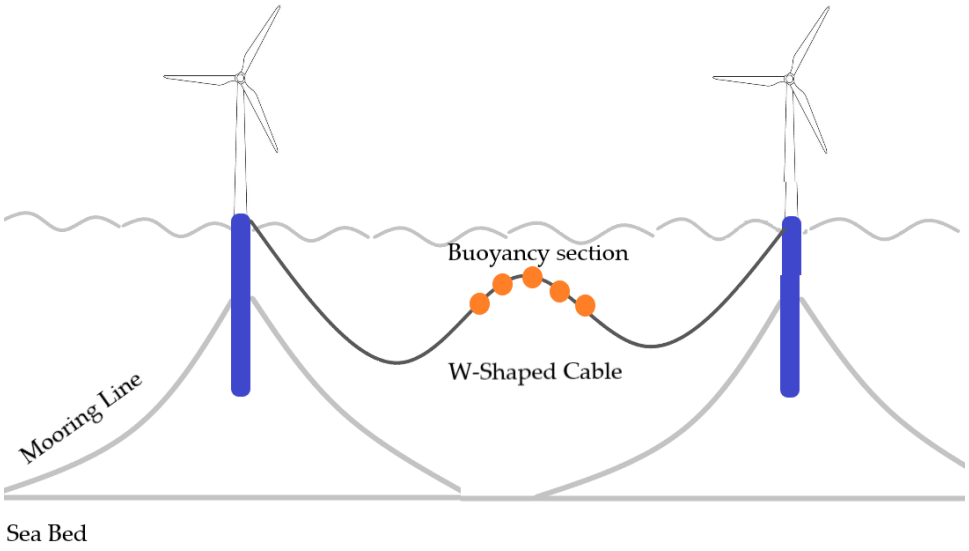

Figure 6.8a W-shaped electrical cable

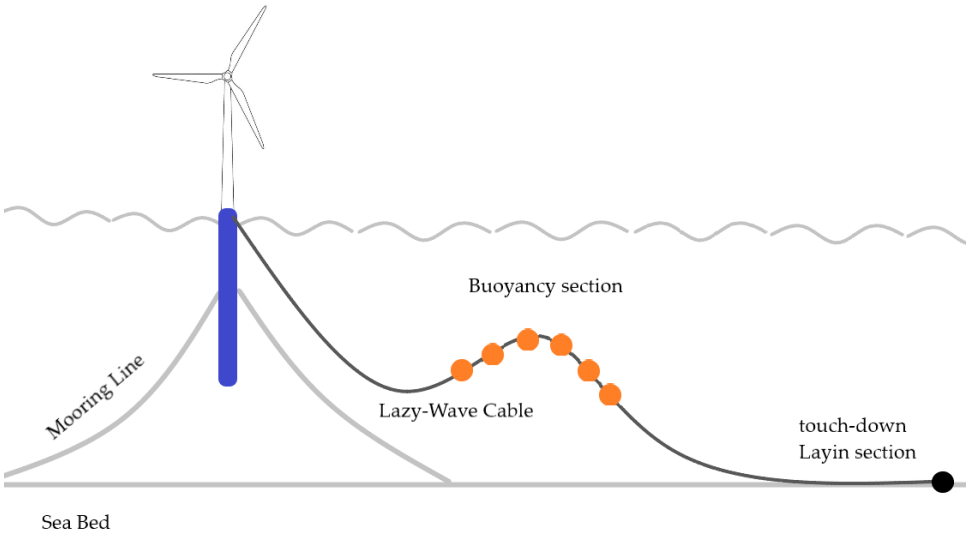

Figure 6.8b Lazy wave electrical cable

6.6 Fatigue life estimation for the electrical cables of a three FOWTs group

This section of the thesis focuses on the fatigue damage of the electrical cables connected to three FOWT with three different cables. As before mentioned, there is different type of collector system configuration and installation possibilities which one of the electrical cables (cable A in a lazy-wave configuration) is modeled during the study in previous chapter, which consider a simple electrical cable connected to single FOWT.

Next step is running the simulations of the three FOWTs to get the dynamic response of the FOWTs and connected power cables and implement fatigue damage in each cable and compare lifetime of the cables in two different configurations of the connected cable.

To implement fatigue damages of each electrical cable, same procedure for the single FOWT is repeated to carry fatigue damages in each cable which the flowchart of figure 5.1 clearly shows the procedure.

Figure 6.9 shows cable configuration for Cable A, B (left side) and Cable C (right side). Cables are considered as 100 elements and 101 nodes in the modeling phase. As the results of fatigue analysis for single FOWT has been shown in the previous chapter of this thesis, point A has more fatigue damage than other parts of the cable, and it is a critical section for the cable. By mentioned consideration, to implement fatigue

analysis in both cables, point A is chosen as a critical point in the cables and the fatigue calculation process is applied at point A.

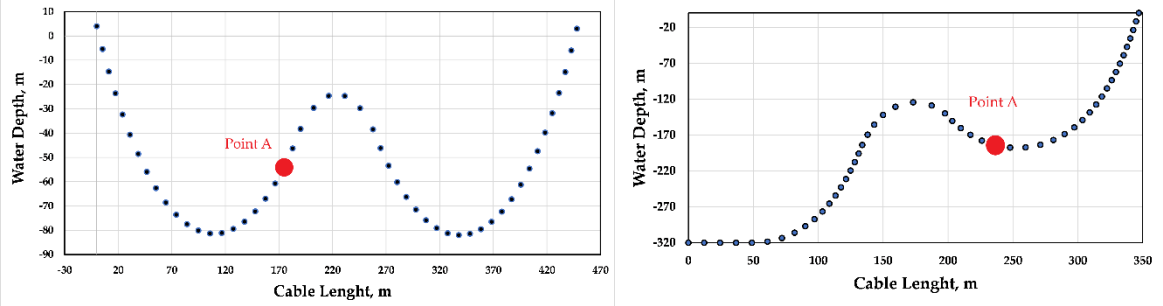

Figure 6.9 Cable Configuration

Environmental condition is the same as table 5.5 which consider 20 sea states. At the end to estimate fatigue life, it is necessary to consider probability of happening of each sea states. Regarding to table 5.5, figure 6.10 shows probability of each sea states.

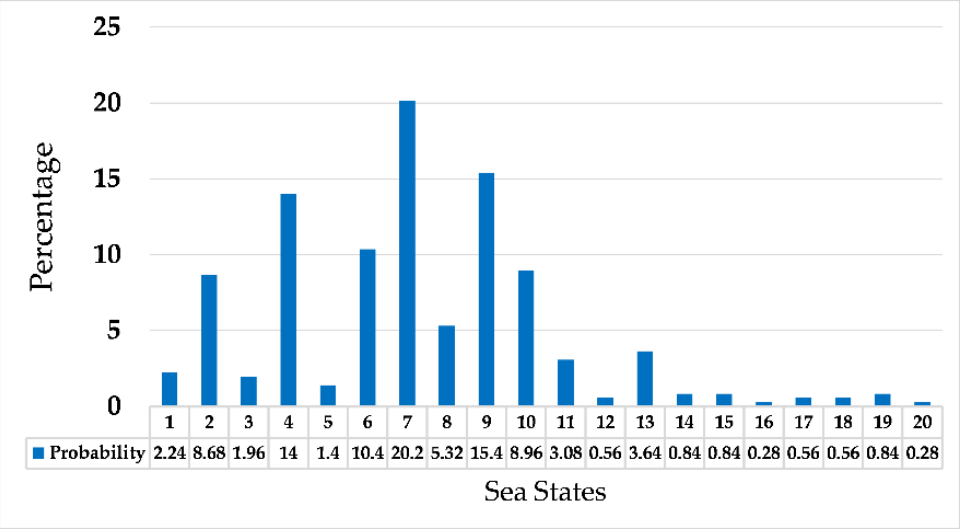

	1	2	3	4	5	6	7	8	9	10	11	12	13	14	15	16	17	18	19	20
Probability	2.24	8.68	1.96	14	1.4	10.4	20.2	5.32	15.4	8.96	3.08	0.56	3.64	0.84	0.84	0.28	0.56	0.56	0.84	0.28

Figure 6.10 sea states probability

As already stated in the previous chapter, 4000 seconds time domain analysis ran in ANSYS AQWA to carry the dynamic responses of the floating structure and connected dynamic power cable. First 400 seconds of the analysis are neglected from ANSYS AQWA output to avoid transitory effects of the analysis, then, 3600 seconds time domain analysis is used to feed inhouse developed MATLAB routine to calculate fatigue damages using rainflow method.

As mentioned in figure 5.1, in this part to calculate fatigue damage of the cables, it is needed to extract N, σ and ε of focused section of the cable (point A), to calculate strain time histories of the cable in all sea states.

Cable tension (N), cable stress (σ) and cable strain (ε) has been shown at figure 6.11 for sea state number 10. Figure 6.11a shows tension force at three cables, figure 6.11b shows stress at mentioned cable and figure 6.11c shows strain at the cables.

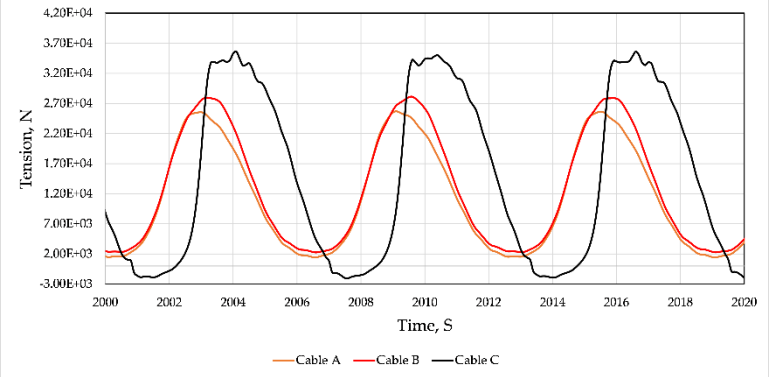

Figure 6.11a Cable Tension at sea state 10

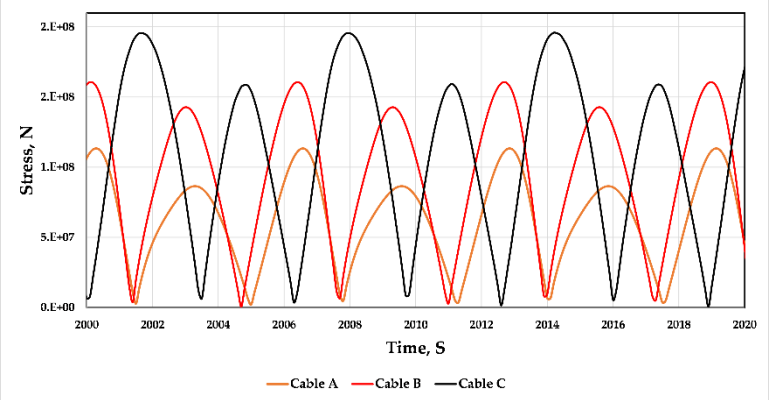

Figure 6.11b Stress of the cable at sea state 10

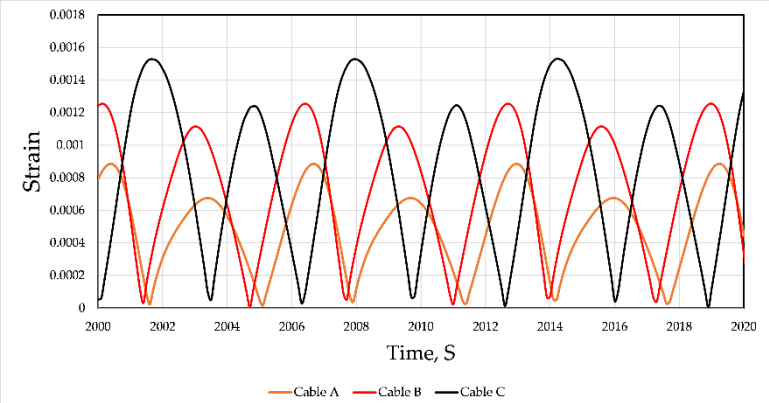

Figure 6.11c Strain of the cable at sea state 10

Referred to stress time histories and strain time histories, by increasing diameter of the cable strain increases and it cause more fatigue damage and less lifetime of the cable.

As mentioned earlier, by having strain time history, applying rainflow method and using given $S-N$ curve it is possible to calculate fatigue damage in each sea states for each cable. Figure 6.12a, 6.12b and 6.12c show annual fatigue damage of the cable A, B and C, respectively.

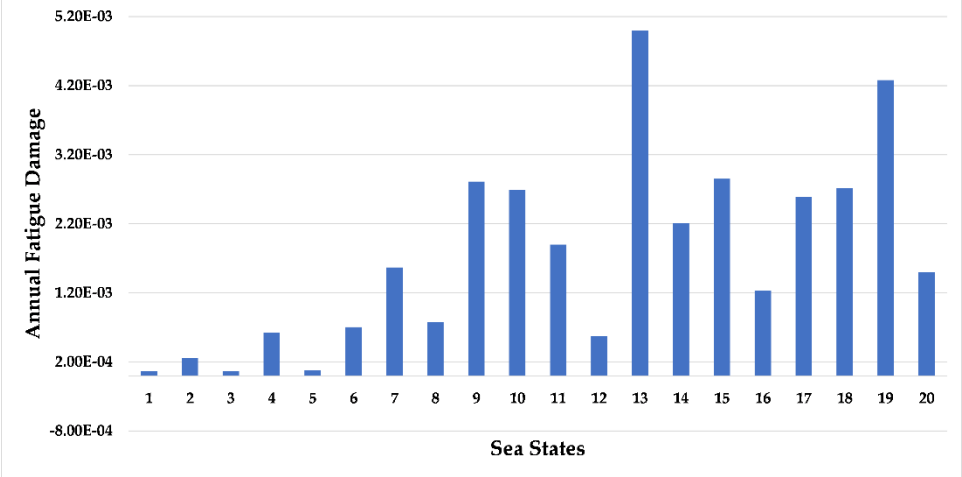

Figure 6.12a annual fatigue damage at cable A

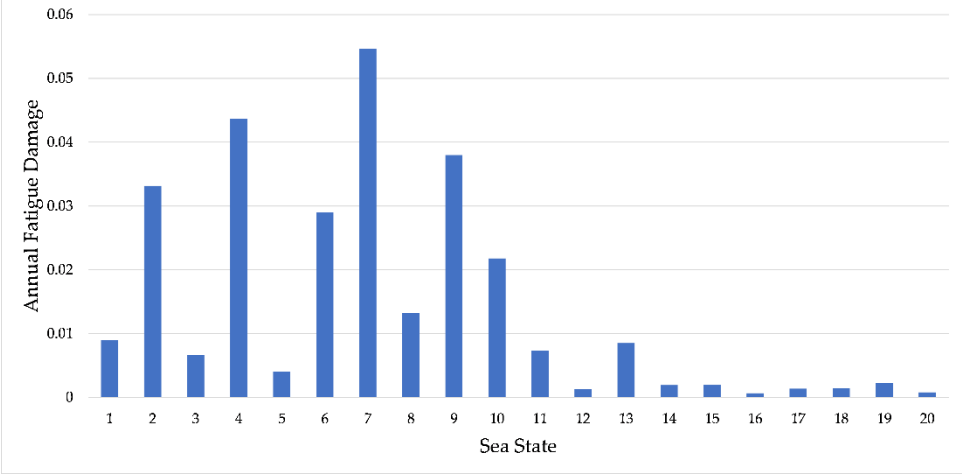

Figure 6.12b annual fatigue damage at cable B

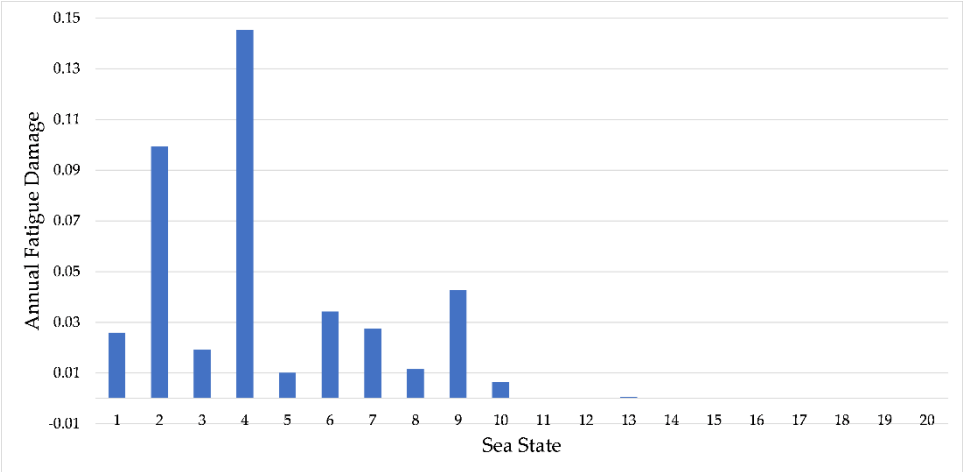

Figure 6.12c annual fatigue damage at cable C

Table 6.4 shows detailed damage of each cable at each cable and lifetime of each cable.

Sea State	Cable A (D=200mm)	Cable B D=(300mm)	Cable C (D=400mm)
1	6.61E-05	0.009001561	0.025904934
2	2.59E-04	0.033163502	0.099530763
3	6.34E-05	0.006666664	0.019331496
4	6.27E-04	0.043709858	0.145218965
5	8.20E-05	0.004090166	0.010094132
6	7.05E-04	0.028971734	0.034287431
7	1.57E-03	0.054648282	0.027583521
8	7.78E-04	0.013248331	0.011560117
9	2.81E-03	0.037986727	0.042722813
10	2.69E-03	0.021787943	0.006485238
11	1.90E-03	0.007352243	0.000198482
12	5.72E-04	0.001315506	2.85998E-05
13	5.00E-03	0.008510141	0.000682349
14	2.20E-03	0.001942276	3.37888E-05
15	2.85E-03	0.001957278	2.93944E-05
16	1.23E-03	0.000656593	7.3287E-06
17	2.59E-03	0.001378844	1.53903E-05
18	2.72E-03	0.001447787	1.61598E-05
19	4.28E-03	0.00227983	2.54468E-05
20	1.50E-03	0.00079775	8.90426E-06
Sum of Annual Damage for All SS's	3.45E-02	2.81E-01	0.423765254
Fatigue Life of the Cable (Years)	2.90E+01	3.56E+00	2.36E+00
Fatigue design life of the cable (with the application of the DNV safety factor (years)	2.90E+00	3.56E-01	2.36E-01

Table 6.4 fatigue damage of the cables

As a result of the analysis, it is obviously clear that the design life of the cable B and C are even less than one year, however, design life of the cable A is less than 3 years.

Chapter 7: Conclusion

7.1 Conclusions

In the present thesis, a detailed study on the fatigue performances of floating offshore wind turbines with connected power cable has been presented. A full procedure for the calculation of the fatigue life of power cables connecting the single FOWT with the cables grid of the farm has been devised. The procedure considers the full non-linear dynamic of the floating support of the turbine joint with the ones of the mooring lines and the electrical cable. the loading regime of a typical marine environment, and under the non-linear dynamic conditions as they can happened during the lifetime of spar-buoy floating offshore wind turbine and dynamic electrical cable (including aerodynamic, hydrodynamic, and wave loads) are considered in the proposed procedure by the implementation of state of the art numerical models, and the climatology of the site is fully taken into account by considering joint occurrences of wind and waves. In a successive step of the study, an attempt has been carried out to propose different layout configurations for the inter-array electrical cables in order to increase the fatigue strength of these components, being at today one of the main weaknesses of FOWT farms.

The analyses are conducted both for single FOWT and multi FOWTs .

The key innovations of the thesis are about two aspects:

- the proposal of an advanced, but affordable procedure for the pooling of the most commonly available information, to provide a comprehensive fatigue analysis of vulnerable FOWT electrical cables;

- the proposal of different inter-array cable layout configurations for the fatigue strength improvements of such a elements.

Practically, in the present study, the fatigue life of the dynamic cables, with consideration of actually installed cables in the operating wind farms were estimated by setting out an ad-hoc complete procedure that:

1) models and analyzes the dynamic response of a spar-buoy floating offshore wind turbine with two numerical code (FAST and ANSYS AQWA);

2) validates dynamic responses of the model by comparing motions of the platform with published results;

3) computes the total strain time histories in the cable cross-section by the benefit of fully non-linear time histories and numerical analyses of the whole floating turbine system included the dynamic electrical cable;

4) evaluates the fatigue damage suffered by the electrical cables under a combination of various marine states and by covering the wide spectrum of climate and operating conditions of the turbine;

5) defines annual events of the various marine states considered for annual damage assessment purposes on the basis of data on the condition of the sea;

6) models more than one wind turbine by consideration electrical grid system of an actually installed wind farm to investigate the lifetime of the dynamic electrical cables;

7) evaluates the fatigue strength of dynamically loaded electrical cables in both single wind turbine and in a wind farm by considering w-shaped and lazy-wave configuration for the electrical cables.

Numerical analysis has been conducted by the joint use of two well-established numerical codes for offshore floating structures, which is very important for allowing multi-physic analyses of such a complex structural system which include structural, hydrodynamics, and aerodynamics interactions. Furthermore, developing in-house MATLAB script for post-processing the extracted data of hundreds of analyses and evaluating fatigue damage in the cross-section of the cable is also another point of novelty of the thesis.

Regarding the fatigue design of dynamic electrical cables, the general engineering findings are:

- FOWT power cables must withstand a dynamic loading regime when they are attached to the support platform. As presented in the results, the fatigue life the examined cases are less than design lifetime of the wind farm with or without consideration of the suggested DNV standards safety factor.

- The proper assessment of all operational conditions (parked versus spinning blades) and environment conditions (different sea states with their occurrences) is necessary for accurate estimates of annual fatigue damage. This

is shown by the significant difference created by the damage measured under different conditions.

- Due to the simultaneous contribution of both bending and axial strains and both elastic and plastic strains to the overall strains used for damage assessment, fatigue damage estimated for the capable is highly dependent on the position along the cable, where the study is based, which ensures that measuring fatigue damage at various positions along the cable is essential for analysis. In addition, cable diameter plays an important role in fatigue analysis, cyclic loading does further fatigue damage to the thicker cable. As the findings showed, the thicker cable has a lower lifetime.

Reference

1. Lefebvre, Simon, and Maurizio Collu. "Preliminary design of a floating support structure for a 5 MW offshore wind turbine." *Ocean Engineering* 40 (2012): 15-26..
2. https://www.ansys.com/products/structures/ansys-aqwa
3. Jonkman, J. M., and M. L. Buhl. "FAST user's guide Tech. Rep." *National Renewable Energy Laboratory* 28 (2005).
4. US Energy information Administration /www.eia.doe.govS
5. IEC, IEC. "61400-3, Wind Turbines-Part 3: Design Requirements for Offshore Wind Turbines." *International Electrotechnical Commission, Geneva* (2009).
6. Det Norske Veritas, 2007. Design of offshore wind turbine structures. DNV-OS-J101.
7. Lloyd, Germanischer, and Germany Hamburg. "Guideline for the certification of wind turbines." *July 1st* (2010)..
8. American Bureau of Shipping, 2013. Guide for building and classing floating offshore wind turbine installations.
9. Det Norske Veritas, 2013. Design of floating wind turbine structures.DNV-OS-J103.
10. Matha, D., 2009. \Model development and loads analysis of an offshore wind turbine on a tension leg platform, with a comparison to other floating turbine concepts". Master's thesis, University of Colorado-Boulder, April.
11. Sclavounos, P. D., et al. "Floating offshore wind turbines: tension leg platform and taught leg buoy concepts supporting 3-5 MW wind turbines." *European wind energy conference EWEC*. 2010.
12. Cordle, Andrew, and Jason Jonkman. *State of the art in floating wind turbine design tools*. No. NREL/CP-5000-50543. National Renewable Energy Lab.(NREL), Golden, CO (United States), 2011.
13. Larsen, Torben Juul, and Anders Melchior Hansen. "How 2 HAWC2, the user's manual." *December 2007* (2007).
14. Association, E. W. E. (2012). The European offshore wind industry key 2011 trends and statistics. Technical report, European Wind Energy Association.
15. Upwind (2011). Design limits and solutions for very large wind turbines; a 20-mw turbine is feasible. Technical report, Upwind.
16. Shikha, T. S. Bhatti, and D. P. Kothari. "Aspects of technological development of wind turbines." *Journal of Energy Engineering* 129.3 (2003): 81-95.
End of Chapter 1
17. Manwell, James F., Jon G. McGowan, and Anthony L. Rogers. *Wind energy explained: theory, design and application*. John Wiley & Sons, 2010.
18. Kaldellis, John K., and Dimitris Zafirakis. "The wind energy (r) evolution: A short review of a long history." *Renewable energy* 36.7 (2011): 1887-1901.

19. Nixon, N. Timeline: The history of wind power. http://www.theguardian.com/environment/2008/oct/17/wind-power-renewable-energy, October 2008.
20. US Department of Energy. 20% Wind Energy by 2030 - Increasing Wind Energy's Contribution to U.S. Electricity Supply. http://www.nrel.gov/docs/fy08osti/41869.pdf, July 2008
21. Global Wind Energy Council. Global Wind Report, April,2018. https://gwec.net/wp-content/uploads/2020/02/Annual-Wind-Report_digital_full-1.pdf
22. European Wind Energy Association. Upwind: Design limits and solutionsfor very large wind turbines. http://www.upwind.eu/~/media/UpWind/Documents/Home/21895_UpWind_Report_low_web.ashx, March 2011.
23. Navigant Consulting, Inc. Offshore wind market and economic analysis,2012 annual market assessment. http://www1.eere.energy.gov/wind/pdfs/offshore_wind_market_and_economic_analysis.pdf, February 2013.
24. IRENA (2019c), Renewable power generation costs in 2018, International Renewable Energy Agency, Abu Dhabi.
25. WindEurope (2019b), Wind energy in Europe in 2018 – Trends and statistics,WindEurope, Brussels.
26. MHI Vestas (2018), "MHI Vestas launches the first 10 MW wind turbine in history", www.mhivestasoffshore.com/mhi-vestas-launches-the-first-10-mw-wind-turbine-in-history/ (accessed 20 September 2019).
27. IRENA (n.d.), Power to change – Solar and wind cost reduction potential to 2030 in the G20 countries,International Renewable Energy Agency, Abu Dhabi.
28. Future of wind. Future of wind. October 2019. ISBN : *978-92-9260-155-3*.
29. Roddier, Dominique, Christian Cermelli, and Alla Weinstein. "WindFloat: A floating foundation for offshore wind turbines—Part I: Design basis and qualification process." *International Conference on Offshore Mechanics and Arctic Engineering*. Vol. 43444. 2009.
30. Skaare, B., Hanson, T. D., Nielsen, F. G., Yttervik, R., Hansen, A. M., Thomsen, K., and Larsen, T.J.,2007. \Integrated dynamic analysis of floating onshore wind turbines". In 2007 European Wind Energy Conference and Exhibition.
31. Jonkman, Jason, and Walter Musial. Offshore code comparison collaboration (OC3) for IEA Wind Task 23 offshore wind technology and deployment. No. NREL/TP-5000-48191. National Renewable Energy Lab.(NREL), Golden, CO (United States), 2010.
32. Jonkman, Jason M., and Marshall L. Buhl Jr. "FAST user's guide." Golden, CO: National Renewable Energy Laboratory 365 (2005): 366.

33. Jonkman, Bonnie J., and Marshall L. Buhl Jr. *TurbSim user's guide*. No. NREL/TP-500-39797. National Renewable Energy Lab.(NREL), Golden, CO (United States), 2006.
33. AQWA Reference Manual, October 2012.
34. Jonkman, Jason M., et al. "AeroDyn v15 user's guide and theory manual." *NREL Draft Report* (2015).
35. Jonkman, Jason M., A. Robertson, and Greg J. Hayman. "HydroDyn user's guide and theory manual." *National Renewable Energy Laboratory* (2014).
36. Iternational Electrotechnical Commission (IEC), 2005. Wind turbines:Part 1: Design requirements. IEC61400-1.
37. International Electrotechnical Commission (IEC), 2009. Wind turbines: Part 3: Design requirements for offshore wind turbines. IEC61400-3.
38. Det Norske Veritas, 2013. Design of floating wind turbine structures. DNV-OS-J103.
39. Jonkman, Jason, et al. *Definition of a 5-MW reference wind turbine for offshore system development*. No. NREL/TP-500-38060. National Renewable Energy Lab.(NREL), Golden, CO (United States), 2009.
40. Jonkman, J., and Matha, D., 2009. \A quantitative comparison of the responses of three floating platforms". In European Offshore Wind 2009 Conference and Exhibition, Stockholm, Sweden.
41. Veritas, Norske. *Design of Offshore Steel Structures, General (LRFD Method)*. Det Norske Veritas, 2000.
42. Feng, Ju, and Wen Zhong Shen. "Co-optimization of the shape, orientation and layout of offshore wind farms." *Journal of Physics: Conference Series*. Vol. 1618. No. 4. IOP Publishing, 2020.
43. Danish Energy Agency. Invitation to dialogue - tenders for horns rev 3 and kriegers flak. Available at: https://ens.dk/sites/ens.dk/files/Vindenergi/invitation_to_dialogue.pdf, 2013..
44. N. G. Nygaard. Systematic quantification of wake model uncertainty. In EWEA Offshore Conference, 2015 .
End of Chapter 2
45. Faltinsen, O.M. Sea loads on ships and offshore structures. s.l. : Cambridge University Press, 1990.
46. (DNV), Det Norske Veritas. RP-C205, ENVIRONMENTAL CONDITIONS AND ENVIRONMENTAL LOADS.
47. Tipler, Paul A. og Mosca, Gene. Physics for scientists and engineers. 2004. 0-7167-4389-2
48. Marintek. SIMO - Theory Manual Version 3.6, rev: 2. 2009.
49. Jonkman, J.M. Dynamics Modeling and Loads Analysis of an Offshore Floating Wind Turbine. s.l. : NREL, 2007. 6.

50. Hansen, Martin O. L. Aerodynamics of Wind Turbines. s.l. : Earthscan. 978-1-84407-438-9.
51. Moriarty, P.J. og Hansen, A.C. AeroDyn Theory Manual. s.l. : National Renewable Energy Laboratory, 2005. 16.
52. DNV. DNV-OS-J101 - Design of offshore wind turbine structures. s.l. : DNV, 2010.
End of Chapter 3
53. Ardelean, Mircea, and Philip Minnebo. "HVDC submarine power cables in the world." *Joint Research Center* (2015).
54. DNV, 2012, "Electrical Power Cables in Subsea Applications" DNV-RP-F401
54. Thies, Philipp R., Lars Johanning, and George H. Smith. "Towards component reliability testing for marine energy converters." Ocean Engineering 38.2-3 (2011): 360-370.
55. Clausen, T., and R. D'Souza. "Dynamic risers key component for deepwater drilling, floating production." Offshore 61.5 (2001): 89-90.
56. Schachner, Josef. *Power connections for offshore wind farms*. na, 2004.
57. Taninoki, Ryota, et al. "Dynamic cable system for floating offshore wind power generation." *SEI Technical review* 84.53-58 (2017): 146.
58. Loos, B. "Operability limits based on vessel motions for submarine power cable installation." (2017).
59. Green, J.; Bowen, A.; Fingersh, L.J.; Wan, Y.H. Electrical collection and transmission systems for oshore wind power. Onshore Technol. Conf. Proc. 2007, 4, 2215–2221.
60. Nasution, F. P.; Sævik, S.; Gjøsteen, J.K.Ø. Fatigue analysis of copper conductor for offshore wind turbines by experimental and FE method. Energy Procedia, 2012, 24, 271–280.
61. DNV, G.; DNVGL-RP-C203: Fatigue Design of Offshore Steel Structures. n. o DNVGL-RP-C203, 176. 2016.
62. LARSEN, C. M. 2009. Marine Dynamics
63. LARSEN, C. M. 1992. Use of Stochastic Dynamic Analysis in Marine Riser Design
64. BERGE, S. 2006. Fatigue and Fracture Design of Marine Structures.
65. Murakami, Yukitaka, ed. *The rainflow method in fatigue: the Tatsuo Endo memorial volume*. Butterworth-Heinemann, 2013.
End of Chapter 4
66. Skaare B, Hanson TD, and Nielsen FG. "Importance of Control Strategies on Fatigue Life of Floating Wind Turbines." 26th International Conference on Offshore Mechanics and Arctic Engineering, 10–15 June, San Diego, CA, 2007. (CD-ROM)
67. Larsen TJ, and Hanson TD. "A Method to Avoid Negative Damped Low Frequent Tower Vibrations for a Floating, Pitch Controlled Wind Turbine." The Second Conference on The Science of Making Torque From Wind, 28–31 August,

Copenhagen, 2007. [Online]. Available: http://iopscience.iop.org/1742-6596/75/1/012073/pdf?ejredirect=.iopscience.
68. Platt, A., Jonkman, B., & Jonkman, J. (2016). Inflowwind users guide. *Technical Report*.
69. Jonkman, J. M., Robertson, A., & Hayman, G. J. (2014). HydroDyn user's guide and theory manual. *National Renewable Energy Laboratory*.
70. Jonkman, J. M., Hayman, G. J., Jonkman, B. J., Damiani, R. R., & Murray, R. E. (2015). AeroDyn v15 user's guide and theory manual. *NREL Draft Report*.
71. Hall, M. (2015). MoorDyn user's guide. *Orono, ME: Department of Mechanical Engineering, University of Maine*.
72. Bouty, C.; Schafhirt, S.; Ziegler, L.; Muskulus, M. Lifetime extension for large offshore wind farms: Is it enough to reassess fatigue for selected design positions?. Energy Procedia,2017, 137, 523-530.
73. Jensen, P. C.; Jacobsen, S, H. Wind Turbines in Denmark, Danish Energy Agency, Denmark,2009.
74. Nasution, F. P.; Sævik, S.; Gjøsteen, J.K.Ø. Fatigue analysis of copper conductor for offshore wind turbines by experimental and FE method. Energy Procedia, 2012, 24, 271–280.
75. Loos,. B. Operability limits based on vessel motions for submarine power cable installation. Master's Thesis Royal Boskalis Westminster NV, Netherlands, 2017.
76. Sobhaniasl, Mohsen, et al. "Fatigue Life Assessment for Power Cables in Floating Offshore Wind Turbines." *Energies* 13.12 (2020): 3096.
77. Karimirad, M.,; Moan, T. Stochastic Dynamic Response Analysis of a Tension Leg Spar-Type Offshore Wind Turbine. Journal of Wind Energy (Wiley), 2013.16,6,953-973. DOI: 10.1002/we
78. Jonkman, J. Definition of the Floating System for Phase IV of OC3. No. NREL/TP-500-47535, National Renewable Energy Lab.(NREL), Golden, United States, 2010 [15] Jonkman, Jason M.,; Buhl Jr, M.L. FAST user's guide, National Renewable Energy Laboratory, Golden, USA, 2005.
79. Zeng, Xiang, et al. "Microstructure and Mechanical Properties of Al–SiC Nanocomposites Synthesized by Surface-Modified Aluminium Powder." Metals 8.4 (2018): 253.
80. Thies, Philipp R., Lars Johanning, and George H. Smith. "Assessing mechanical loading regimes and fatigue life of marine power cables in marine energy applications." Proceedings of the Institution of Mechanical Engineers, Part O: Journal of Risk and Reliability 226.1 (2012): 18-32.

81. Rychlik, I.; A new definition of the rainflow cycle counting method. Int. Journal of Fatigue., 1987, 9, 119–121.

82. Karlsen, Stian, et al. "Dynamic deep water power cables." Proceedings of the 9th International Conference and Exhibition for Oil and gas resources development of the Russian Arctic and CIS continental shelf, RAO/CIS Offshore, St Petersburg. 2009.
83. Rentschler, Manuel UT, Frank Adam, and Paulo Chainho. "Design optimization of dynamic inter-array cable systems for floating offshore wind turbines." Renewable and Sustainable Energy Reviews 111 (2019): 622-635.
84. Veritas, Det Norske. "DNV-OS-J103: Design of Floating Wind Turbine Structures." *Nor-way: DNV, DNV* (2013).
End of chapter 5
85. Bresesti, Paola, et al. "HVDC connection of offshore wind farms to the transmission system." *IEEE Transactions on energy conversion* 22.1 (2007): 37-43.
86. Lumbreras, S., and A. Ramos. "Offshore wind farm electrical design: a review." *Wind Energy* 16.3 (2013): 459-473.
87. Bauer, Joanna, and Jens Lysgaard. "The offshore wind farm array cable layout problem: a planar open vehicle routing problem." *Journal of the Operational Research Society* 66.3 (2015): 360-368.
88. Quinonez-Varela, G., et al. "Electrical collector system options for large offshore wind farms." *IET Renewable Power Generation* 1.2 (2007): 107-114.

Appendix A: Matlab Fatigue Calculation Function

This code calculates strain time history based on 6 parameters of the electrical cable. and at the end using rainflow script computes the cycles and amplitude of the provided rainflow signal.

```
function [rf]=F_calc100(N, X_2, X_1, Z_2, Z_1 , D,)
% This function compute Fatigue Damage based on 5 csv
input files from
% ansys
%Fatigue Analysis
%Loading Tables
N=(N); %Axial Stress Time Histories (TH)
Na=N(:,2);
X2=(X_2);   %X2 TH
Xa=X2(:,2);
X1=(X_1); %X1 TH
Xb=X1(:,2);
Z2=(Z_2); %Z2 TH
Za=Z2(:,2);
Z1=(Z_1); %Z1 TH
Zb=Z1(:,2);
%Constants
EI=%Const ;
E=%Const;
%R is D/2
R=D/2;
%A is Cross Sectional Area
A=3.14*(R^2);
StressYield= %Const;
%Removing Transitory Part
Na([1:4000],:) = [];
Xa([1:4000],:) = [];
Xb([1:4000],:) = [];
Za([1:4000],:) = [];
Zb([1:4000],:) = [];
npoints=length(Na); %Length of the vectors used for
calculation
I = EI/E;
E1 = E/20;
StrainYield = StressYield/E;
%M = Chi*E*I;
% Chi is curvature of the Cable
Chi=zeros(npoints,1);
Stresslin=zeros(npoints,1);
```

```
Strain=zeros(npoints,1);
Dx=zeros(npoints,1);
Dz=zeros(npoints,1);
Dz0=Za(1)-Zb(1);
AxialStress=zeros(npoints,1);
AxialStrain=zeros(npoints,1);
BendingStress=zeros(npoints,1);
BendingStrain=zeros(npoints,1);
%Calculating Curvature
for i=1:npoints
    Dx(i) = Xa(i)-Xb(i);
    Dz(i) = Za(i)-Zb(i);
    if Dz0<0
        if Dz(i)>0
            Chi(i)=(Dz(i)/Dx(i))+Dz0;
        else
            Chi(i)=(Dz(i)/Dx(i))-Dz0;
        end
    else
        if Dz(i)>0
            Chi(i)=(Dz(i)/Dx(i))-Dz0;
        else
            Chi(i)=(Dz(i)/Dx(i))+Dz0;
        end
    end
end
avgChi=mean(Chi);
Chi = (Chi-avgChi);
%Calculating Strain
for i=1:npoints
    Stresslin(i) = abs(Na(i)/A)+ abs(Chi(i)*E*R);

    if Stresslin(i) <= StressYield
        Strain(i) = (Stresslin(i)/E);
    else
        Strain(i) =(((Stresslin(i)-
StressYield)/E1)+StrainYield);
    end
end
ChiAA=abs(Chi);
StressAA=Stresslin;
%Rainflow
SSS = Strain;
tp = sig2ext(SSS);
rf = rainflow(tp);
end
```

Appendix B: MATLAB Fatigue Damage Calculator Script

This script compute fatigue damage for each sea states, based on previous function.

```
%Fatigue Calculator
clear;
clc;
    % Cable Diameter Input
    D_Cable10= 0.20
    % S-N_Curve_Constants
    C=%Constant
    B=%Constant
    %Input_Cable10
for i =1:%Number of files
    C10_N=[%directory of input file];
    C10_N=csvread(C10_N,6)
    C10_X44=[%directory of input file];
    C10_X44=csvread(C10_X44,6)
    C10_X43=[%directory of input file];
    C10_X43=csvread(%directory of input file)
    C10_Z44=[%directory of input file];
    C10_Z44=csvread(C10_Z44,6)
    C10_Z43=[%directory of input file];
    C10_Z43=csvread(C10_Z43,6)

[rf_Cable10]=Fatgiue_Calculator_Function(C10_N,C10_X44,C1
0_X43,C10_Z44,C10_Z43,D_Cable10);
    rf__Cable10_i{i}=rf_Cable10;
    %Rainflow_Cable10
    [no_Cable10, xo_Cable10]=rfhist(rf_Cable10); % taken
from rfhist.m(rainflow script);
    n_cycle_Cable10=no_Cable10;
    amp_Cable10=xo_Cable10;
    %Damage_Cable10
    %NNN_Cable10=C.*(amp_Cable10.^B);

f_damage_Cable10=(n_cycle_Cable10)./(C.*(amp_Cable10.^B))
;
    f_damage_Cable10_i{i}=f_damage_Cable10;
    Total_Damage_Cable10=sum(f_damage_Cable10);
    Total_Damage_Cable10_i(i)=Total_Damage_Cable10;
end
```

Appendix C: Paper I

Article

Fatigue Life Assessment for Power Cables in Floating Offshore Wind Turbines

Mohsen Sobhaniasl [1], Francesco Petrini[2]*, Madjid Karimirad [3] and Franco Bontempi [4]

[1] Sapienza University of Rome; mohsen.sobhaniasl@uniroma1.it
[2] Sapienza University of Rome; francesco.petrini@uniroma1.it
[3] Queen's University Belfast (QUB); madjid.karimirad@qub.ac.uk
[4] Sapienza University of Rome; franco.bontempi@uniroma1.it
* Correspondence: francesco.petrini@uniroma1.it

Received: date; Accepted: date; Published: date

Abstract: In this paper, a procedure is proposed to determine the fatigue life of the electrical cable connected to a 5MW floating offshore wind turbine supported by spar-buoy at a water depth of 320 meters by using a numerical approach that takes into account site-specific wave and wind characteristics. The effect of the intensity and the simultaneous action of wave and wind are investigated and outcomes for specific cable configurations are shown. Finally, the fatigue life of the cable is evaluated. All analyses have been carried out using Ansys AQWA computational code, which is a commercial code for the numerical investigation of the dynamic response of floating and fixed marine structures under the combined action of wind, waves and current. Furthermore, this paper applies FAST NREL numerical code for comparison with ANSYS AQWA results.

Keywords: Wind energy, Floating offshore wind turbine, Dynamic analysis, Fatigue life assessment, Flexible power cables

1. Introduction

Power cables are wideley used in power transmission lines and electrification of floating oil and gas production infrastructures, where they have to withstand considerable cyclic loads induced by the combination of floating body dynamics with wind, waves and current effects [1,2].

One of the main design issues for power cables in marine applications is the fatigue strength, fatigue assessment studies have demonstrated that accurate analysis of the complex dynamic behavior induced by the offshore environment must be carried out for fatigue assessment purposes, Dai et al (2020) [3] presented experimental and numerical studies on dynamic stress and curvature in steel tube umbilicals, the results show tha curvature, also when small, governs the fatigue problem, Yang et al. (2018) [4] presented a parametric study of the dynamic motions and mechanical characteristics of power cables for wave energy conversion (WEC) system. The results show large curvature responses of the cable typically occur at high wave heights and near the wave period of resonance, Yang et al (2017) [5], still regarding the same WEC system, demonstrated that minor fouling can increase the fatigue life of the power cable.

A relatively new application area for marine power cable elements is in floating offshore wind turbines (FOWTs) [6] and farms. In fact, wind energy has become one of the most important renewable energy sources in recent decades. Its development requires increasing electric transmission capacity and better ways to preserve system reliability. Wind-generated power continues to grow rapidly throughout the world, offshore wind farms are expected to account for a large portion of total wind energy output and may even contribute significantly to total electricity production in some countries [7]. The cost-effective operation of marine energy conversion systems needs reliable design of marine

power cables, which are currently the components for which design procedures mainly needs further developments due to their limitate fatigue strength. FOWTs in particular, together with their mooring systems and connected power cables must withstand various environmental actions: correlated variability in the wind, current, and wave loads cause variable and uninterrupted dynamic motion and stress in the power cables connecting the single FOWTs each other and/or with the land. The accumulation of variable stress results in cumulative damage to fatigue [8], which for this kind of systems is a weak point in the design panorama, and it is something that, together with other design or operating issues, currently prevent the large-scale installation and diffusion of floating offshore wind farms as a reliable system for energy generation and as an evolution of the currently widely diffused fixed-foundation offshore wind farms. These weaknesses are particular relevant for the electrical cables connecting each other single turbines in the farm [9] named "inter-array" or "umbilical" cables.

Therefore, the definition of advanced and reliable tools for the investigation of fatigue damage is necessary, and the topic is highly recognized by the research community [9] and the industry [10], [11]. Design approaches in this area intend to ensure the required fatigue life for the structure or key parts of it [12], and are devised toghether with appropriate inspection programs for monitoring fatigue damage initiations or progresses.

This paper proposes a procedure for the fatigue life evaluation of a power cable which is attached to a single FOWT in lazy wave geometrical configuration, by considering: i) the correlated intensities of wind, ocean current and wave actions [13]; ii) the different operating conditions of the turbine, and; iii) the complete non-linear dynamics of the turbine-cable coupled system [14]; iv) the difference between fatigue actions in different locations along the cable. Several modelling issues are faced to increase the confidence in the results obtained by the Multiphysics modelling of the system. The wind field sampling by the rotor in operating conditions, the fluid-structure interaction between the wind and the FOWT due to the platform large displacements, the joint bending and axial induced strain in the cable, the non-linearity involved in the problem (due to both large displacements and the appearing of plastic strains) are included in the analyses by making reliable assumptions and by calibrating the procedures employing sensitivity analyses. The objective of this paper is to provide a reliable procedure for assessing the fatigue failure of the power cable of FOWTs. The proposed procedure is applied to the umbilical cable attached to the spar-buoy supported 5 MW NREL wind turbine in a water depth of 320 meters considering site-specific wind, wave and current for short term sea state of the China sea. The case study is modelled both in the FAST NREL code [15] and in the ANSYS AQWA Commercial code [16]. The obtained results offer supporting data for the a-priori identification of weakenesses and critical components for fatigue strenght and to evaluate the desired level of reliability before deployment.

2. Analysis Method for Fatigue Life evaluation

As well known, the simplified relation between the stress of amplitude Si and the associated number of cycles Ni that leads to fatigue failures of mechanical components under constant-amplitude oscillating load can be represented for different intensities by the S-N (σ-N) fatigue curve [17]. The S-N curve is a characteristic of the materials, of the shape of the component or of the design configuration of the structure. Under the indications provided in DNV design standards [18,19], the fatigue damage for different levels of stress oscillation magnitudes can be calculated for pertinent components of FOWTs by the Palmgren's- Miner assumption by the Equation 1 [17]

$$Dm = \Sigma \frac{ni}{Ni_{cyces}} \tag{1}$$

where Dm is the accumulated fatigue damage due to all considered stress oscillations magnitudes, ni is the number of the stress oscillations with magnitude Si, Ni_{cyces} is the number of cycles of stress oscillations with magnitude Si which leads to fatigue failure.

Electrical cables connecting FOWTs in floating offshore wind farms are of the umbilical typology, providing a service-support from the main station to the single FOWTs. Such as umbilical cables, are

of the optical powered submarine type and are provided to supply electrical power or to send operating control inputs and data to underwater elements in the offshore oil and gas infrastructures [20]. Umbilical cables are implemented in floating offshore wind farms and connected to each FOWT for the same purposes, then their integrity and service ability are crucial for the correct coordination and operation of the FOWTs in the farm.. The stress condition in such non-homogeneous cross-section of the umbilical cables is quite complex, with non-linear local stress due to contact and friction between the components of the tube, and the model and aleatory uncertainty due to this complexity is critical for the reliability of any fatigue analysis. For sake of simplicity, and in line with state of the art literature paper on the topic [9] the cable will be modelled in this paper with a homogeneous-material equivalent cross-section.

As an alternative to the σ-N plane, fatigue curves may also be represented by the total strain (ε) versus the number of cycles (N) as detailed below. Equation 1 is usable for both stress versus number of cycles curve and strain versus number of cycles (ε-N). The evaluation of the total strain time history in a critical fatigue-prone location of the cable, and corresponding to a specific sea state, is conducted by a non-linear numerical analysis of the coupled FOWT-electrical cable system, and ε accounts for both elastic (ε_e) and plastic strain (ε_p) and may then be expressed as follows [21]:

$$\varepsilon(t) = \varepsilon_e(t) + \varepsilon_p(t) = \frac{\sigma_{el}(t)}{E} + \varepsilon_p(t) \tag{2}$$

where E is the Young's elastic modulus assigned to the equivalent homogenous material modelling the cable, and σ_{el} is the elastic tension stress of the electrical cable, evaluated step-by-step as the maximum cross-section tensile stiffness in the homogeneous material cross-section by considering both the axial and bending contributions:

$$\sigma_{el}(t) = \frac{N(t)}{A} + \chi(t) \cdot E \cdot \frac{D}{2} \tag{3}$$

in which, by referring to the circular cross-section of the cable, N is the axial force, A is the area, χ is the bending curvature, and D is the diameter.

The plastic strain contribution ε_p enters in the game only when the total stress, evaluated by the equation (3), is larger than the yielding stress σ_y of the cable, which can be evaluated from the strain-stress constitutive law assumed for the equivalent homogeneous material used for modelling the cable (see Figure 1) as detailed in equation (4)

$$\varepsilon_p(t) = \frac{\sigma_y}{E} + \frac{\sigma_y - \sigma_{el}(t)}{E'} \tag{4}$$

where E' is the material plastic modulus.

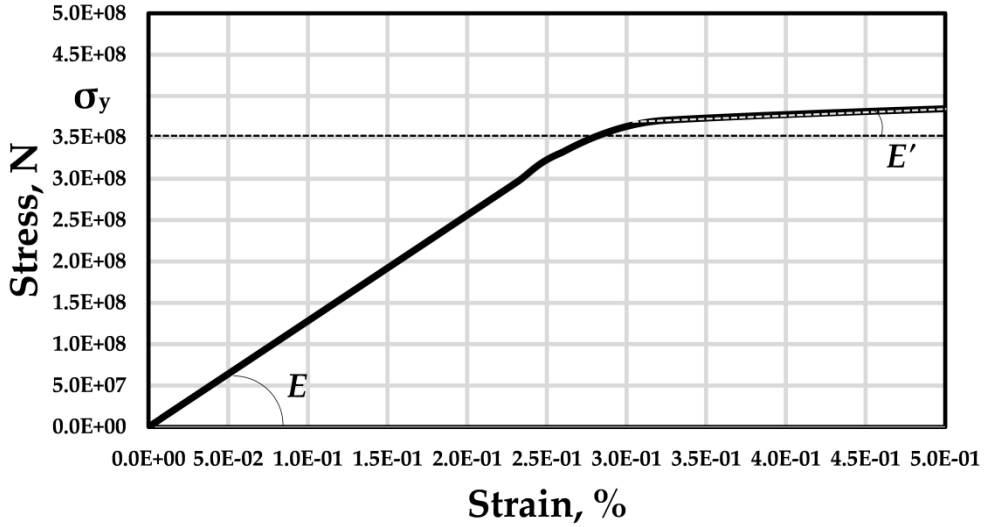

Figure 1. Stress-strain constitutive relationship of the cable.

The non-linear stress-stress behavior and relaxation characteristics make the impact of plastic strains plays a non-negligible role in the electrical cable fatigue analysis. Inside the umbilical cable, the conductors, that are commonly made of pure Electrolytic Tough Pitch (ETP) copper, are vulnerable to fatigue accumulation and mechanical failure, as highlighted by Karlsen and co-authors (2009) [11], which state that *"the material has excellent conductivity but poor mechanical properties, which include stress-relaxation (creeping) and non-linear stress-strain behaviour, and they suggests using ε-N curves (referring to strain) instead of traditional σ-N curves"*.

NIST Monograph 177 [22] summarizes the results of a total of 126 plastic strain-controlled tests and 150 stress-controlled tests performed on a large set of coppers, made by annealed material and cold-worked material. The stress-controlled test data may be converted to elastic strain values according to Equation 2 with ε_P=0.

The *ε-N* fatigue curve considering the effect of both elastic and plastic strain can be expressed by the Coffin-Manson relation [21]:

$$\varepsilon\left(N_{cycles}\right) = \varepsilon_e\left(N_{cycles}\right) + \varepsilon_p\left(N_{cycles}\right) = = C_1 \cdot N_{cycles}^{-\beta_1} + C_2 \cdot N_{cycles}^{-\beta_2} \quad (5)$$

where $\varepsilon\left(N_{cycles}\right)$ are the strain amplitudes leading to failure at N_{cycles} number of cycles, C_i and β_i (with i=1,2) are appropriate material constants, provided by Thies et al. (2011) [23] for a typical FOWT umbilical cable as C_1 = 0.7692, β_1 = 0.5879, C_2 = 0.0219, β_2 = 0.1745This curve is shown in Figure 2, and it is the same used in the present paper forfatigue analyses.

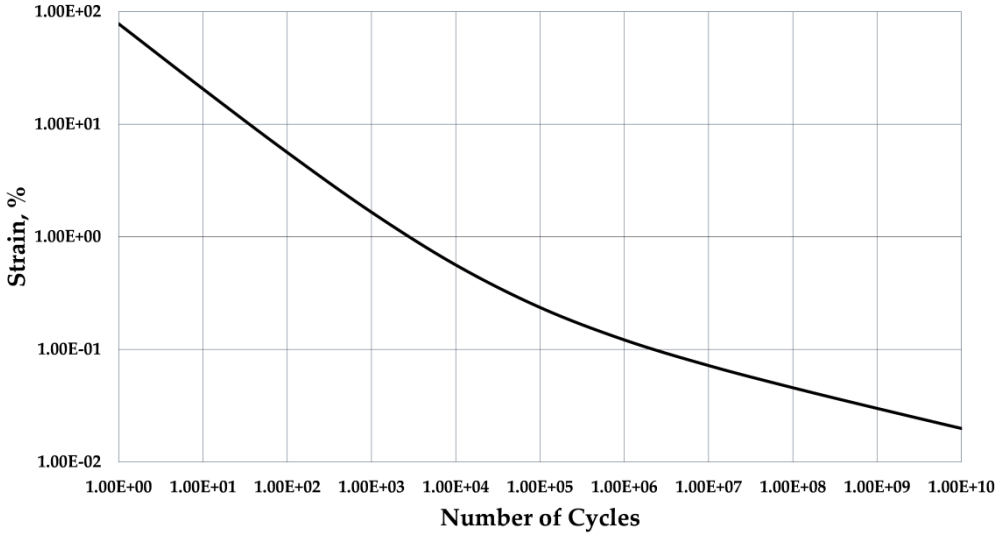

Figure 2. Strain-cycle (*ε-N*) fatigue curve for ETP copper. Adapted from Ref. [11].

According to abovementioned calculation, the total strain time history in a critical cross-section of the cable has to be evaluated and then processed by a cycle counting, leading to a set of amplitudes-No of cycle histograms which are compared with the fatigue curve of the cable in order to assess the fatigue damage *Dm* associated with each single time history. One of the most popular cycle counting methods is Rainflow method [24].

In the FOWT context, the fatigue damage is calculated for each considered sea state. Then, from the climate statistics of the site where the floating offshore wind farm is located, the joint probability distribution of the sea states in the reference period of the analysis *Tr* (e.g. 1-year) is estimated, and the occurrences in *Tr* of the damage associated to each sea state can be evaluated.

3. Case study

The NREL 5-MW wind turbine on the OC3-Hywind spar buoy FOWT is chosen as a case study for the evaluation of the fatigue life of an inter-array turbines (umbilical) cable. The case study has been chosen for its simplicity in design, suitability to modelling, and the existence of literature numerical

results [25]. As already said, the case study is modelled both in FAST and ANSYS AQWA software. Structural, hydrodynamic and mooring line properties of the model are reported in appendix A.

Figure 3 illustrates the models NREL 5-MW wind turbine on the OC3-Hywind spar on FAST (right) and the model with the same properties in ANSYS AQWA (left). It is worth noting that the electrical cable is modelled in ANSYS AQWA but it is not in FAST, the motivations for this are given in next section 4. Tables in the Appendix show structural and hydrodynamic properties and the mooring properties of the model. The lazy wave configuration of the electrical cable is taken from Rentschler et al. ([9]), in which a hydrostatic optimization of the layout of the cable is carried outd with a genetic algorithm, with the goal of minimizing the cable fatigue and by chosing the position of the buoyancy elements as design variables, resulting in a lower waveform position as optimal solution, with anaccumulative length of the buoyancy parts from 18 % to 23 % of the total cable length.

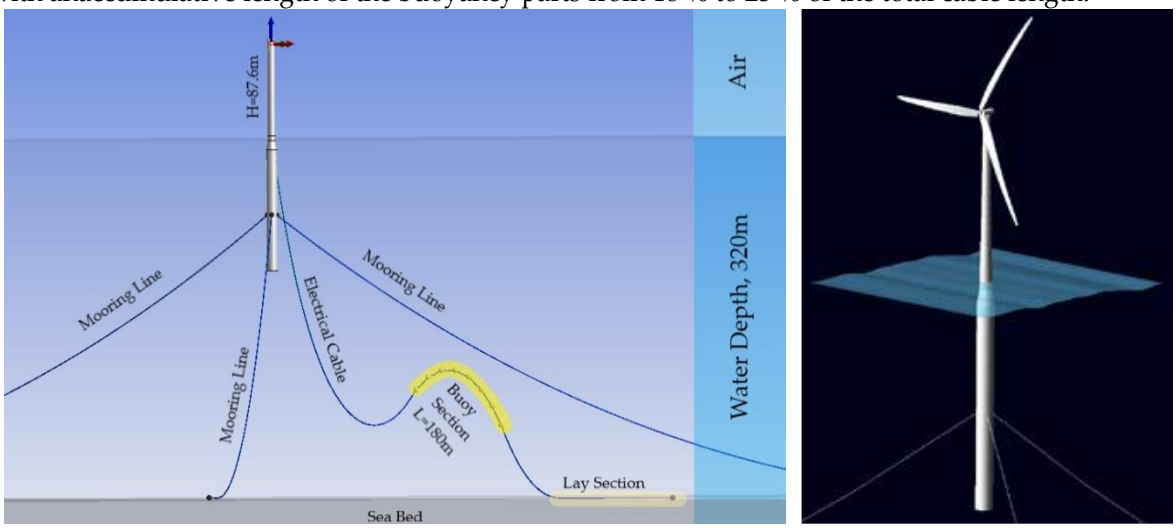

Figure 3. Left: Model in ANYSY AQWA, Right: Model in NREL FAST [22]

For the simulations of this paper, a typical cross-section of the electrical cable has been utilized , with a single layer of galvanized steel armour wires and extruded XLPE isolators. The mechanical characteristics of the cable have been assumed from the literature [6], [27]. The values for the diameter, weight and strength are shown in Figure 4, with reference to Figure 1, the linear and non-linear elastic module E and E' and the yielding stress σ_y are equal to 128 GPa, 6.4 GPa and 350 MPa, respectively.

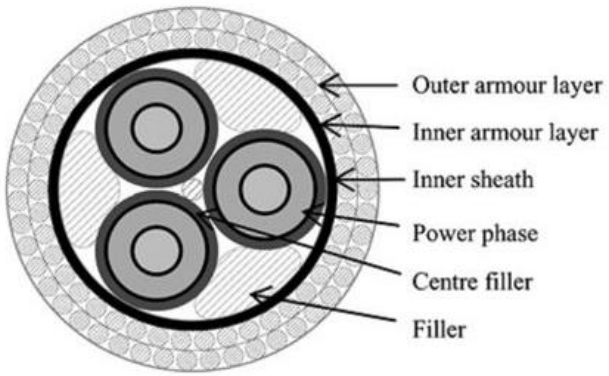

Cable Specification	
Nominal Diameter	0.2 m
Nominal weight in seawater	39 Kg
Bending Stiffness	10 kNm²
Axial stiffness	700 MN
Minimum Breaking Load	100 kN

Figure 4. Cable specifications [27]

4. Modeling Spar Buoy Supported Platform and The Cable

Depending on the wind speed and the environmental conditions, the configuration of the rotor changes: it is in operational, rotating blades conditions, when the wind speed is between the cut-in and

the cut-out values, while the wind turbine is parked for the wind speeds higher than the cut-out value, with blades parallel to the wind [28]. Time history analyses are conducted for 4000 seconds for different environmental conditions, and the first 400 seconds are removed to neglect transitory effects of the simulation and waiting for to the model to reach the stationary operation state.

The used version of the FAST Code (version 8) does not allow to add extra non-structural elements (like power cable, etc.), but there are some possibilities to add extra elements in ANSYS AQWA, this is the motivation why the electrical cable and the fatigue analyses have been conducted in ANSYS AQWA. On the other side, one of the issues faced in the used version of ANSYS AQWA (version 18.2) is the difficulty of modelling the rotating blades in operating conditions, then the rotor-nacelle assembly is modelled there as a concentrated mass at the hub height. To mitigate this weakness, total rotor aerodynamic load time history (force in the x-direction) named "*RtAeroFxh*" output [15], as extracted from a preliminary simulation FAST (where the electrical cable is not modelled) in a certain sea state case, is successively applied to the hub in the model in ANSYS AQWA (where the electrical cable is now modelled and meshed by 100 finite elements). Since hydrodynamic loads are evaluated in ANSYS AQWA based on the implemented wave theory and by making use of the Morrison's equation, to avoid double-counting of hydrodynamic effects during the simulation in ANSYS AQWA, the *RtAeroFxh* aerodynamic force should be evaluated by not taking into account the three following effects: i) presence of waves; ii) action of a sea current and; iii) inertial effect of water volumes moving with the platform; because all these effects will be taken into account in the subsequent ANSYS AQWA simulation.

One of the procedures that can be implemented for avoiding the double-counting is by running the preliminary FAST analysis by fully restraining the bottom DOFs of the platform and maintaining the over-water dynamics (named "Fixed DOFs at spar" option). This procedure would completely neglect the double-counting of all the three listed effects but, on the other hand, this option would also neglect some fluid-structure interaction (FSI) effects that have a non-negligible impact on the *RtAeroFxh* (e.g. the wind incoming velocities and angles of attack are not combined with the correct translational velocities and rotational displacements experimented by the rotor during the large pitch, thrust and heave displacements of the floating platform when relative wind-rotor velocities and rotational angles are obtained for aerodynamic load calculation purposes). The second strategy for facing the double-counting problem is to run the preliminary FAST analysis by assuming a "still water" (no sea current and no waves) and by allowing the floating platform DOFs. By adopting this strategy, the FSI effects are mostly taken into account (the relative velocities between the wind and the rotor and tower will take into account the large displacements of the floating platform induced by the wind itself) also if the impact on the relative traslational velocities of the hydrodynamic forces (less important than that of wind, which are due to both translation and rotation of the tower) is not considered and, at the end of the process, there will also be a (partial) double-counting of the inertial effect of water volumes moving with the platform. Then a compromise should be put in place to run the analysis by the joint use of the two computational codes. In order to show the differences found in the *RtAeroFxh* by running the preliminary analysis with three different strategies: the above mentioned "Fixed DOFs at spar" and "Still Water" options, and the analysis carried out by considering all the loads in FAST ("wave and current" mode, something that would cause the above-mentioned double-counting effect if the extracted *RtAeroFxh* is successively applied to ANSYS AQWA), the time histories of the *RtAeroFxh* obtained for the three cases are compared in Figure 5 for one of the sea states considered in the following fatigue analysis: sea state 15 as identified in Table 2 by grey highlighting (wind velocity at the hub height equal to 21.7m/s, current velocity equal to 0.5m/s, wave height equal to 4.5m with period of 10s).

From Figure 5 (b), it is clear that the "Fixed DOFs at spar" option provides conservative results with respect to the "Still Water" option, while is also obvious that the inclusion of the waves and current would produce an additional contribution (the one that, if included, would be double counted in ANSYS AQWA) that is relevant for the examined load case. From Figure 5(c) it is shown that frequency content slightly changes between the three options (with different frequencies contents for the "Wave

and Current" case with respect to the other two). Based on this analysis, final choice has been made by opting for the "Fixed DOFs at spar" strategy in subsequent fatigue calculation as this is on the conservative side with respect to the "Still Water" model.

In order to further discuss the adopted strategy in coupling the two codes, it is worth to say that a step-by-step "*two-way*" coupling, that is the continuous data exchange between the two codes in order to take into account for the interactions of sub-domains (e.g. aerodynamics-hydrodynamics) which are evaluated in the two different numerical codes, would be able to solve the above mentioned problems regarding the double counting or the neglection of some effects. When, as in this paper, some "*one-way*" coupling is put in place, the two codes elaborate separately the subdomains of the problem, and for just one of them the elaboration takes into account the data coming from the other domain/code (in this paper for example we lost the effect of the ANSYS AQWA results on the FAST evaluations). Therefore, the use of the one-way coupling implies the acceptance of a compromise regarding the effects we lost and the accuracy of the obtained results. The correct strategy to pursue the one-way coupling is to adapt/calibrate the separate subdomains models in a way that minimizes the aspects we lost but, more importantly, keeps the design/analysis on the conservative side. In our case we adapted the FAST model, used for aerodynamic subdomain evaluation, with the main goal of being on the conservative side, but with the secondary goal of not being too conservative (and far from accuracy) by trying to neglect the double-counting of the displacements induced by the hydrodynamic forces.

4.1 Model Verification

Due to the above mentioned joint use of the two codes, the procedure needs to be validated, especially regarding the evaluation of the hydrodynamic loads obtained by the two codes: having the same response of the model under hydrodynamic loads is a primary condition in order to assume that the obtained results are reliable and that the above-mentioned procedure of extracting the aerodynamic loads from FAST leads to a consistent dynamics of the system. With this purpose, a set of validation analyses (comparison of the platform dynamics obtained by FAST and ANSYS AQWA and comparison with literature results for the same problem under different load conditions) are carried out and based on published results of Phase IV of NREL 5 MW FOWT [26]. Fully nonlinear analysis in ANSYS AQWA and FAST are performed with all wind turbine DOF's (surge, sway, heave, pitch, roll, yaw). Environmental condition for validation simulation is shown in table 1. Hydrodynamic, structural and mooring line properties considered the same as in [26] while the electrical cable is not modelled in this validation phase.

Figure 6 shows time histories of the platform surge, heave and pitch displacement considering load case shown in Table 1 as obtained in the present study by ANSYS AQWA and FAST and compared with results published in [26] as obtained with FAST ("OC3" in the Figure) for validation purposes. The simulation shows there is a good agreement between the results of FAST and ANSYS AQWA.

In the Fatigue analysis presented in the next section, the motion responses of the spar-buoy platform were calculated in ANSYS AQWA under the combination of wind, current, and wave loads. Concerning the wind, in each analysis, in addition to the time history of the total force acting on the rotor *RtAeroFxh* as extracted from FAST, the mean wind (equation (6) below) is applied to the tower above the sea. The Airy theory for regular waves [26] is applied for waves' dynamics computation, while Morrison's equations [26] is applied for hydrodynamic forces evaluation. To model the environmental condition, regular sea states are assumed.

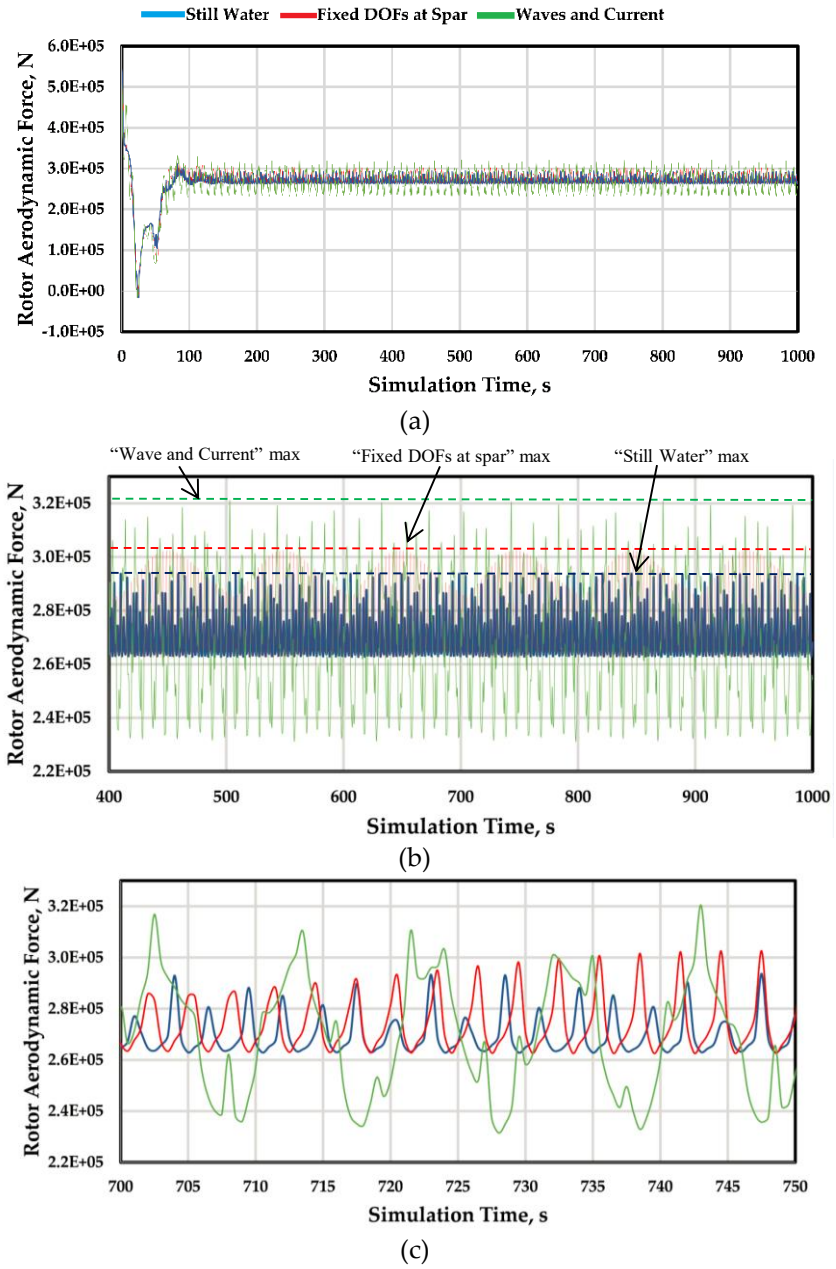

Figure 5. Rotor Aerodynamic Force *RtAeroFx* as extracted from FAST for the sea state 15 and the three strategies that would be adopted for neglecting the double-counting of the hydrodynamic effects. 0-100 sec scale (a); 400-1000 sec scale (b); 700-750 sec time interval (c).

Table 1. Environmental conditions used for model verification purposes [26]

Enabled DOFs	Platform, Tower
Wind Condition	None
Wave Condition	Regular Airy: H=6 m and T= 10s
Analysis Type	Time-series solution

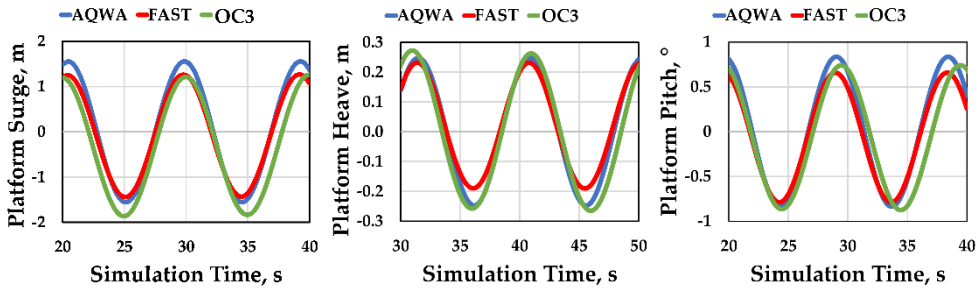

Figure 6. Comparison of the time histories of the platform main DOFs under the load case shown in table 1, as obtained by FAST an ANSYS AQWA models. Surge (a), Heave (b), Pitch (c).

5 Fatigue Analysis

The above-mentioned general procedure for fatigue life evaluation has been applied to the case study by using the validated numerical models as described above. The complete flowchart of the fatigue analysis procedure adopted in this study is shown in Figure 7, the goal is to determine the fatigue life in the cross-section of the cable that is located at a critical position along with the cable development for fatigue.

As already said, for each considered loading condition (sea state "SS" in what follows) the aerodynamic forces time histories are extracted from FAST (in "Fixed DOFs at spar" conditions and without modelling the electrical cable), and applied to the top of the tower in the ANSYS AQWA model. Then the structural response is evaluated in ANSYS AQWA by a fully non-linear time-domain analysis considering also the model provided by the electrical cable. The outputs that are relevant for fatigue damage assessment in the electrical cable with the method described in the previous section 2 (axial force and bending curvature in the cross-section of the cable at the location which is relevant for fatigue) are then extracted to feed an in-house developed MATLAB routine which implements the evaluation of the total strain time history as described in Equations (2)-(4). The bending curvature of the cable is obtained step-by-step as spatial first derivative of the bending deflection starting from the time histories of the displacements of the two nodes adjacent to the focused location. When the time history of the total strain in the given location for a certain SS is obtained, a MATLAB routine for rainflow cycle counting method [24] is applied and the fatigue damage for the considered SS is evaluated at the focused location by the comparison of the cycle-counting histogram with the ε-N fatigue cure shown in Figure 2. The procedure is repeated for all the relevant SSs (for a total of 20 SSs reported in Table 5). Finally, the damages obtained are multiplied by their pertinent annual occurrences evaluated by a fitted Weibull distribution indicating the climate of the FOWT location. The total annual fatigue damage *Dm_year* is then evaluated as the sum of the annual fatigue damages induced by the single SSs and the fatigue life of the cable *Lf* is evaluated as the inverse of the annual fatigue damage, while the design fatigue life *Lf_d* is obtained by considering a safety factor SF_DNV equal to 10 as indicated in DNV standards [29].

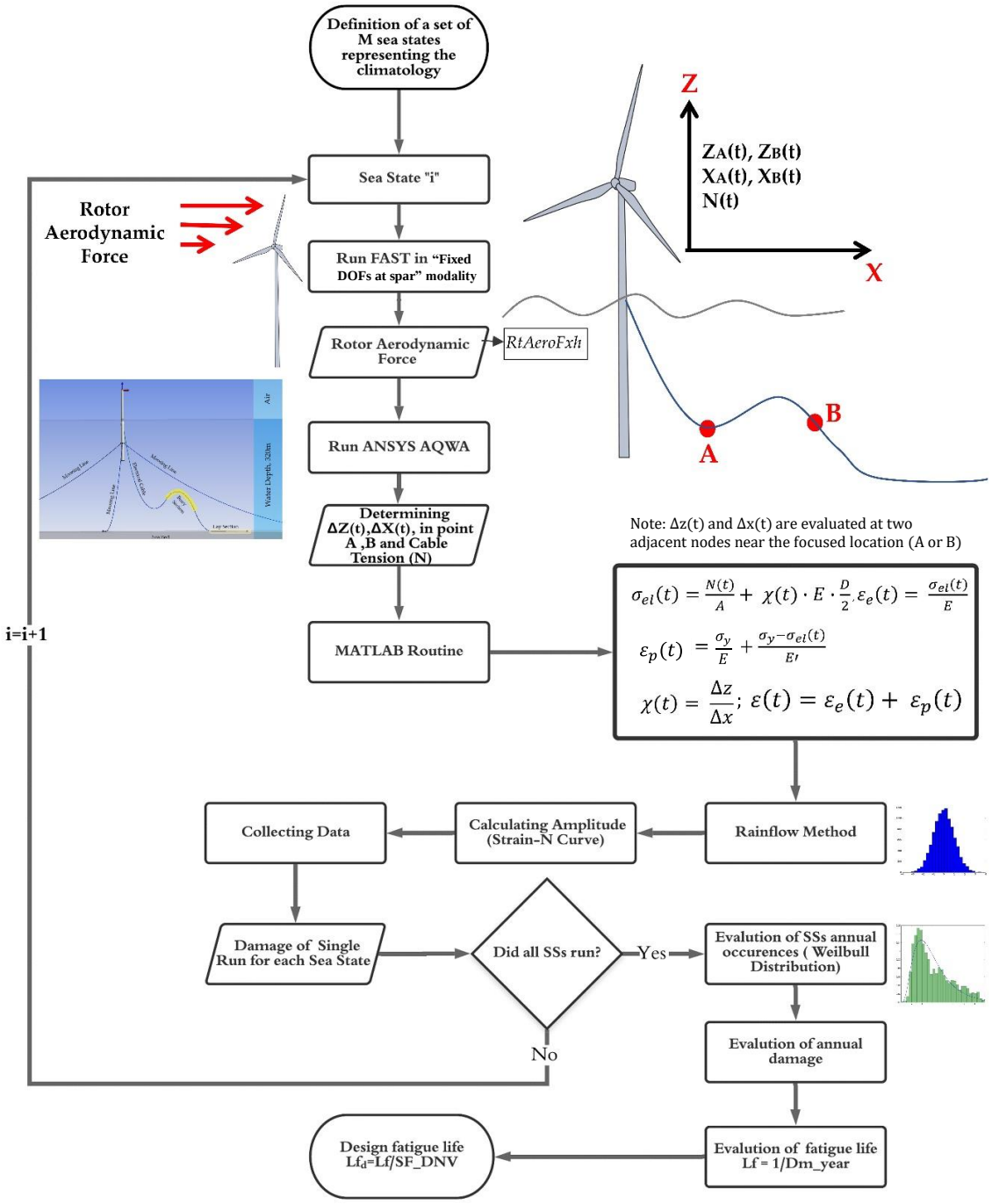

Figure 7. Fatigue Analysis of Dynamic Electrical Cable

Figure 8 shows the electrical cable configuration. As already said, the electrical cable configuration provided in [9] is used in the simulations. The cable is hanging off a fixed point on the spar-buoy platform at the sea surface, and the electrical cable modelled by 100 elements. The fatigue of the cable is calculated at different locations along the cable to individuate the most critical cross-section for fatigue. The fatigue damage is highly influenced by the position of the cross-section along the cable. For demonstration purposes, in the following the fatigue life is evaluated for locations A and B along the cable as shown in Figure 8.

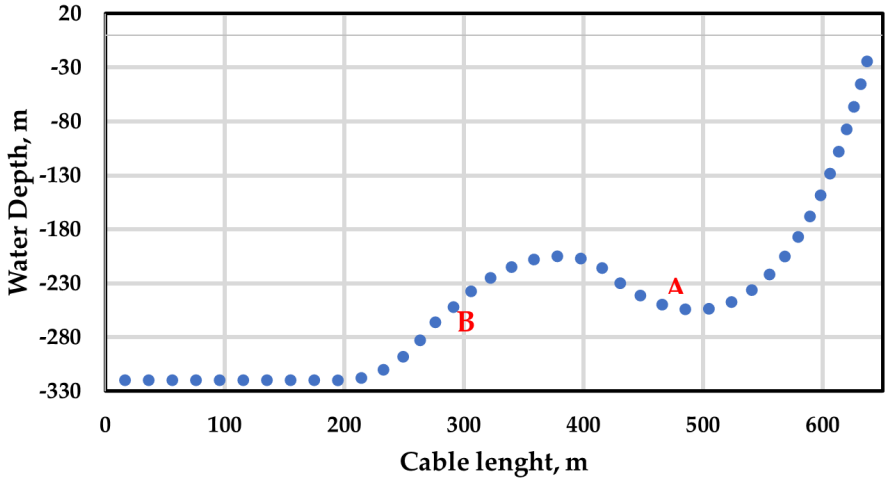

Figure 8. Electrical Cable layout

5.1 Environmental conditions and considered SSs

The SS conditions for fatigue life evaluations are selected from the South China Sea S4 area, the angle of incidence of wind and waves is fixed to the direction coinciding with to the X-axis, that is orthogonal to the cable longitudinal extension, since this is recognized to be the most critical configuration for fatigue in umbilical cables. The chosen sea states are listed in Table 2 in accordance with the wave scatter diagram of South China Sea S4 [30] in one year period. The wind speed profile representing the variation of the mean wind with the height above the still water level $U(z)$, is evaluated by the power-law model shown in equation (6), where U_{10} is 10 mins average wind speed at 10m height above the sea still water level, α is power-law profile [29]:

$$U(z) = U_{10} \cdot \left(\frac{z}{10}\right)^{\alpha} \tag{6}$$

Also in Table 2, Hs is the waves height and T is the waves period, Cv is the current velocity, and P is the annual probability of each sea state as evaluated by a Weibull probability distribution function adopted in fitting the number of occurrences of the sea states. Equation 7 describes Weibull probability density function, while Figure 9 shows Weibull probability distribution function.

$$PDF_{weibull} = \frac{\beta}{V}\left(\frac{U_{10}}{\gamma}\right)^{\beta} e^{-\left(\frac{U_{10}}{\gamma}\right)^{\beta}} \tag{7}$$

Where, in this paper $\beta = 2.49$ and $\gamma = 10.4\ m/s$ are the values assumed for the shape parameter and scale parameter [31] in order to fit the available SSs data.

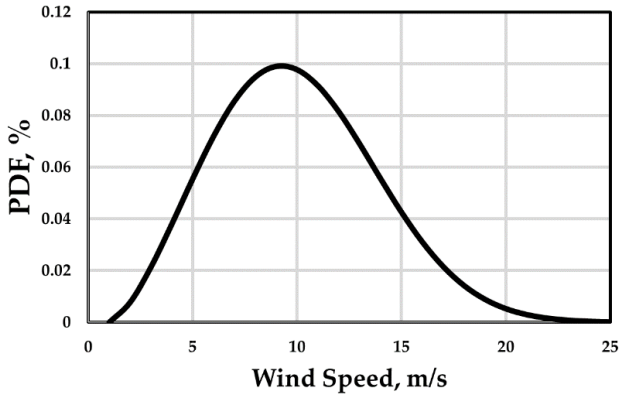

Figure 9. Weibull distribution adopted for U_{10}

Table 2. Short Term Sea States (in grey the sea state used for comparison in Figure 5) [30]

SS	U_{10} (m/s)	U(H) (m/s)	Hs (m)	T (s)	Cv (m/s)	P (%)
1	5.6	7.279722555	0.675	4	0.168	2.24096
2	6	7.799702738	0.675	5	0.180	8.68372
3	7	9.099653194	1.050	4	0.210	1.96084
4	7.80	10.13961356	1.050	6	0.234	14.006
5	8.5	11.04957888	1.550	4	0.255	1.4006
6	9	11.69955411	1.550	5	0.270	10.36444
7	9.40	12.21953429	1.550	7	0.282	20.16864
8	10.8	14.03946493	2.175	5	0.324	5.32228
9	11.2	14.55944511	2.175	7	0.336	15.4066
10	12	15.59940548	2.875	6	0.360	8.96384
11	13.2	17.15934602	3.625	6	0.396	3.08132
12	14.5	18.84928162	4.000	6	0.432	0.56024
13	15.0	19.49925684	4.500	7	0.450	3.64156
14	16.1	20.92920235	5.000	7	0.483	0.84036
15	16.7	21.70917262	4.500	10	0.501	0.84036
16	17.2	22.35914785	4.500	11	0.516	0.28012
17	17.4	22.61913794	5.500	10	0.522	0.56024
18	18	23.39910821	5.500	11	0.540	0.56024
19	19.1	24.82905372	6.750	10	0.573	0.84020
20	20	25.99900913	3.625	12	0.600	0.280
		Sum of Probability				100

Wind turbines are typically designed for 20-25 years [32], Under average wind conditions, an onshore wind turbine can produce electricity for 4,000-7,000 hours a year, corresponding to 70-80% of the total hours in the year [33] On the above basis an average number of 15 windy hours each day for a total of 365 days during the year (5475 hours per year) is considered in evaluating the occurrences of the SSs.

5.2. Fatigue Life Estimation

As already said, in order to avoid transitory effects of the simulation in rainflow method calculations, first 400 seconds are removed from the ANSYS AWQWA analysis output before feeding the cycle-counting MATLAB routine. As an instance, Figure 10 shows time histories of the cable axial force as obtained at location A from the SS 10 simulation in Table 2. The results obtained for the annual fatigue damage at location A for the 20 SSs are shown in Figure 11, while Figure 12 shows the percentage of the contribution of each SS to the annual fatigue damage. As said above, the annual fatigue damage due to a particular SS is evaluated by multiplying the fatigue damage obtained by the non-linear time history analysis conducted in ANSYS AQWA by the number of annual occurrences of that SS.

Finally, the Table 3 represents the evaluation of the annual fatigue damage *Dm_year* due to all the 20 SSs considered with their occurrences, obtained as the sum of the annual fatigue damages obtained for all SSs. From these results, it is evident how the Location A is critical for fatigue and that it suffers important damage who quantifies the fatigue life *Lf* of the umbilical cable to about 10 years, if scaled by the safety factor SF_DNV reduces to 1 year. This result confirms that fatigue in electrical cables is a weak point for this kind of structures.

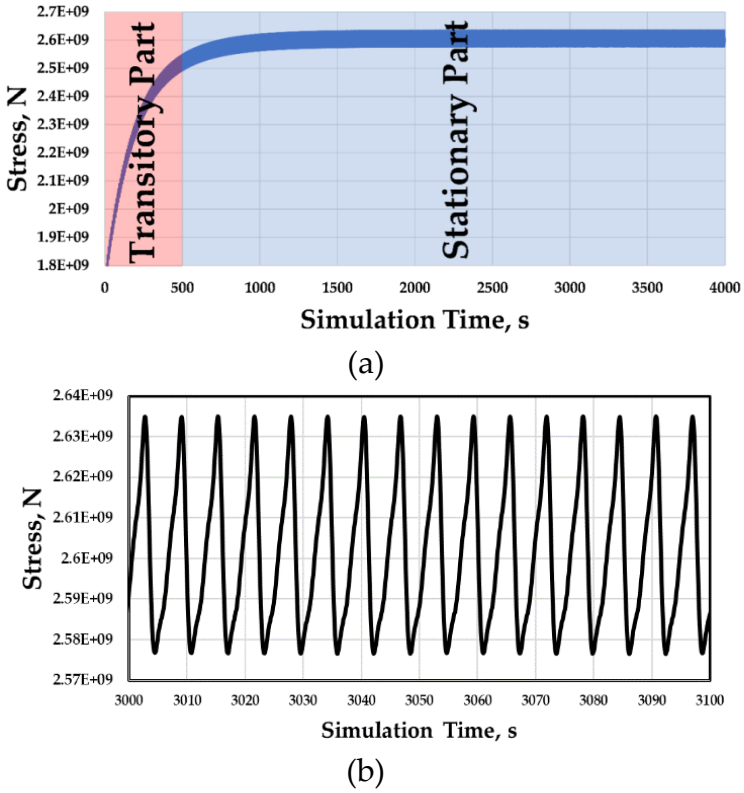

Figure 10. Example of axial stress time history in the cable at location A and for the SS no. 10. Whole (a); focus (b)

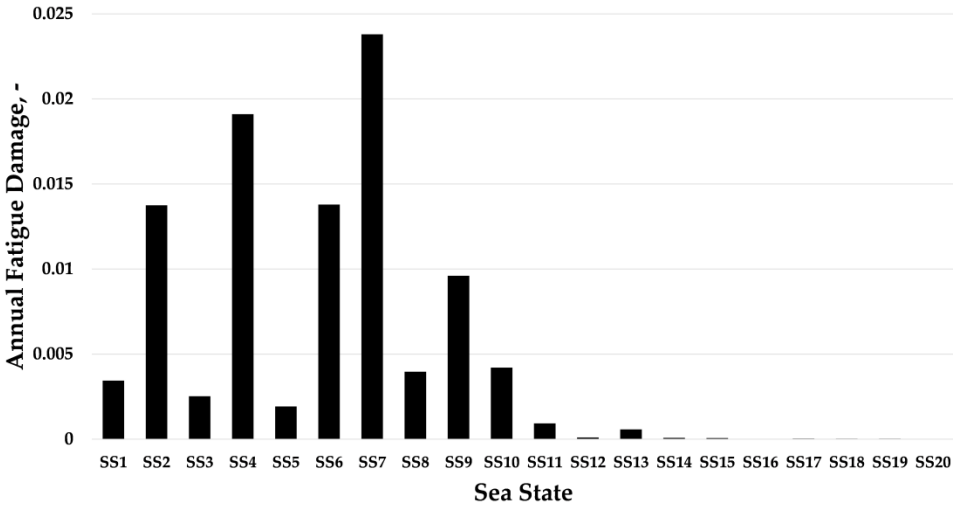

Figure 11. Annual fatigue damage induced at location A for all considered SSs

Table 3. Annual fatigue damage and fatigue life estimation

Sea State	Annual Fatigue Damage. Location A	Annual Fatigue Damage. Location B
1	3.442737E-03	2.68358E-04
2	1.3747238E-02	9.76374E-04
3	2.526371E-03	2.0901E-04
4	1.9108678E-02	1.10222E-03
5	1.923422E-03	1.13001E-04
6	1.37916E-02	8.4595E-04
7	2.380188E-02	1.44312E-03
8	3.962855E-03	2.18672E-04
9	9.60747E-03	3.96218E-04
10	4.204048E-03	1.88023E-04
11	9.2328E-04	3.25774E-05
12	1.00209E-04	3.50426E-06
13	5.72823E-04	1.28245E-05
14	8.0497E-05	1.65752E-06
15	6.27443E-05	1.28641E-06
16	1.97191E-05	3.1258E-07
17	3.50939E-05	5.99213E-07
18	2.66189E-05	5.45779E-07
19	2.54863E-05	9.23608E-07
20	5.53736E-06	4.84702E-07
Sum of the annual damage for all SSs	9.796831E-02	5.81566E-03
Fatigue life of the cable *Lf* (years)	10.2074	171.9495
Fatigue design life of the cable Lf_d (with the application of the SF_DNV Safety Factor (years)	1.02074	17.19495

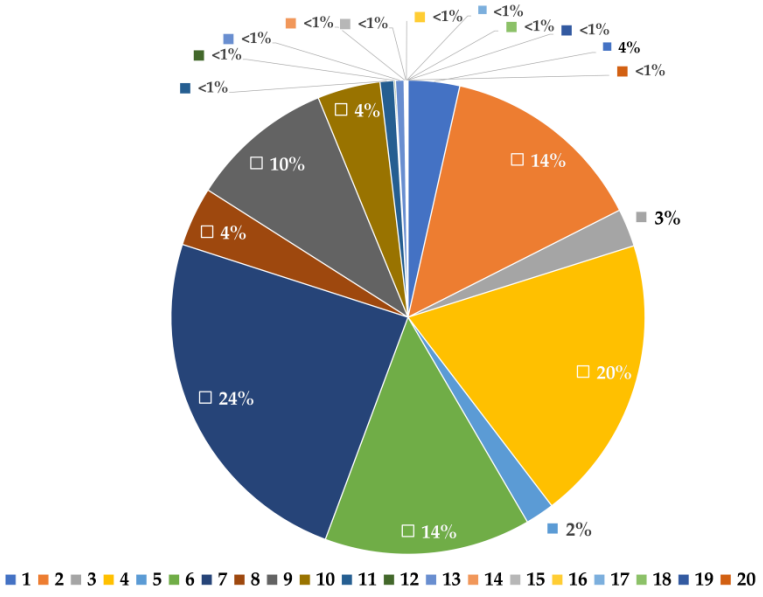

Figure 12. Relative contribution at location A to the annual fatigue damage of all considered SSs

From Table 3 it is also evident how the evaluated fatigue damage is strongly dependent from the location along the cable: location B experiments much less damage (more than 10 times lower) than location A.This difference in the fatigue damage is due to the fact that the experimented oscillations and bending deformations of the cable decrease from A to B due to the presence of the buoy section of the cable development, being the cable stabilized by the buoyancy (see Figure 3).

Fatigue life assessment is highly dependent on the cable diameter and the location of the calculation point for the fatigue analysis. As already mentioned above, two different points are used in fatigue analysis in this research to calculate strain amplitude of the points (Figure 8). The suggested safety factor (SF) of 10 based on recommendations [29] is applied in the present study to assess the fatigue life.

6. Conclusion

The paper has assessed the fatigue life expected for an umbilical cable subjected to the loading regime of a typical marine environment and under the non-linear dynamic conditions as they can be expected in a spar-buoy floating offshore wind turbine.

Main novelty of the paper lies in bringing together mostly available knowledge to provide a comprehensive procedure/tool for the fatigue analysis of the vulnerable electrical cables of FOWTs. Such a tool cnanot avoid complex structural dynamics analyses by putting in place simplistic assumptions about loads, their occurrences and numerical models. In fact in the paper the fatigue life of the cable's copper conductor was estimated for the FOWT site by setting out an ad-hoc complete procedure that: i) computes the total strain time histories in the cable cross-section by the avail of fully non-linear time histories numerical analyses of the whole turbine system including the electrical cable; ii) evaluates the fatigue damage induced by a number of different sea states and by covering the wide range of climate and operating conditions of the turbine; iii) defines annual occurrences of the different considered sea states for annual damage evaluation purposes based on the sea state statistics. Numerical analyses have been conducted by the joint use of two well-established numerical codes for offshore floating structures, which is important for allowing multi-physic and multi-scale analyses of such a complex structural systems: critical points arising from this coupling have been spotted out (e.g. correct consideration of the FSI and large displacements) and the associated analysis steps/choices for making the design remaining on the conservative side under the current integration level of the two codes have been discussed, which is also a point of novelty for the paper.

Regarding the fatigue design of FOWTs electrical cable, general engineering findings are:

- floating offshore wind turbine power cables must withstand a dynamic loading regime when they are attached to the support platform (spar-buoy, TPL, etc.) and are susceptible to fatigue failures. The fatigue life of the examined case is 10 years if not scaled with the safety factor prescribed by the DNV standards. When a value of 10 is applied as a safety factor, the design fatigue life reduces to 1 year only;
- the correct evaluation of all the operating (parked VS rotating blades) and climate conditions (different sea states with their occurrences) is fundamental to obtain reliable estimations of the annual fatigue damage, this is evidenced by the large difference obtained by the damage evaluated by different conditions;
- due to the concurrent contribution of both bending and axial strains, and both elastic and plastic strains to the total strains used for damage evaluation, the fatigue damage evaluated for the cable is strongly dependent on the location along the cable development where the analysis is focused, then evaluating the fatigue damage in different locations along the cable is crucial for the analysis.

All the above general consideration suggest that the development of reliable-advanced tools for fatigue damage calculation like the one presented in this paper, which can include non-linearities of the structural behaviours, statistics of the climatology at the site, complex dynamic behaviours of

rotating blades and aero-hydrodynamics under large displacements, is an important topic for the reliable evaluation of the fatigue of electrical cables, something that is a design weakness in floating offshore wind turbine systems.

Further developments for the research are under development and includes:

- consideration of the effects of irregular sea states;
- refinement of the wind action and the fluid-structure interaction model by a two way-coupling between the two codes used for the analysis, with the inclusion of the aerodynamic damping;
- refinement of the electrical cable modeling (currently modeled as an equivalent homogeneous element);
- exploration of more complex dynamic configuration of the electrical cable (modeling of more than one turbine, different cable layouts);

Author Contributions: Conceptualization, Karimirad M., Petrini F.; methodology, Karimirad M., Petrini F. and Bontempi F.; software, Sobhaniasl M. and Petrini F.; formal analysis, Sobhaniasl M.; writing—original draft preparation, Sobhaniasl M.; writing—review and editing, Karimirad M. and Petrini F.; supervision, Bontempi F. All authors have read and agreed to the published version of the manuscript.

Funding: This research was funded by Sapienza University of Rome, "Fondi di avvio alla Ricerca", grant number AR118164360855CD.

Conflicts of Interest: The authors declare no conflict of interest.

Appendix A

Table 4. Structural Properties of the Model [25]

Description	Unit
Gravitational acceleration (m/s^2)	9.80665
Hub mass (kg)	56780
Hub inertia about rotor axis [3 blades] or teeter axis [2 blades] (kg m^2)	115926
Generator inertia about HSS (kg m^2)	534.116
Nacelle mass (kg)	240000
Nacelle inertia about yaw axis (kg m^2)	2.60789E+06
Yaw bearing mass (kg)	0
Platform mass (kg)	7.46633E+06
Platform inertia for roll tilt rotation about the platform CM (kg m^2)	4.22923E+09
Platform inertia for pitch tilt rotation about the platform CM (kg m^2)	4.22923E+09
Platform inertia for yaw rotation about the platform CM (kg m^2)	1.6423E+08

Table 5. Hydrodynamic Properties of the Model [25]

Description	Unit
Water density (kg/m^3)	1025
Water depth (meters)	320
Displaced volume of water when the platform is in its undisplaced position (m^3)	8029.21
Incident wave kinematics model	Regular
Analysis time for incident wave calculations (s)	3630
Time step for incident wave calculations	0.25
Significant wave height of incident waves (meters)	6
Peak-spectral period of incident waves	10
Range of wave directions(degrees)	90
Wave Type	Stokes 2nd-order wave theory
Low frequency cutoff used in the summation-frequencies (rad/s)	0.1
High frequency cutoff used in the summation-frequencies (rad/s)	1.9132
Current profile model	No Current
Analysis time for wave (s)	2000
Time step for wave (s)	0.0125
Additional Linear Damping in Surge N/(m/s)	100,000
Additional Linear Damping in Sway N/(m/s)	100,000
Additional Linear Damping in Heave N/(m/s)	130,000
Additional Linear Damping in Yaw Nm(rad/s)	13,000,000
Hydrostatic Restoring in Heave (N/m)	332,941
Hydrostatic Restoring in Roll (Nm/rad)	-4,999,180,000
Hydrostatic Restoring in Pitch (Nm/rad)	-4,999,180,000

Table 6 Mooring Lines Properties of the Model [25]

Description	Unit
the mass per unit length of the line (kg/m)	77.7066
the line stiffness, product of elasticity modulus and cross-sectional area (N)	384.243E6
Diameter (m)	0.09

References

1. De Alegria, I. M.; Martín, J. L.; Kortabarria, I.; Andreu, J.; Ereño, P. I. Transmission alternatives for offshore electrical power. *Renew. Sustain. Energy Rev.* **2009**, *13(5)*, 1027-1038.
2. Green, J.; Bowen, A.; Fingersh, L. J.; Wan, Y. H. Electrical collection and transmission systems for offshore wind power. *Offshore Technol. Conf. Proc.*, **2007**, 4, 2215–2221.
3. Dai, T., Sævik, S. and Ye, N. Experimental and numerical studies on dynamic stress and curvature in steel tube umbilicals. *Marine Structures*, **2020**, p.102724
4. Yang, S.H., Ringsberg, J.W. and Johnson, E. Parametric study of the dynamic motions and mechanical characteristics of power cables for wave energy converters. *Journal of Marine Science and Technology*, 2018,*23*(1), pp.10-29
5. Yang, S.H., Ringsberg, J.W., Johnson, E. and Hu, Z. Biofouling on mooring lines and power cables used in wave energy converter systems—analysis of fatigue life and energy performance. *Applied Ocean Research*, **2017**,*65*, pp.166-177
6. Nasution, F. P.; Sævik, S.; Gjøsteen, J.K.Ø. Fatigue analysis of copper conductor for offshore wind turbines by experimental and FE method. *Energy Procedia*, **2012**, 24, 271–280.
7. Watson, S.; Moro, A.; Reis, V.; Baniotopoulos, C.; Barth, S.; Bartoli, G.; Bauer, F.; Boelman, E.; Bosse, D.; Cherubini, A.; Croce, A.; Fagiano, L.; Fontana, M.; Gambier, A.; Gkoumas, K.; Golightly, C.; Latour, M.I.; Jamieson, P.; Kaldellis, J.; Macdonald, A.; Murphy, J.; Muskulus, M.: Petrini, F.; Pigolotti, L.; Rasmussen, F.; Schild, P.; Schmehl, R.; Stavridou, N.; Tande, J.; Taylor, N.; Telsnig, T.; Wiser, R. Future emerging technologies in the wind power sector: A European perspective. *Renewable and Sustainable Energy Reviews*, **2019**, 113, Article number 109270
8. Lotsberg, I. *Fatigue Design of Marine Structures*. Cambridge University Press.; Cambridge, 2016. doi:10.1017/CBO9781316343982
9. Rentschler M.U.T.; Adam, F.; Chainho, P. Design optimization of dynamic inter-array cable systems for floating offshore wind turbines. *Renew. Sustain. Energy Rev.*, **2019**, 111, 622–635.
10. Deltares. Joint industry project cables lifetime monitoring. 2018. URL https://www.deltares.nl/app/uploads/2018/04/PB_Joint-Industry-Project-Cables-Life-Time-Monitoring_v2.pdf.
11. Karlsen, S.; Slora, R.; Heide, K.; Lund, S.; Eggertsen, F.; Osborg, P. A. Dynamic deep water power cables. In Proceedings of the 9th International Conference and Exhibition for Oil and gas resources development of the Russian Arctic and CIS continental shelf, RAO/CIS Offshore, St Petersburg, 2009.
12. Homb, H. R. Fatigue Analysis of Mooring Lines on the Floating Wind Turbine Hywind Demo, Master's thesis, NTNU, Norway, 2013.
13. Manenti S., Petrini F. Dynamic Analysis of an Offshore Wind Turbine: Wind-Waves Nonlinear Interaction, *Proceedings of the 12th biennial ASCE Aerospace Division International Conference (Earth & Space 2010)*, Honolulu, USA, 2010. ISBN 978-0-7844-1096-7
14. Karimirad, M. Modeling aspects of a floating wind turbine for coupled wave-wind-induced dynamic analyses. *Renewable Energy*, **2013**, 53, 299-30
15. Jonkman, J M.; Buhl Jr, M.L. FAST user's guide, National Renewable Energy Laboratory, Golden, USA, 2005.
16. Canonsburg, T.D. AQWA User Manual, ANSYS, Inc, 2012.

17. DNV, G.; DNVGL-RP-C203: Fatigue Design of Offshore Steel Structures. n. o DNVGL-RP-C203, 176. 2016.
18. DNV, GL; DNV-OS-J101–Design of offshore wind turbine structures. 2014.
19. Veritas, D. N. Design of floating wind turbine structures, Offshore Standard DNV-OS-J103.2013.
20. Cárdenas, N. O.; Machado, I. F.; Gonçalves, E. Cyclic loading and marine environment effects on the properties of HDPE umbilical cables. *Journal of materials science*, **2007,**42(16), 6935-6941.
21. Dieter, G. E.; Bacon, D. *Mechanical metallurgy* ,New York, USA, 1986,Vol. 3.
22. Drexler, E. S.; Simon, N.J.; Reed R.P. *Properties of copper and copper alloys at cryogenic temperatures*. *No. NIST-MN-177. NIST*, National Inst. of Standards and Technology (MSEL), Buolder, USA,1992
23. Thies, P.R.; Johanning ,L.; Smith, G.H. Assessing mechanical loading regimes and fatigue life of marine power cables in marine energy applications. Journal of Risk and Reliability, **2012**, vol. 226. p. 18–32.
24. Rychlik, I. A new definition of the rainflow cycle counting method. *Int. Journal of Fatigue.,* **1987**, *9*, 119–121.
25. Jonkman, J. Definition of the Floating System for Phase IV of OC3. No. NREL/TP-500-47535, National Renewable Energy Lab.(NREL), Golden, United States, 2010.
26. Jonkman, J. *Definition of the Floating System for Phase IV of OC3* (No. NREL/TP-500-47535). National Renewable Energy Lab.(NREL), Golden, CO (United States),**2010**
27. Loos, B. Operability limits based on vessel motions for submarine power cable installation. Master's Thesis Royal Boskalis Westminster NV, Netherlands, 2017.
28. Karimirad, M.; Moan, T. Stochastic Dynamic Response Analysis of a Tension Leg Spar-Type Offshore Wind Turbine. *Journal of Wind Energy (Wiley)*, **2013**.16,6,953-973. DOI: 10.1002/we
29. DNV-RP-F401, Electrical Power Cables in Subsea Applications, 2012
30. Qiao, D.; Yan, J.; Ou, J. Fatigue analysis of deepwater hybrid mooring line under corrosion effect, *Polish Marit*,**2014**., 21, 3,. 68–76.
31. Chang, R.; Zhu, R.; Badger, M.; Hasager, C. B.; Xing, X.; Jiang, Y. Offshore wind resources assessment from multiple satellite data and WRF modeling over South China Sea. *Remote Sensing*, **2015**, 7(1), 467-487.
32. Bouty, C.; Schafhirt, S.; Ziegler, L.; Muskulus, M. Lifetime extension for large offshore wind farms: Is it enough to reassess fatigue for selected design positions?. *Energy Procedia*,**2017**, 137, 523-530.
33. Jensen, P. C.; Jacobsen, S, H. *Wind Turbines in Denmark,* Danish Energy Agency, Denmark,2009.